50272-101

REPORT DOCUMENTATION PAGE	1. REPORT NO. NCEER-93-0010	2.	3. PB93-227494

4. Title and Subtitle
Seismic Performance of Shear-Critical Reinforced Concrete Bridge Piers

5. Report Date
May 12, 1993

6.

7. Author(s)
J.B. Mander, S.M. Waheed, M.T.A. Chaudhary and S.S. Chen

8. Performing Organization Rept. No.

9. Performing Organization Name and Address
State University of New York at Buffalo
Department of Civil Engineering
Buffalo, New York 14260

10. Project/Task/Work Unit No.

11. Contract(C) or Grant(G) No.
(C) BCS 90-25010
(G) NEC-91029

12. Sponsoring Organization Name and Address
National Center for Earthquake Engineering Research
State University of New York at Buffalo
Red Jacket Quadrangle
Buffalo, New York 14261

13. Type of Report & Period Covered
Technical Report

14.

16. Abstract (Limit: 200 words)
This report summarizes an investigation of the behavior of a beam to column joint of a 32 year old shear-critical bridge pier and a companion one-quarter scale model of the two column prototype bent under reversed cyclic lateral loading. The prototype specimen was retrieved from the field and prepared for testing by welding a self equilibrating reaction frame onto the reinforcing steel of the cap beam. The model and the prototype were tested under constant vertical (gravity) loads. The cyclic lateral loading was applied through a horizontally connected actuator in case of the model and two parallel actuators inclined at $24°$ with the horizontal were used for the prototype testing in order to simulate lateral force effects in an entire two-column bent. Experimentally observed shear strengths were compared with code-based strength evaluation techniques. Evaluation shows that the pier would possess inadequate shear capacity and thus be classified as shear-brittle with no ductility capability. It is also shown that if code-based evaluation procedures are followed this class of bridge pier is classified as unsafe and shear-brittle, but may be capable of resisting minor earthquakes through elastic response. However, if a dependable ductile mechanism is assumed, as demonstrated by good experimental behavior, a safe seismic response can be assumed for all Seismic Performance Categories in the United States.

17. Document Analysis a. Descriptors

b. Identifiers/Open-Ended Terms

Reinforced concrete bridge piers.   Beam column joints.   Experimental tests.
Reversed cyclic lateral loads.   Code-based strength evaluation.   Shear strength.
Energy-based damage analysis.   Earthquake Engineering.

c. COSATI Field/Group

18. Availability Statement	19. Security Class (This Report)	21. No. of Pages
Release Unlimited	Unclassified	176
	20. Security Class (This Page) Unclassified	22. Price

(See ANSI-Z39.18)   See Instructions on Reverse   OPTIONAL FORM 272 (4-77)
(Formerly NTIS-35)

Seismic Performance of Shear-Critical Reinforced Concrete Bridge Piers

by

J.B. Mander, S.M. Waheed, M.T.A. Chaudhary and S.S. Chen

State University of New York at Buffalo
Department of Civil Engineering
Buffalo, New York 14260

Technical Report NCEER-93-0010

May 12, 1993

NOTICE

Seismic Performance of Shear-Critical
Reinforced Concrete Bridge Piers

by

J.B. Mander[1], S.M. Waheed[2], M.T.A. Chaudhary[2] and S.S. Chen[1]

May 12, 1993

Technical Report NCEER-93-0010

1 Assistant Professor, Department of Civil Engineering, State University of New York at Buffalo
2 Graduate Research Assistant, Department of Civil Engineering, State University of New York at Buffalo

NATIONAL CENTER FOR EARTHQUAKE ENGINEERING RESEARCH
State University of New York at Buffalo
Red Jacket Quadrangle, Buffalo, NY 14261

PREFACE

The National Center for Earthquake Engineering Research (NCEER) was established to expand and disseminate knowledge about earthquakes, improve earthquake-resistant design, and implement seismic hazard mitigation procedures to minimize loss of lives and property. The emphasis is on structures in the eastern and central United States and lifelines throughout the country that are found in zones of low, moderate, and high seismicity.

NCEER's research and implementation plan in years six through ten (1991-1996) comprises four interlocked elements, as shown in the figure below. Element I, Basic Research, is carried out to support projects in the Applied Research area. Element II, Applied Research, is the major focus of work for years six through ten. Element III, Demonstration Projects, have been planned to support Applied Research projects, and will be either case studies or regional studies. Element IV, Implementation, will result from activity in the four Applied Research projects, and from Demonstration Projects.
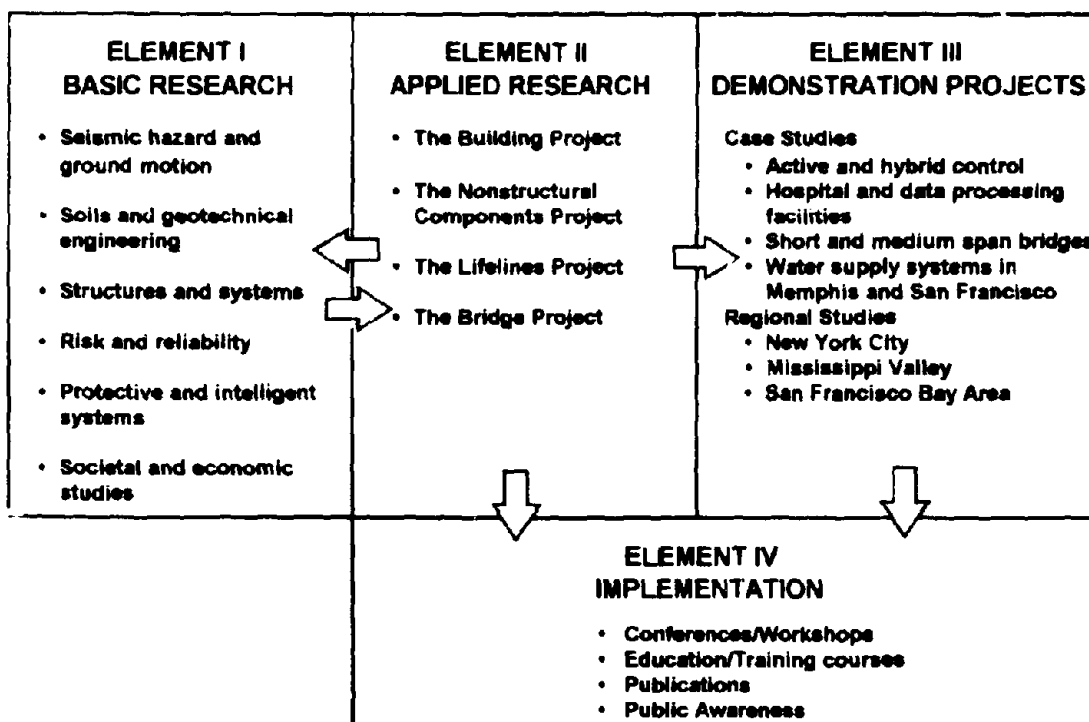
Research tasks in the **Bridge Project** expand current work in the retrofit of existing bridges and develop basic seismic design criteria for eastern bridges in low-to-moderate risk zones. This research parallels an extensive multi-year research program on the evaluation of gravity-load design concrete buildings. Specifically, tasks are being performed to:

1. Determine the seismic vulnerability of bridge structures in regions of low-to-medium seismicity, and in particular of those bridges in the eastern and central United States.

2. Develop concepts for retrofitting vulnerable bridge systems, particularly for typical bridges found in the eastern and central United States.

3. Develop improved design and evaluation methodologies for bridges, with particular emphasis on soil-structure mechanics and its influence on bridge response.

4. Review seismic design criteria for new bridges in the eastern and central United States.

The end product of the **Bridge Project** will be a collection of design manuals, pre-standards and design aids which will focus on typical eastern and central United States highway bridges. Work begun in the **Bridge Project** has now been incorporated into the **Highway Project**.

This report summarizes the results of experiments of an actual 32 year old bridge pier joint and a companion quarter-scale two-column bent. The load-deformation characteristics, including the energy absorption capacities for reversed cyclic loading, were similar for the prototype subassembly and the model test. These tests show that there is little strength deterioration up to column drift angles of two percent. The shear capacity predictions by codes were shown to be too conservative for these piers with little transverse reinforcement. The accompanying analytical study included a new energy-based strength deterioration model.

ABSTRACT

This report summarizes an investigation of the behavior of a beam to column joint of a 32 year old shear-critical bridge pier and a companion one-quarter scale model of the two column prototype bent under reversed cyclic lateral loading. The prototype specimen was retrieved from the field and prepared for testing by welding a self equilibrating reaction frame onto the reinforcing steel of the cap beam. The model and the prototype were tested under constant vertical (gravity) loads. The cyclic lateral loading was applied through a horizontally connected actuator in case of the model and two parallel actuators inclined at 24° with the horizontal were used for the prototype testing in order to simulate lateral force effects in an entire two-column bent.

Lateral loads were applied with increasing drift angles to ± 4 percent. A moderately ductile failure initiated through flexure but was later dominated by shear when drift angles exceeded ± 2 percent for both model and prototype specimens. Final failure was attributed to fracture and bond deterioration of the longitudinal bars for the model and the prototype respectively. The results of model and the prototype tests were compared with one another. Overall performance of the model and prototype were remarkably similar.

Shear accounted for between 25 and 60 percent of the plastic deformations in the columns. The experimentally observed shear strengths were compared with code based strength evaluation techniques. The evaluation methods show that the pier would possess inadequate shear capacity and thus be classified as shear-brittle with no ductility capability. An energy based damage analysis procedure is proposed. This improved evaluation procedure is a rational method and is capable of predicting the cumulative displacement ductility failure limit state. The seismic vulnerability of this class of shear-critical bridge pier is examined using the ATC 6-2 methodology. It is shown that if code-based evaluation procedures are followed this class of bridge pier is classified as "unsafe" and shear-brittle, but may be capable of resisting minor earthquakes through elastic response. However, if a dependable ductile mechanism is assumed, as demonstrated by good experimental behavior, a "safe" seismic response can be assumed for all Seismic Performance Categories in the United States.

ACKNOWLEDGEMENTS

vii

TABLE OF CONTENTS

TABLE OF CONTENTS (cont'd)

LIST OF ILLUSTRATIONS

Preceding page blank

LIST OF ILLUSTRATIONS (cont'd)

LIST OF ILLUSTRATIONS (cont'd)

LIST OF TABLES

SECTION 1
INTRODUCTION

1.1 Research Context

To date most existing bridges in the eastern and central United States have been designed predominantly for carrying gravity loads. Some lateral loading might have been considered in the design process to account for: centrifugal forces on curved bridges, hydrodynamic loading on piers in river crossings including the effects of a debris raft, traction forces and wind loading. However, these lateral loads with respect to the weight of the bridge are typically small. Even though bridges in the eastern and central United States are situated in low to medium seismic risk zones, the seismic design of bridge substructures has historically been ignored in these regions. This raises a leading question: How will such bridges perform in the event of an earthquake when they are subjected to large dynamic seismic loads that may arise from ground shaking?

The large number of bridge failures during recent earthquakes has emphasized the need to improve design standards for new bridges. While considerable improvement has been made in seismic design standards since the 1971 San Fernando earthquake, the dependability of existing bridges under seismic loads remains an unresolved question. Especially failures of older bridges and the accompanying loss of life in the 1989 Loma Prieta earthquake brought an increased awareness of the vulnerability of existing bridge systems. The research presented herein addresses such bridges and is part of a larger program sponsored by NCEER to investigate the seismic vulnerability of the existing highway bridge system, particularly in the eastern and central United States. It also endeavors to study the effect of conservatism built in design and construction which can result in an unknown intrinsic strength and ductility capacity, that can be mobilized to resist seismic loading. This study is a step towards formulating evaluation procedures for prediction of bridge behavior under earthquakes to achieve confidence while making decisions regarding the existing dependability, or the requirement of seismic retrofitting

or replacement.

The present state-of-the-art in Earthquake Engineering requires that in the event of an earthquake, the loss of life should be minimized; structures may suffer structural damage, but prevention of complete collapse must be ensured. The traditional way of achieving this for reinforced concrete structures is by the formation of a ductile structural mechanism with the dissipation of energy in carefully detailed ductile plastic hinge zones. The ability of the structure to behave in a desirable ductile fashion therefore depends primarily on the adequacy of the reinforcing steel detailing.

A considerable amount of model testing on bridge components under simulated seismic loading has been carried out over the past two decades, but the reliability of these results and whether they can or cannot be applied to aged existing bridge structures needs verification through comparative studies. The present study constitutes an experimental investigation on a prototype cap to column connection retrieved from such a bridge and a companion one-quarter scale model of the entire pier of a shear-critical bridge pier. The prototype bridge is a typical gravity load designed slab on steel girder bridge constructed in the late 1950's in the state of New York. An effort is also made to compare the performances of the model and the prototype.

This present report is first of a series on the seismic evaluation and retrofitting of reinforced concrete bridge piers. Similar studies have already been completed on the evaluation and seismic retrofit of reinforced concrete frame buildings, designed only for gravity loads. These studies include an Evaluation Series and a Retrofit Series. The Evaluation Series consists of:

Part I: *Design and Properties of a One-Third Scale Model Structure* by Bracci, Reinhorn and Mander (1992a).

Part II: *Experimental Performance of Subassemblages* by Aycardi, Mander and Reinhorn (1992).

Part III: *Experimental Performance and Analytical Study of Structural Model* by Bracci, Reinhorn and Mander (1992b).

The Retrofit Series consists of:

1-2

Comprehensive in Scope

The comprehensive report covers topics from earthquake-resistant design to the development of repair technology for earthquake-damaged structures It contains photographs, charts, and technical illustrations along with step by-step procedures, with special sections detailing case examples of U S and Japanese repairs Emphasis is given to the importance of information collection and dissemination of information to the public

Topics include

Step-By-Step Procedures

☐ Emergency investigations & actions

☐ Damage inspection

☐ Damage analysis

☐ Temporary & permanent repair methods

River, Coastal & Erosion Control

☐ Bank   ☐ Sluice

☐ Bulkhead   ☐ Gate

☐ Sluiceway   ☐ Weir

Sewage Pipe

☐ Main pipe   ☐ Inverted siphon

☐ Branch pipe   ☐ Inlet

☐ Manhole

Road Facilities

☐ Bridges*   ☐ Common sewage

☐ Banking   ☐ Culvert

☐ Slope   ☐ Foot path bridge

☐ Soil cutting of   ☐ Signposts
   face of slope   ☐ Information boards

☐ Tunnels

*Following is an example of the type of detailed information found in a typical section of the repair manual

---

Highway Bridge Repair

Investigation of damage
Evaluation of damage
Temporary repair method
Permanent repair method

☐ General   ☐ Upper construction

☐ Foundation   ☐ Supporting section

☐ RC bridge pier   ☐ Expansion joint

☐ Steel bridge pier ☐ Others

☐ Abutment

Applications In A Variety Of Fields

The manual is well-suited for applications in a variety of fields including:

☐ Construction Companies, Offices & Contractors

☐ Regional Construction Bureaus

☐ Ministries of Construction

☐ Civil & Consulting Engineers

☐ Public Works Officials/Staffs

☐ Transportation Officials/Engineers

Ordering Information

Cost of the repair manual is $65 plus postage and handling Checks and purchase orders are accepted For more information, or to place your order call 716 636 3391 or complete the attached form and mail to

Repair Manual
National Center for
Earthquake Engineering Research
State University of New York at Buffalo
118 Red Jacket Quadrangle
Buffalo, NY 14261

Order Form

Manual for Repair Methods of Civil Engineering Structures Damaged by Earthquakes

_____ copies, @ $65 per copy $ _____

U S Postage $4 00 per copy   _____

Foreign Postage $8 00 per copy _____

Total $ _____

_____ _____ Check enclosed
_____ _____ Purchase order enclosed

Send my order to

Name _____

Position _____

Company _____

Address _____

City/State _____ Zip Code ____

Country _____

Telephone _____

Signature _____ Date ____

Make checks payable to
   Research Foundation

Mail to
National Center for
Earthquake Engineering Research
State University of New York at Buffalo
118 Red Jacket Quadrangle
Buffalo, NY 14261

Part I: *Experimental Performance of Retrofitted Subassemblages* by Choudhuri, Mander and Reinhorn (1992).

Part II: *Experimental Performance and Analytical Study of Retrofitted Structural Model* by Bracci, Reinhorn and Mander (1992c).

1.2 Scope of Present Study

The present study consists of two parts: experimental and analytical. The experimental part of the study is divided into the study of the model pier and the prototype. Section 2 provides a description of the bridge and design, construction, instrumentation and testing of the model pier, while experimental results of the model study are presented in Section 3. Section 4 describes the test setup, instrumentation and testing procedure for the prototype. Observations and results of the prototype testing are discussed in Section 5.

The analytical part presented in Section 6 constitutes of the evaluation of the flexure and shear strengths for both the prototype beam-column joint and the quarter scale model by code based formulations and their comparison with the experimental results. A comparison is also made of the hysteretic performances and energy absorption patterns of the model and the prototype. Finally the damage potential of the prototype bridge under earthquake loading in various seismic zones is studied employing the AASHTO/ATC guidelines. The conclusions drawn from this study are presented in Section 7.

SECTION 2

MODEL DESIGN, CONSTRUCTION, AND INSTRUMENTATION

2.1 Introduction

In this section a description is given of the prototype bridge, the prototype beam-column joint specimen, and design, construction and instrumentation of the quarter scale bridge pier model.

2.2 The Prototype

The bridge selected for the present study was the East Jewett-Holmwood road bridge crossing the eastern branch of Cazenovia Creek. The bridge, owned by Erie County, is located near the town of East Aurora, New York. The plan, elevation and section of the bridge are shown in Fig. 2.1. The bridge consisted of a 32' wide roadway with 3.5' wide sidewalks on both sides. The three spans were 40', 88' and 60' in length. The wearing surface was 2" thick asphalt supported by a composite superstructure consisting of 8" thick concrete deck slab over five WF steel girders equally spaced at 8'-3" centers. The steel girders for the central span were seated on high bolster bearings while the end spans were seated on low steel pintle rocker/sliding bearings. Both piers consisted of two column bents with tapering square columns supported on a deep beam over a spread footing foundation.

The Jewett-Holmwood bridge was originally constructed in 1957. Due to considerable deterioration of concrete in the deck and piers the bridge was dismantled for reconstruction in 1990. At that time, a beam-column joint of the pier was retrieved from the site and brought into the SUNY at Buffalo Civil Engineering laboratory for testing. In Fig. 2.2a, the elevation of the western pier is shown, where the shaded portion represents the portion which was retrieved from the field for laboratory testing. The test setup was designed in accordance with the forces which would be experienced

2-1

by the prototype as shown in Fig. 2.2b. Details about the testing arrangements are presented in Section 4.

The columns were reinforced with 16 #7 bars enclosed by #3 hoops at 12" centers. Figs. 2.3 and 2.4 show the reinforcement details of the pier. Test cylinders (3" diameter x 6" long) of concrete were core drilled and taken out of the specimen. Compression test results revealed cylinder strengths of 7400 psi and 9000 psi for column and capping beam respectively. It may be of interest to note that the specified strength found in the construction drawings was $f_c' = 3,500$ psi.

2.3 Scale Model Design

In the area of structural research, scale model experimentation is a powerful tool in developing an understanding of structural behavior in many complex dynamic loading situations, especially where sophisticated non-linear analytical techniques are not fully developed. Experimental methods are also able to take into account many of the secondary effects and indeterminate factors which are commonly neglected in analytical modeling procedures in order to obtain a tractable solution.

For the purpose of the model pier experiment, modeling laws based on constant stress and strain similitude in the model and prototype were used; thus:

stress and strain ratios $\qquad \dfrac{f_p}{f_m} = \dfrac{\epsilon_p}{\epsilon_m} = 1$

geometric modeling scale $\qquad \dfrac{L_p}{L_m} = \lambda = 4$

area ratio $\qquad \dfrac{A_p}{A_m} = \lambda^2 = 16$

force ratio $\qquad \dfrac{F_p}{F_m} = \lambda^2 = 16$

bar force ratio $\qquad \dfrac{(A_b f_y)_p}{(A_b f_y)_m} = \lambda^2 = 16$

moment ratio $\qquad \dfrac{M_p}{M_m} = \lambda^3 = 64$

2-2

In the above ratios, the subscripts m and p stand for the model and the prototype, respectively. These relationships were required to simulate the behavior of the prototype during the experiment.

To simplify the construction of the model, some deviations in geometry from the true similitude were made as can be seen in Fig. 2.2(a) and Fig. 2.5. To hold down the pier model to the strong floor and thus simulate a fixed base, the length of the base was adjusted to conform to the configuration of holes in the laboratory strong floor.

Based on the geometric limitations of the holding down locations of the laboratory strong floor, as well as the limitations of the reaction frame and actuators, it was established that a ¼ scale model should be used. This would enable as large as possible model to be constructed, and still capture all the construction details. It was also as small as the model could be constructed using deformed model reinforcement. Figs. 2.5 and 2.6 show the working drawings for the model. Front and side elevations and plan view are shown in Fig. 2.5, while Fig. 2.6 shows the steel reinforcement details.

2.4 Materials for the Model
2.4.1 Model Concrete

Model pier was built in the following four states:

Stage 1:	Construction of the Base
Stage 2:	Construction of the Foundation Beam
Stage 3:	Construction of the Columns
Stage 4:	Construction of the Cap Beam

Concrete for stages 1 and 3 was mixed in the laboratory while the larger quantities for stages 2 and 4 were provided by a local ready-mix supplier.

The proportions by weight for the Stage 1 mix were:

Water : *Cement* : *Aggregate (Sand + Coarse)* = 0.49 : 1 : 3.8 (1.7 + 2.1)

and for Stage 2 mix:

Water : *Cement* : *Aggregate(Sand* + *Coarse)* = 0.43 : 1 : 3.4(1.5 + 1.9)

Aggregate for these two stages was ¾″ crushed stone and sand was a blend of coarse and fine in 4:1 ratio. Type III (rapid hardening) cement was used in all mixes.

For each pour, 16 4″x8″ cylinders were cast to determine the compressive strength, except for Stage 1 in which 3″ diameter cylinders were cast. Results of these tests are presented in Table 2.1.

TABLE 2.1: Concrete Compressive Strength for various Pours of the Model Pier

Concreting Stage	Slump (inches)	7 Days Strength (psi)	28 Days Strength (psi)	Age at Time of Testing (days)	Strength at Testing (psi)
Stage 1: Base	3	2960	3020	180	--
Stage 2: Foundation Beam	4	2390	2940	162	3080
Stage 3: Columns	2.5	4500	5050	149	5350
Stage 4: Cap Beam	3	3050	3080	100	4100

2.4.2 Model Steel

The exact required model bar diameters are generally impossible to find in the marketplace. Therefore, an attempt was made to obtain model bars with diameters as close as possible to the required size, but more importantly, to model the yield force similitude of the prototype versus model bars. The prototype steel yield stress was assumed to be 60 ksi and modeling was done based on this value, but later steel samples

were extracted from the prototype pier after testing, from the regions which were least affected during the test. Monotonic testing of these samples in tension showed yield strengths of 38 ksi and 40 ksi for hoops and longitudinal bars respectively. The results of the test parameters are presented in Table 2.2. Table 2.3 shows the bar sizes in the prototype and the model. Results of the coupon tests for the prototype and the model reinforcement are presented in Fig. 2.7.

TABLE 2.2: Prototype Pier Reinforcing Steel, Stress - Strain Properties

	f_y (ksi)	E_y (ksi)	E_{sh} (ksi)	ϵ_{sh}	f_{su} (ksi)	ϵ_{su}
Longitudinal bars #7	40.0	29000	1250	0.007	75	0.116
Transverse hoops #3	38.0	29000	750	0.010	60	0.106

TABLE 2.3: Prototype & Model Reinforcement

Prototype			Model				Modeling Ratios	
Bar Desig-nation	Bar Diameter (inches)	Area (in.^{2})	Bar Desig-nation	Bar Dia-meter (inches)	Area (in.^{2})	Measured Yield Stress (ksi)	$\dfrac{(A_s)_p}{(A_s)_m}$	$\dfrac{(A_s f_y)_p}{(A_s f_y)_m}$
#3	0.375	0.110	Gauge 12 wire	0.104	0.008	54	14	22
#4	0.500	0.196	D1	0.113	0.010	140	9	22
#5	0.625	0.307	D2	0.160	0.020	85	15	12
#6	0.75	0.442	D4	0.225	0.040	85	11	8
#7	0.875	0.601	D4 D4(a)	0.225 0.225	0.040 0.040	85 65	15	12 14
#8	1.000	0.785	D5	0.252	0.050	83	22	12

*Assumed prototype steel yield stress is 60 ksi.
**D4(a) means annealed bars.

2-5

2.5 Stages of Model Construction

The model pier was built in the following four stages described in the following:

Stage 1: Pier Base

The base for the model was $8' \times 2' \times 7.5''$ in size and was built by making a hollow box consisting of two 8' and two 2' long and 7.5" high wood pieces nailed at the ends. This box was then nailed to a $4' \times 8'$ plywood sheet which served as the flooring. Along the length, the long sides of the form were braced at third points.

Provision for lifting and moving the 3.5 ton model and anchoring the specimen to the strong floor was embedded in the base and is shown diagrammatically in Fig. 2.8. At each end this lifting mechanism was made on a $2' \times 2' \times 0.5''$ steel plate consisting of 24" long, 1.5" diameter steel pipe welded across the plate such that the pipe was located 15" away from the end of the base. The mechanism to hold down the pier consisted of welding four nuts over 1.25" diameter holes drilled in the plate. Then 1" pieces of 1" diameter pipe were welded on top of these nuts which were later plugged with wood plugs and sealed with silicon caulk to prevent the ingress of cement. These nuts were designed to accommodate the 1" dia holding down bolts which were passed up from beneath the laboratory strong-floor.

As these plates had to be subjected to all the uplift and most of the shear during testing, two #6 bars were added to improve the base strength capacity. Then the bottom 12 gauge 2" square steel mesh was placed with a 0.5" cover above the flooring. The top mesh was then put in place with 0.5" top cover. The next step was to put all the reinforcement abutting from the base and to tie it to the bottom and top steel meshes. Finally laboratory mixed concrete was poured and a key was left in the middle to form the construction joint for foundation beam concrete.

Stage 2: Foundation Beam

The construction of the foundation beam consisted of firstly tying the six horizontal rebars, secondly placing the formwork, thirdly fixing the column steel starter bars, and finally pouring the ready-mixed concrete.

Stage 3: Columns

Steel tying was limited to only tying the hoops at 3.5" intervals. Formwork for the tapering columns was constructed from trapezoidal pieces of plywood and 2×4 timber. The forms were fixed and braced to the foundation beam. The small volume of concrete required for this pour was mixed in the laboratory in a single batch.

Stage 4: Cap Beam

The major work in this stage was the preparation of the steel reinforcement cage. An arrangement for anchoring the top loading girder was also provided. This consisted of a bearing plate with a U-shape shear connector welded to the $6''\times16''\times\frac{3}{4}''$ plate as shown in Fig. 2.9.

One such bearing plate with a single U-shape stud was placed near each end of the cap beam and a third bearing plate with two U-shape shear studs was placed at the center of the cap. Finally the ready mix concrete was poured and vibrated.

2.6 Test Rig

Fig. 2.10 shows the setup in which the specimen was tested. The specimen was anchored to the 18 inch thick laboratory strong floor. Lateral load was applied to the specimen by a 250 kips capacity servo-controlled actuator. The vertical load, representing the dead load of the bridge spans was applied by a 22 kips actuator via a transverse loading beam seated on the specimen's longitudinal steel girder (W14 x 257).

The test setup was carried out by firstly lifting the specimen over the strong floor anchorages. Secondly, the lateral load transferring beam (12' W14 x 257) was connected to the three steel plates embedded in the cap beam for this purpose with two 3/4" diameter A325 Grade 8 bolts in each plate. This arrangement is shown in Fig. 2.11. The bolts were torqued to 250 kips-inch to prevent slip between the beam and the plates. This beam was then connected to the actuator assembly, correctly aligned, and the holding down anchorages fastened.

In order to prevent sliding of the base on the strong floor, the specimen was tension-anchored to the reaction frame with two high strength (Grade 160) 1" diameter

threadbars. These bars were only effective during the actuator's push cycle when the ties were in tension. When the actuator was in the pull cycle, base sliding was prevented by the holding-down bolts acting in shear as well as friction between the model base and the strong floor.

Axial load was applied with the 22 kips hydraulic actuator through the arrangement shown in Fig. 2.10. Transfer of axial load to the specimen was through the W10 x 77 cross-beam. This system amplified the actuator force by a factor of 3.2, potentially delivering up to 70.4 kips of vertical load into the specimen. The bearing seating of the W10 x 77 cross-beam on to the W14 x 257 lateral loading beam is shown in Fig. 2.12.

2.7 Instrumentation

Displacements, column rotations, and forces were monitored as follows:

Displacements

Fig. 2.13(b) shows the arrangement of the sonic transducers used to measure lateral movement of the pier and the north column. This experiment was controlled by relative drift movement of the north column. Herein, drift was defined by the difference of movement between sonic transducers # 8 and 7. Thus

$$D = \frac{\Delta_8 - \Delta_7}{L_c} \tag{2-1}$$

where L_c = clear length of the column, Δ = displacement of the indicated sonic transducer, and D = drift index.

Even though the base was securely fixed to the strong floor as described above, any slight movements could be monitored by sonic transducer # 10. The displacement of the north column was measured at the six points coinciding with the linear potentiometers' locations. This was done in an endeavor to enable analysis of shear and flexural displacements. All sonic transducers were fixed on to a rigid reference frame secured to the strong floor.

2-8

Curvatures

Fig. 2.13(a) shows the arrangement of seven pairs of linear potentiometers, located at opposite column faces, which were used to enable the measurement of the northern column curvatures over sequential gauge lengths of that column. The gauge length for the potentiometer pairs were adjusted to ensure that some movement would be detected in each section. Two potentiometers were mounted on one aluminum seat; one covering an upper gauge length, the other the adjacent lower one. The seat was glued to a 1/4" wide aluminum strip which was epoxied to the column at appropriate gauge length mark. Similarly, striking plates made of aluminum angle were mounted at each alternate gauge length mark. This arrangement was such that at one end of the gauge length there was a potentiometer mounted on an aluminum seat and on the other end there was the striking plate to provide a contact surface for the brass rod coupled to the potentiometer. It should be noted that the surface mounting arrangement for the potentiometers only provided reliable strain readings until the onset of concrete spalling. Even though this approach has its shortcomings, it was felt to be more expedient than casting mounting rods transversely through the column section.

Loads

Lateral and vertical forces were monitored through load cells connected in series to their respec·ive actuators.

2.8 Data Acquisition

During the active period of the test the output voltages of all the instruments were recorded using a Optim Megadac 5533A Data Acquisition System. From these records force-displacement (drift) and moment-curvature relations were established.

During the test, the lateral load measured by the load cell on the horizontal actuator and the displacement of the sonic transducer on the load transferring beam (W14 x 257) was plotted on a Type 70790A analogue Hewlett-Packard X-Y Plotter. This backup system also provided an immediate insight to the behavior of the model during testing.

Prior to testing, the position of reinforcement in the column was drawn on all the four faces of both columns to detect the nature and position of crack and failure. Before the actual test, all the instruments were set at their balance points and it was also ensured that these are in working order after giving them a small manual movements.

2.9 Photographic Record

Figs. 2.14 to 2.16 present a photographic record of the model experiment. Fig. 2.14 shows the reinforcing steel cages at various stages of construction prior to pouring the concrete. Fig. 2.15 shows the finished one-quarter scale model prior to attaching the instrumentation. Fig. 2.16 shows a number of different views of the test setup including the instrumentation, prior to commencing the testing.

BRIDGE PLAN

BRIDGE ELEVATION

SECTION A-A

PIER PLAN
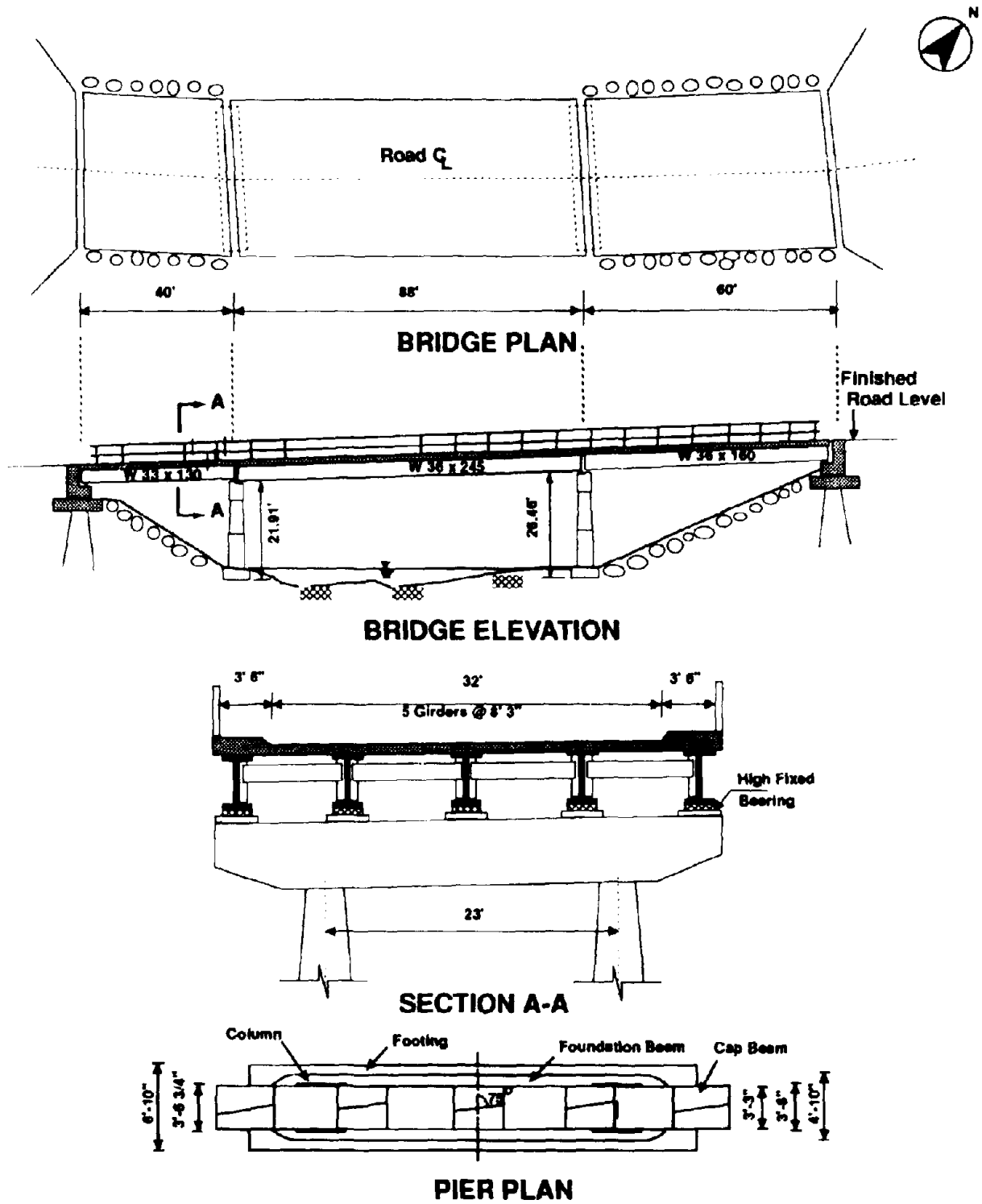
Fig. 2.1 Jewett-Holmwood Road Bridge over East Branch of Cazenovia Creek

39'-4"

Portion Retrieved
from the field

6'-7$\frac{7}{16}$"

23'- 0"

7'-9$\frac{11}{16}$"

33'-5$\frac{3}{8}$"

12 0 12   36"
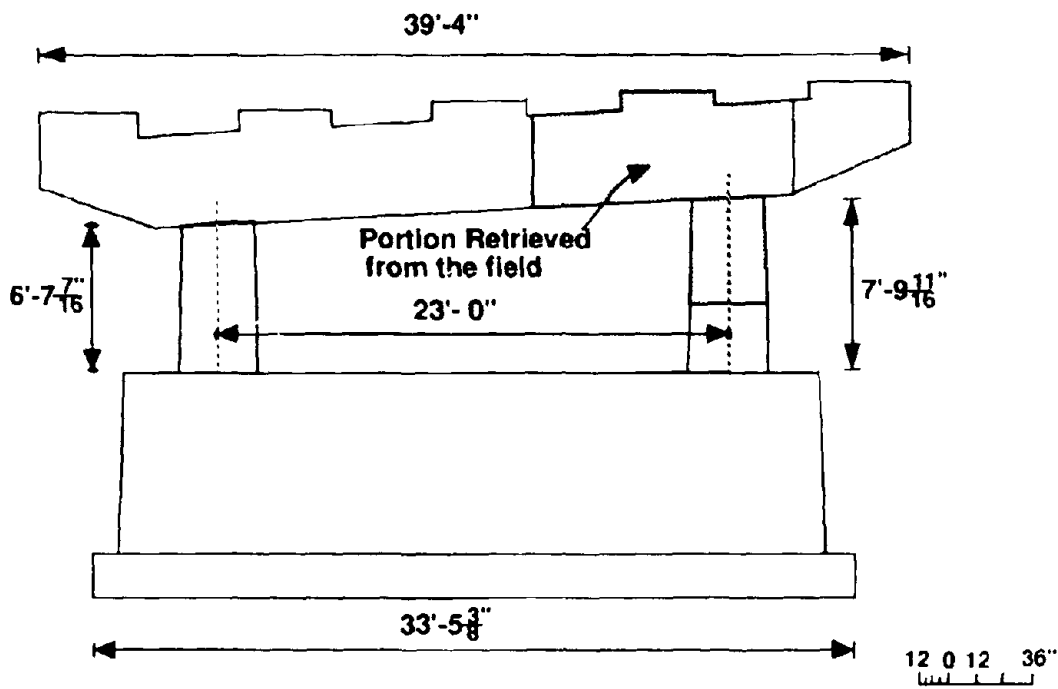
Fig. 2.2a. Elevation Showing Location of the Prototype Specimen

Dead Load

F

Specimen

Gravity Reaction

(i) Gravity plus Lateral Loading on Bridge Pier

R

Inflection
Points

(Lateral Load)

R

Specimen Reaction

(ii) Bending Moment Diagram under
Gravity plus Lateral Loading

(iii) Specimen, Loads and Reactions
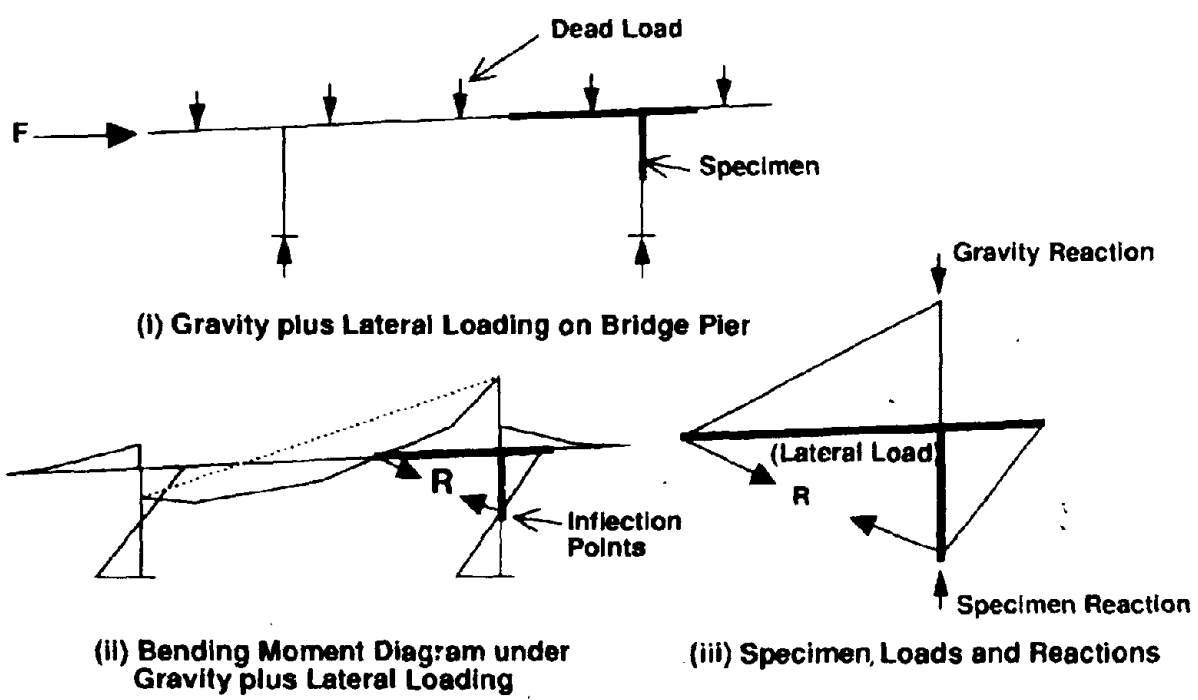
Fig. 2.2b. Rationale for the Prototype testing configuration

2-12
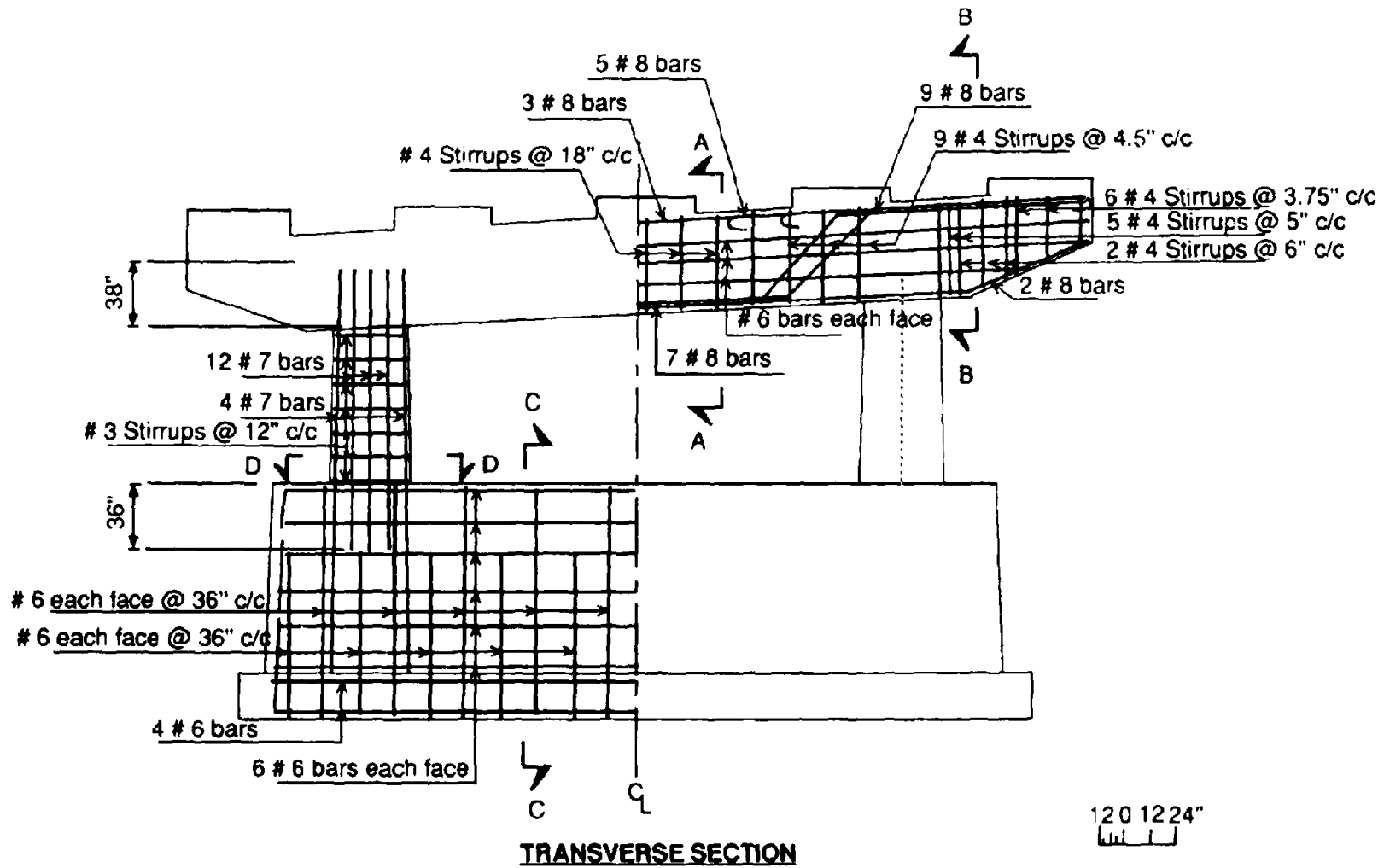
Fig. 2.3 Reinforcement Details (Prototype)

SECTION A-A

3'-3"

4'-6"

9-# 8 bars
9-# 8 bars
2-# 6 bars
2-# 6 bars
4 stirrups @ 18"
2-# 6 bars
9-# 8 bars

SECTION B-B

3'-3"

4'-6"

3-# 8 bars
2-# 6 bars
2-# 6 bars
4 stirrups @ 6"
2-# 6 bars
9-# 8 bars
9-# 8 bars

SECTION D-D

16-# 7 bars
3 Stirrups @ 12" c/c

SECTION C-C

Batter 1/2" per foot

8'-0"

2'-0"

6'-8"

6 bars @36" c/c
6-# 5 bars
6 bars @ 18" c/c
2-# 6 bars

12   0   12"
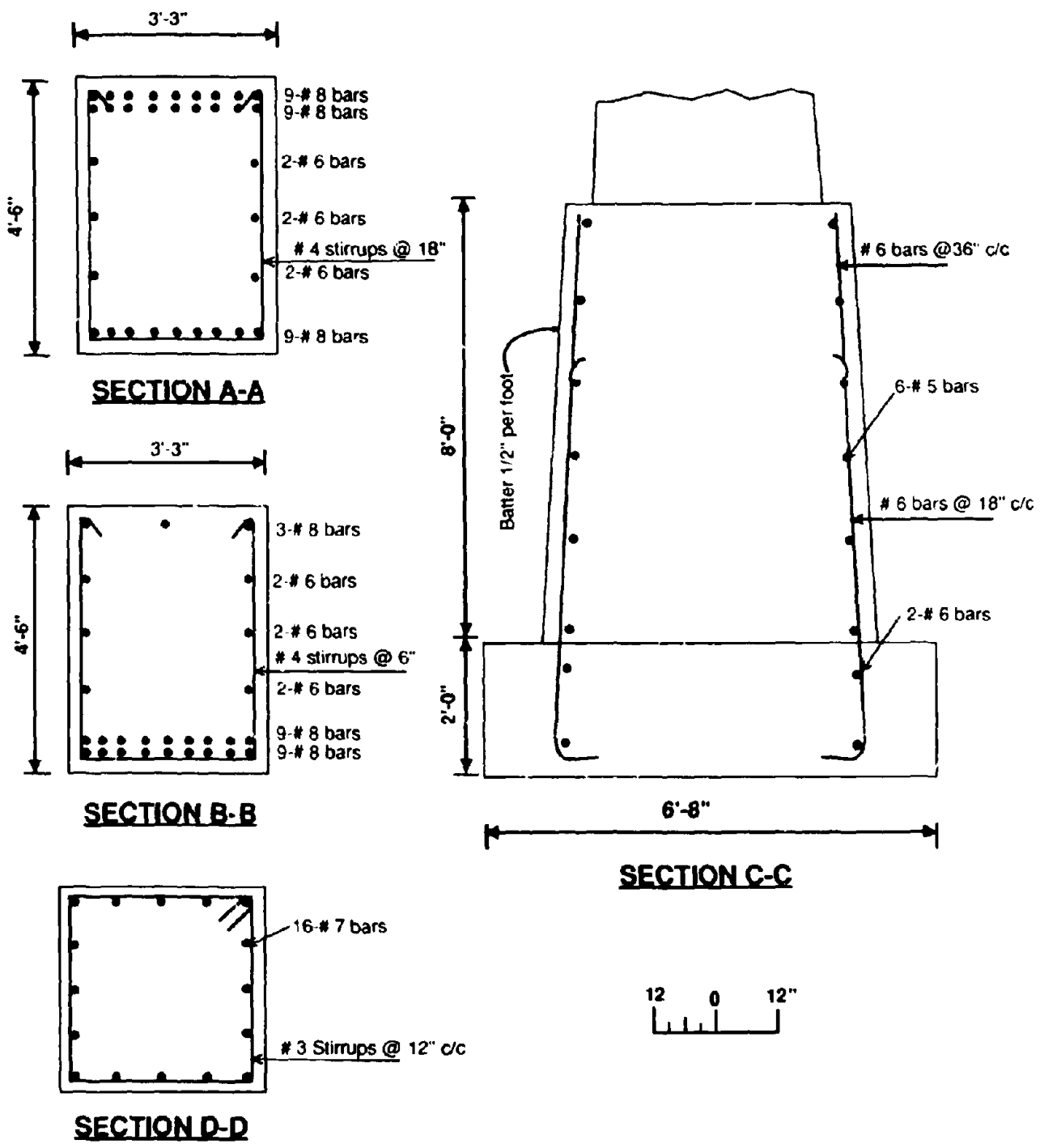
Fig. 2.4 Reinforcing Details of Beams and Columns (Prototype)

2-14
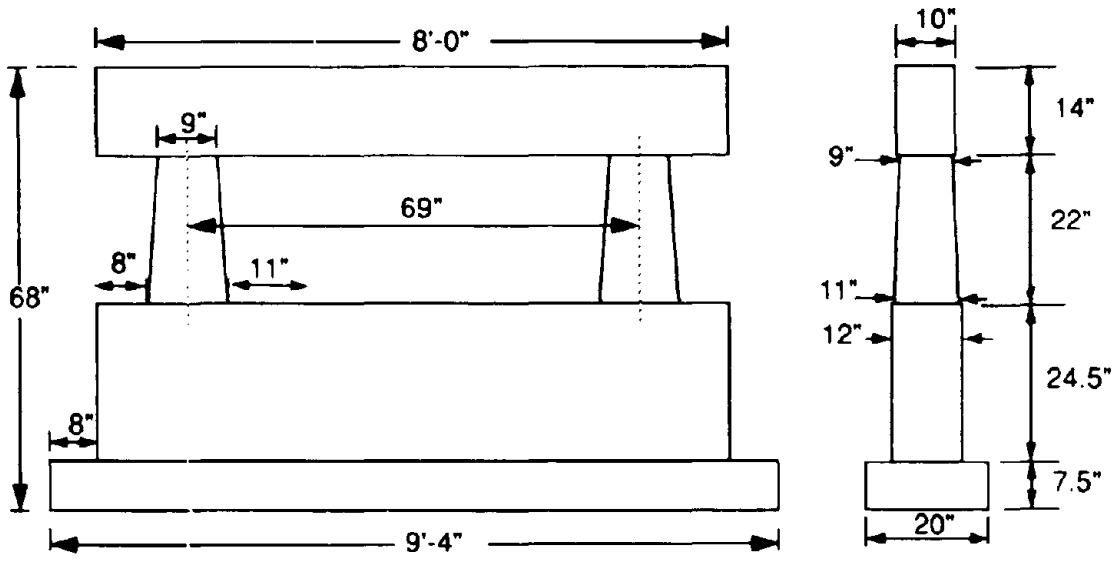
FRONT ELEVATION   **SIDE ELEVATION**
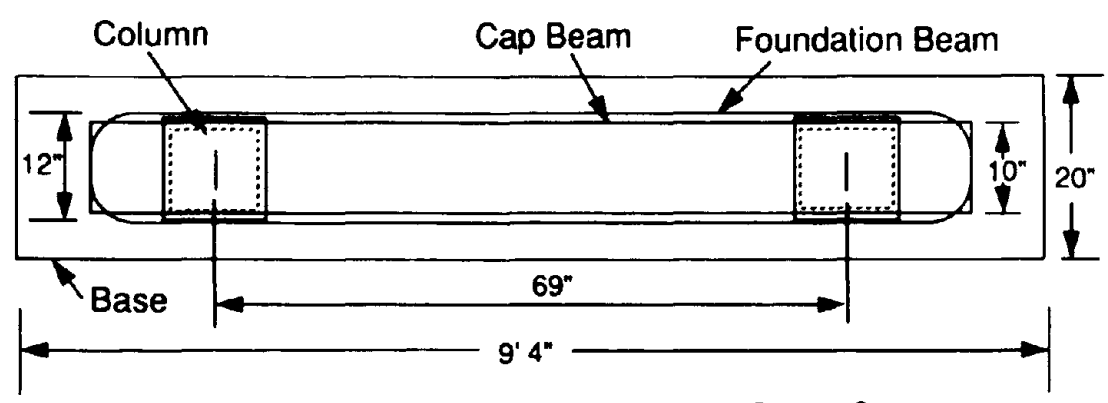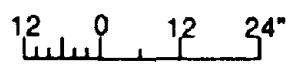
PLAN VIEW

Fig. 2.5 Quarter Scale Bridge Pier Model
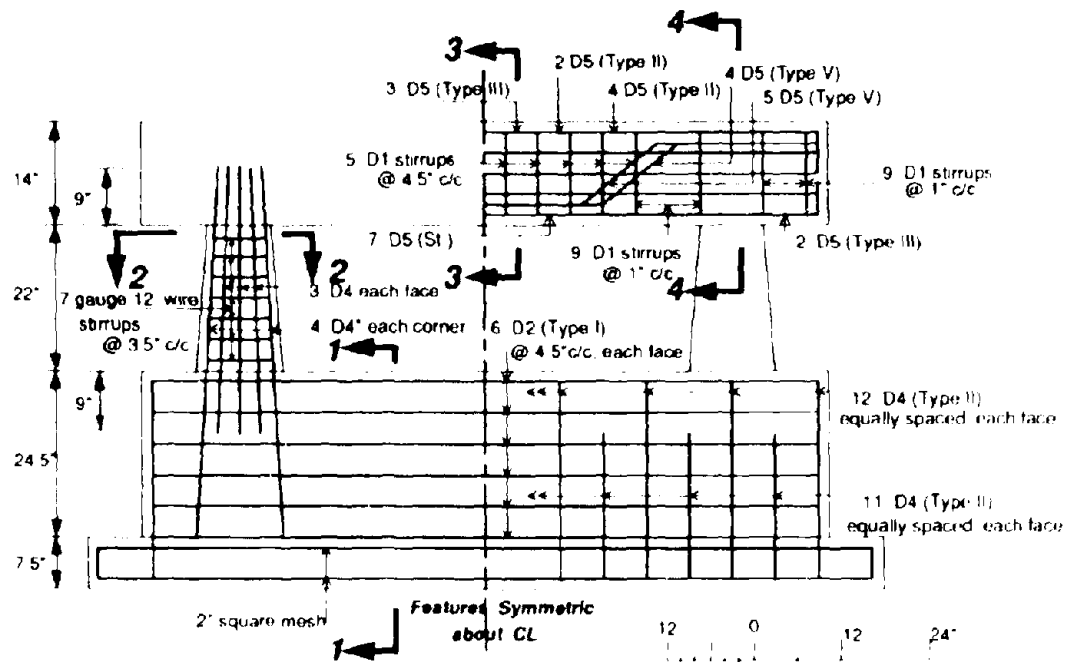
ELEVATION
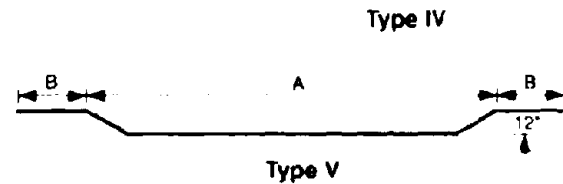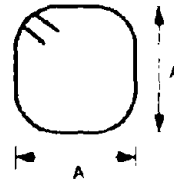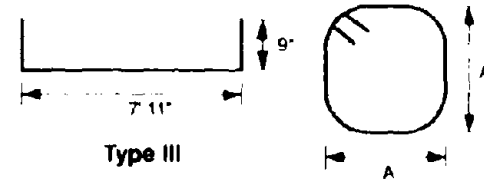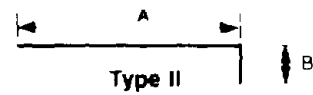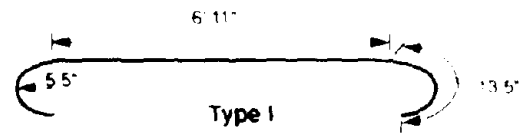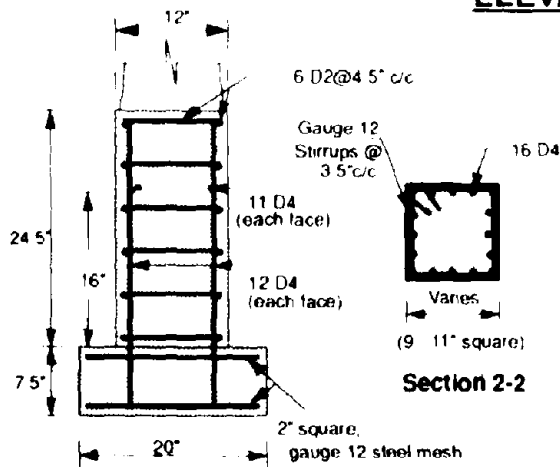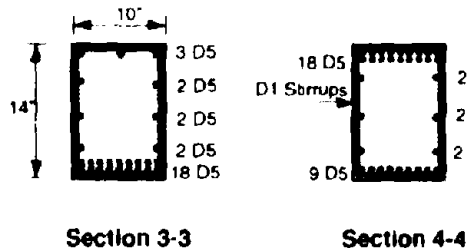
SECTIONS

BAR SHAPES

Fig. 2.6 Reinforcement Details for Pier Model

2-16
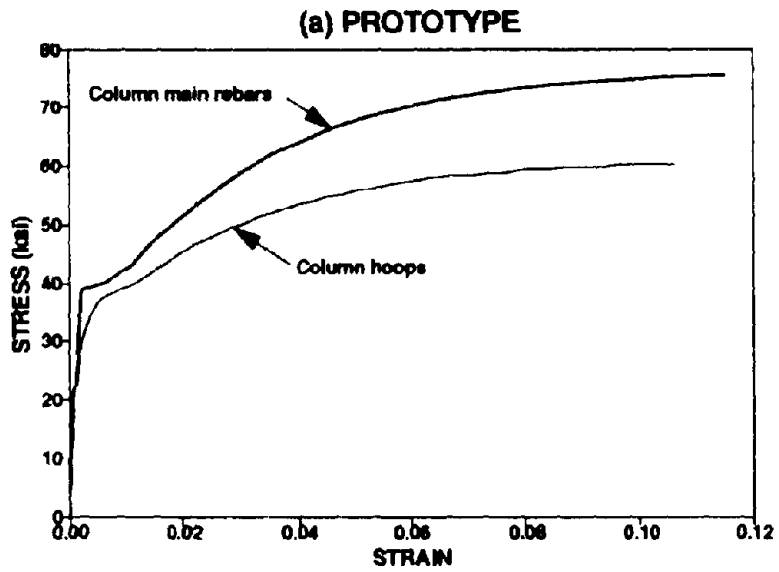
Fig. 2.7 Measured Stress vs Strain Behavior of the Reinforcement for (a) Prototype, and (b) Model

2-17
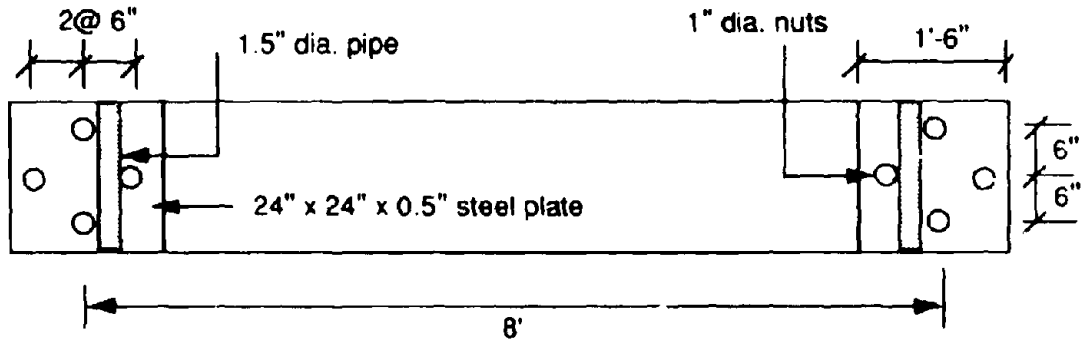
Fig 2.8 Plan view of Lifting and Holding Arrangement
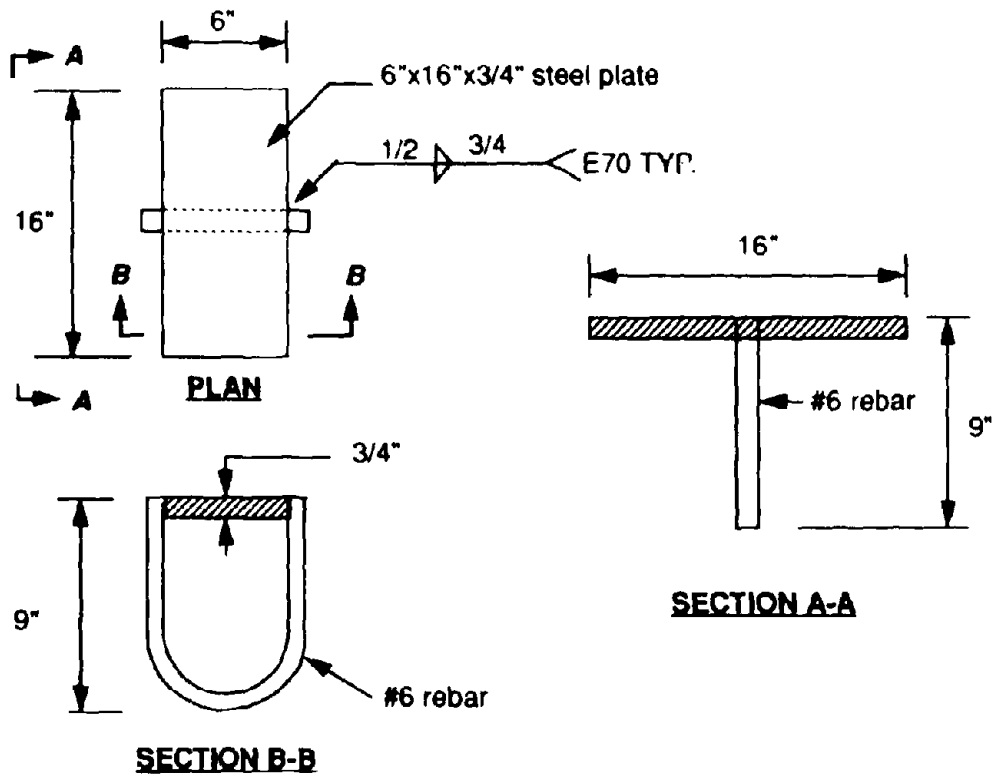
Fig 2.9 Details of Shear Stud
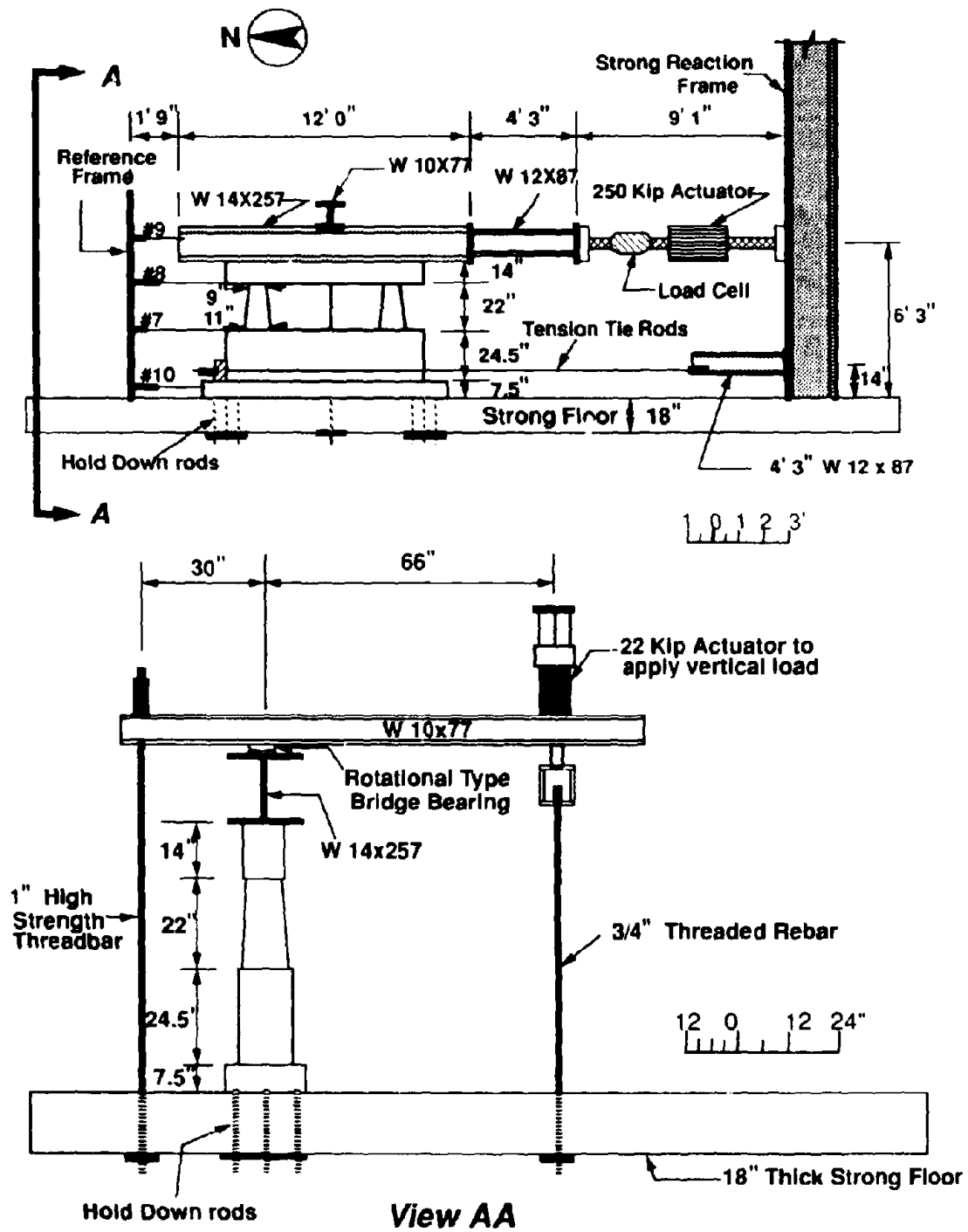
Fig. 2.10 Test Rig for Model Pier Test
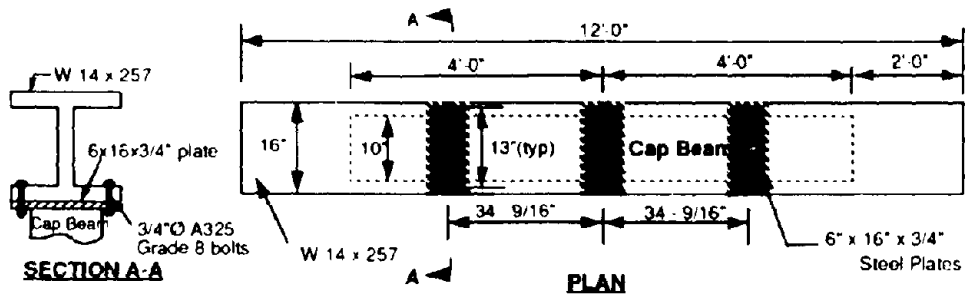
Fig 2.11 Lateral Load Transfer Arrangement
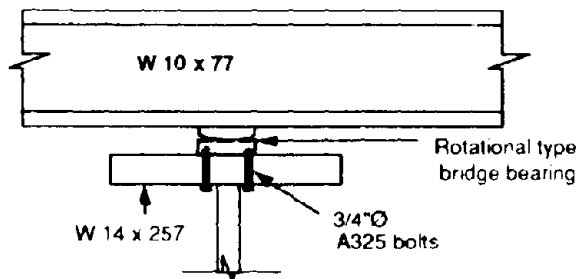
Fig. 2.12 Axial Load Transfer Arrangement
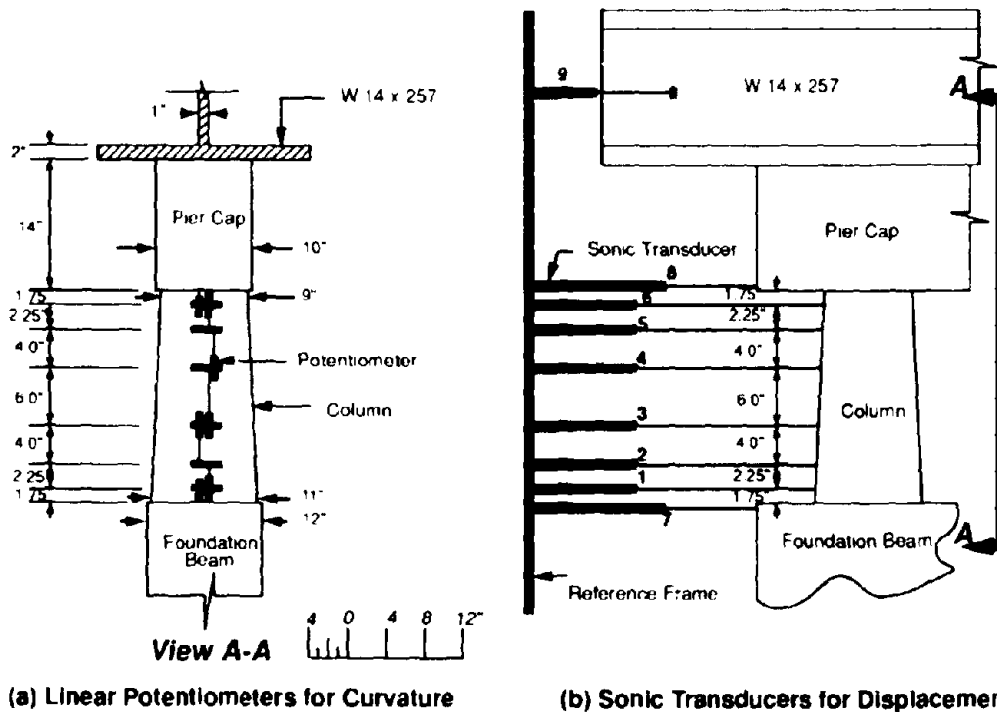
(a) Linear Potentiometers for Curvature (b) Sonic Transducers for Displacement

Fig. 2.13 Instrumentation for Curvature and Displacement Measurement

2-20
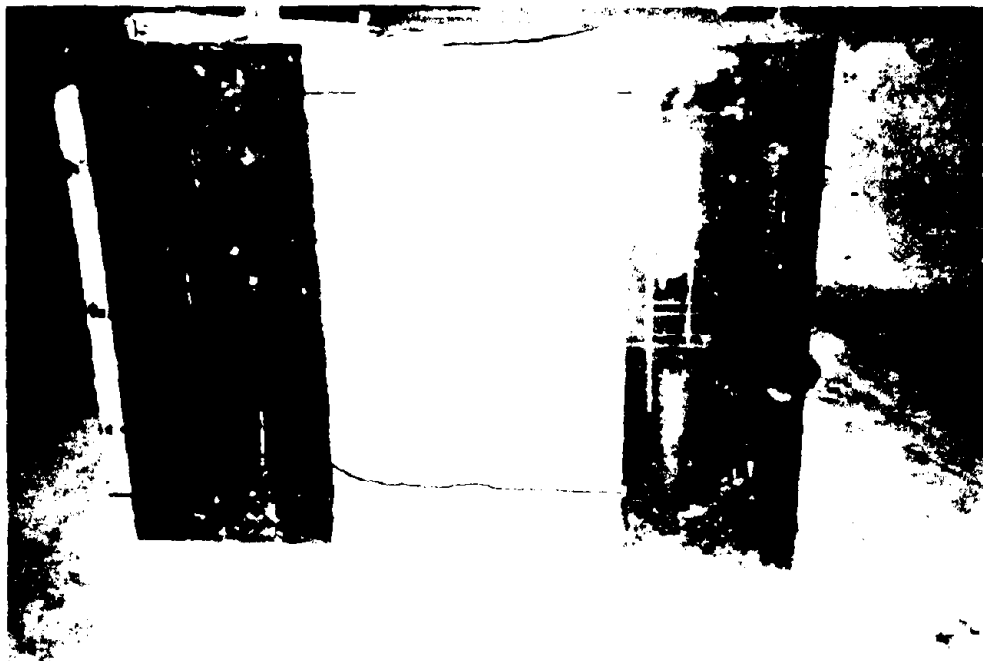
Fig. 2.13 Preparation of Beams 3 and 4
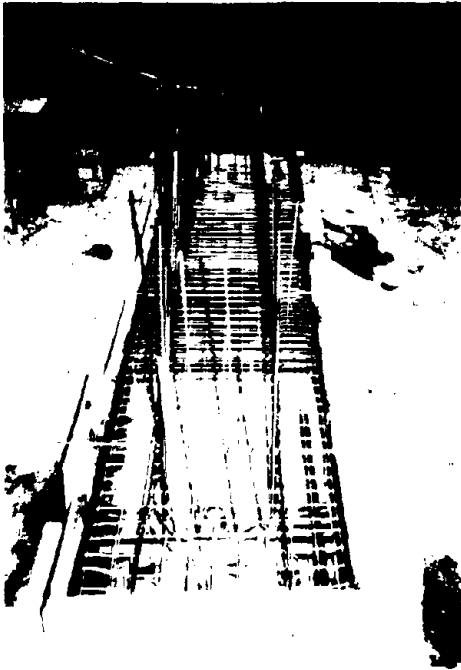
Fig. 2.14 Construction Stages of the Pier Model
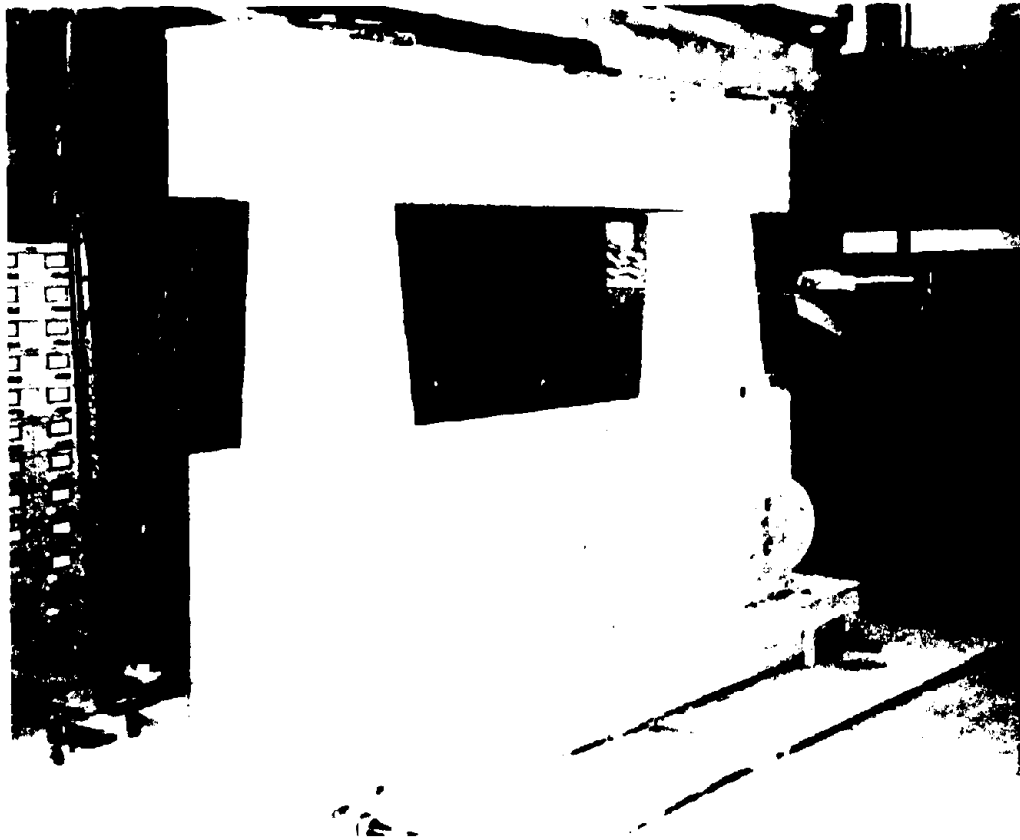
Fig. 2.15 Quarter Scale Bridge Pier Model
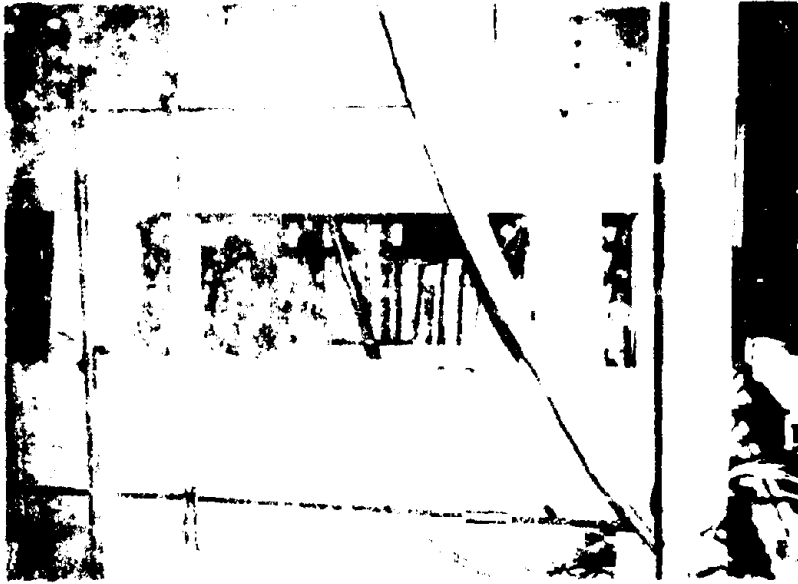
Figure Photographs of Testing Set up

SECTION 3
EXPERIMENTAL RESULTS AND OBSERVATIONS
FOR THE MODEL

3.1 Introduction

In this section an account is presented of the testing procedure, observations made during testing and results obtained after data reduction.

3.2 Testing Procedure

The model was tested in two stages using different frequencies of loading. These first and second stages will be referred hereinafter as Quasi Static and Quasi Dynamic loading respectively. The Quasi Static stage consisted of two cycles of loading at each drift level of $\pm 0.25\%$, $\pm 0.5\%$, $\pm 0.75\%$, $\pm 1.0\%$, $\pm 1.5\%$, and $\pm 2.0\%$. The horizontal load was applied as a sine wave with a frequency of 0.01 Hz. The Quasi Dynamic stage consisted of 5 and 20 cycles at 0.1 Hz. of loads at $\pm 3.0\%$ and $\pm 4.0\%$ drift amplitudes, respectively. A constant axial load of 9 kips was kept in the vertical actuator throughout the experiment. This axial load transferred to the model as 29 kips. By adding the 7 kips weight of the load transferring equipment, a total of 36 kips of vertical force was applied to the specimen. This axial load represents the scaled dead load on the prototype pier.

During testing, all instruments were continuously monitored and records logged using the Megadac Data Acquisition system with data sampling rates of 1 and 10 Hz. for the Quasi Static and Quasi Dynamic tests respectively.

3.3 Visual Observations

All components of the model were closely observed for cracks during the testing procedure but special attention was focused on the columns as failure was anticipated to initiate from here. Cracks were marked and photographs taken for future reference.

Herein an account of the performance of the model pier during each drift amplitude is given.

No cracks were visible in any part during the ±0.25% drift cycles, the behavior essentially being elastic. During the ±0.5% drift cycle, the first noticeable crack appeared at the foundation beam-column interface of the south column as shown in Fig. 3.1a & b. This is attributed to tensile cracking. This crack propagated across the entire height of the foundation beam and was visible on both sides. This crack appeared only on the north side of this column. Such tensile cracking was not evident at the cap beam-column interface. The reason may be the presence of rather congested reinforcement in this part as compared to the base and relatively weak concrete of the foundation beam. In the next drift level at ±0.75%, some new cracks opened around the column base and the previous cracks showed growth in width. So far no visible cracks occurred in the column. The situation remained the same for the ±1.0% drift level with no cracks appearing in the column or the cap beam. At the ±1.5% drift level, the commencement of cracking away from the column ends was observed. These were in the form of diagonal shear cracks initiating from near the column ends. More cracks formed at the column top than the bottom. Some typical shear cracking was also visible in the cap beam in the column support regions. During the ±2% drift level of the Quasi Static loading stage, more cracks in the end regions of the column formed, but all these cracks were very small in width and there was no apparent spalling of concrete at all (Fig. 3.1c). This indicated good serviceability of the model under Quasi Static loading.

The columns showed some plastification during the first cycle at ±3% drift level of the Quasi Dynamic loading stage. Concrete cover to the reinforcing bars on the inner column faces was partially lost in the hinge regions. Therefore, after the end of this loading sequence, all the instruments were taken away from the instrumented north column except the control sonic transducers (Fig. 3.1d).

The final phase of the test(±4% drift level) severely damaged the specimen as depicted in Fig. 3.2. Firstly the concrete in the hinge zones was badly cracked and later crushed and thrown out from there, thus leaving no protection for the reinforcing bars which eventually fractured due to low cycle fatigue at mid hinge length (in the top hinge)

and nearly at the base (fatigue cracks were evident) in the bottom hinge. It was also observed that the bottom hinge length was inadequate (Fig. 3.3a). Even at the end of the test, the columns were able to take the full applied axial load. Apart from hair-line cracks in the column support regions, the cap beam suffered no damage (Fig. 3.3b).

3.4 Experimental Results

i) Hysteretic Performance

The lateral load versus column drift performance of the pier for Quasi Static as well as Quasi Dynamic loading stages are presented in Fig. 3.4. It is evident from this figure that the columns and thus the pier behaved in a ductile fashion as the hysteresis loops show good energy dissipation characteristics. The pier behaved elastically during the $\pm 0.25\%$ drift cycles. As the drift levels increased, the pier started entering the plastic range. It is interesting to note that during the Quasi Static loading stage, there was no apparent degradation in strength as the drift amplitude increased, even though some decrease in strength in the second cycle of a given drift amplitude can be noted. During the Quasi Dynamic loading stage, a progressive decrease in strength can be observed at the $\pm 3\%$ and $\pm 4\%$ drift amplitudes, evidently due to the increased number of load cycles at these amplitudes. This can be attributed to the partial loss of concrete cover in the plastic hinge zones after the $\pm 3\%$ drift cycles, loss of vertical bar anchorage bond, and loss of concrete shear strength capacity. As might be expected, the strength degradation during the 20 cycles at the $\pm 4\%$ drift amplitude is significant. Not only was the concrete in the hinge zones badly cracked and spalled, but also the longitudinal reinforcing bars buckled and fractured due to low cycle fatigue.

The specimen exceeded its nominal strength, calculated in Section 6.2, in the reverse loading cycles but failed to achieve this in the forward loading cycles. This difference may be due to the following: (i) two different types of annealed bars used for longitudinal reinforcement in the column corners; (ii) the presence of a major crack in the foundation beam along the inner face of the south column (during the forward loading cycle, this column is the heavier one and the crack would have reduced the strength of the column as indicated in Fig. 3.1a & b.); and (iii) the initial loading direction for all

load cycles was negative which may have pre-weakened the shear strength capacity of the pier due to crack opening for the positive loading half-cycles.

In Fig. 3.4, the lateral load resistance capacity of the pier model is also expressed in a dimensionless form as a base shear coefficient C_c defined as

$$C_c = \frac{F}{W} \qquad (3\text{-}1)$$

where F = lateral Force, W = axial load on the columns including pier self weight = 38.6 kips

ii) Section Curvatures and Strains

Although the entire column height was monitored for rotations with linear potentiometers, it is evident from photographs that plastification and column rotations were restricted to the two end gauge lengths. Similarly, due to concrete spalling in the end zones, the contact between the potentiometer mountings and the pier was lost and it was not possible to obtain data for drift levels of $\pm 3\%$ and $\pm 4\%$.

Rotation over a given gauge length is calculated from:

$$\theta = \frac{\Delta_p}{L_p} \qquad (3\text{-}2)$$

and curvatures from:

$$\phi = \frac{\theta}{L_g} = \frac{\Delta_p}{L_p L_g} \qquad (3\text{-}3)$$

where Δ_p = algebraic difference of potentiometer readings, L_p = center-to-center distance between potentiometer pairs, and L_g = gauge length over which curvature is measured.

The rotations over the two end gauge lengths are plotted in Fig. 3.5. These locations incorporate the plastic hinges at both ends of the column.

3-4

Lateral load vs. curvature hysteresis curves for the lower and upper gauge lengths of the column are shown in Fig. 3.6. The curvatures for the second gauge lengths adjacent to the end zones are plotted in Fig. 3.7. It is to be noted that the curvature hysteresis performance at the lower gauge length is nearly the same in both directions of loading and it appears to be well within the plastic range while at the upper gauge length the performance in the forward loading direction is nearly half that in the reverse loading cycle and a lack of spread of plasticity is evident. This may be attributed to two reasons:

a)   At the upper end of the column, the plastic hinge length is much greater than at the lower end and one can compare the performances of the adjacent gauge lengths (Fig. 3.7) which show some energy dissipation in the gauge length adjacent to the top one but virtually nothing for the one adjacent to the bottom. But the plastic hinge rotations for the top and bottom hinges present a more regular pattern as shown in Fig. 3.5. Hinge rotation is taken as the combined rotation of the two respective end gauge lengths. It is observed that hinge rotation in the forward and reverse cycles are approximately the same for the top and bottom hinges with rotation in the forward loading cycle being abou. 75% that in the reverse direction for both hinge locations.

b)   It is suspected that due to weak foundation beam concrete, there might have been some strain penetration at the lower gauge length. Thus, the strains recorded there are larger, and hence the curvatures as well.

The same reasoning applies for the differences in the strain profiles for the lower and upper gauge lengths shown in Figs. 3.8 and 3.9 respectively and for the gauge lengths adjacent to the lower and upper ones in Fig 3.10 and 3.11 respectively.

Distribution of section curvatures along the column height are shown in Fig. 3.12. It indicates larger curvatures at the ends, in the reverse loading direction than the forward direction. Note the inactivity of the region between the hinges. This plot is corresponding to the peak potentiometer readings for the first cycle of each drift amplitude.

iii) Synthesis of Various Components of Column Displacement

Various components of column displacement, i.e. total, flexural and shear are shown in Fig. 3.13(a) along the column height, while synthesis of column drift into these components vs lateral force is shown in Fig. 3.13(b). All displacements are with reference to the column base. Total displacements were found from the readings of sonic transducers #1 to 8. The plotted values are the peak values for a given drift level during the first loading cycle. Flexural displacements were computed by using the moment area theorems which can be mathematically stated as:

$$\Delta_{AB} = \int_{x_A}^{x_B} \phi \cdot x \, dx \qquad (3\text{-}4)$$

Eq. 3-4 implies that the deflection of point B relative to a tangent drawn to the elastic curve at point A is equal to the first moment of area of the curvature diagram (between points A & B) about B. This integral can be numerically evaluated by dividing the curvature diagram, between points A and B, into n strips of height $(L_g)_i$ with curvature (ϕ_i) being measured at the center of each gauge length $(L_g)_i$ as shown in Fig. 3.14. Therefore Eq. 3-4 can be written as:

$$\Delta_{AB} = \sum_{i=1}^{n} (\phi_i L_{g_i}) x_i \qquad (3\text{-}5)$$

where x_i = Moment arm of the i th strip about B.

Using the relationship defined in Eq. 3-3,

$$\Delta_{AB} = \sum_{i=1}^{n} (\theta_i x_i) \qquad (3\text{-}6)$$

The shear component of displacement was inferred as the difference between the total and flexural displacements.

The following observations are made:

3-6

1) The flexural displacements' profile along the column height is smooth giving confidence in the instrumentation accuracy. During the last two drift levels ($\pm 1.5\%$ and $\pm 2\%$), the flexural displacements along the entire column height are greater in the reverse direction of loading than the forward direction, although the total displacement in both directions for these drift levels is nearly the same. The difference is accounted for by the shear component. This is explained by the fact that the hinge length at the top is greater than the bottom and when the pier is under forward loading, the inner column face is in tension and as this region developed hinge first (due to smaller cross sectional area), it reached its flexural capacity first and the subsequent displacements were predominantly due to the shear component. The same phenomena can be observed at the bottom that with increasing drift amplitudes, the shear component grew in the hinge zones and first equalled and then exceeded its flexural counterpart.

2) Apart from the hinge zones, the displacements are the desirable flexural type while in the hinge zones shear is equally dominant. This indicates the good overall performance of the pier.

iv) Cyclic Loading and Energy Absorption Considerations

Fig. 3.15 shows a plot of peak force during each loading cycle. The drop in maximum force during the second and subsequent cycles of each drift level is quite noticeable. The specimen picked up strength until reaching a maximum during the first $\pm 1.5\%$ drift amplitude loading cycle. There is a sharp decline in maximum lateral load carried by the pier in the first few loading cycles of $\pm 4\%$ drift level until the instance of first longitudinal rebar fracture after which the loss of strength is gradual reaching a nearly constant value in the last cycles.

The plot of energy absorbed by the pier; which is equal to the amount of work done on it, is shown in Fig. 3.16. A cycle of loading is defined as one full reversal between positive and negative forward and reverse drift amplitudes. Area within a Force-Displacement hysteresis loop for a cycle measures the energy absorbed in that cycle. This

can be found by numerical integration using the trapezoidal rule resulting in :

$$E = \sum_{i=1}^{n} \left(\frac{F_i + F_{i-1}}{2} \right) (x_i - x_{i-1}) \qquad (3\text{-}7)$$

where F_i = force and x_i = displacement for the ith step.

Fig. 3.16 shows that there is a gradual increase in energy absorption with increasing drift amplitudes up to the $\pm 3\%$ drift level. This peak was followed by a steady drop off in absorbed energy. The observation made for the drop of peak force in the $\pm 4\%$ drift level loading cycles holds true in the case of energy absorbed also.

Fig. 3.17 presents a plot of cumulative energy vs cumulative drift. It is evident that there is an increase in energy absorption all the way up to loading cycle 22 corresponding to first fracture of longitudinal reinforcing bar. After the first longitudinal rebar fracture, the slope of the curve has started to drop but did not reach the asymptote at the end of test, indicating that there is still some life left in the apparently devastated specimen.

The degradation of strength is also examined by Peak Force vs Cumulative Drift plot shown in Fig. 3.18. Cumulative drift is defined as the sum of all positive and negative drift peaks occurring prior to a given stage of testing. Thus 2 cycles of drift amplitude $\pm 0.5\%$ contributes a cumulative drift of 2.0%. It is observed that at the instant of first longitudinal rebar fracture 74% of the total energy was absorbed in 41% of total cumulative drift. This implies that, as expected, the lateral load carrying capacity of the pier model was severely impaired after the longitudinal rebar fracture.

(a)

(b)

(d)

(c)

Fig. 3.1 **Progressive Damage of the Model till the end of ±3.0% Drift Amplitude Loading**
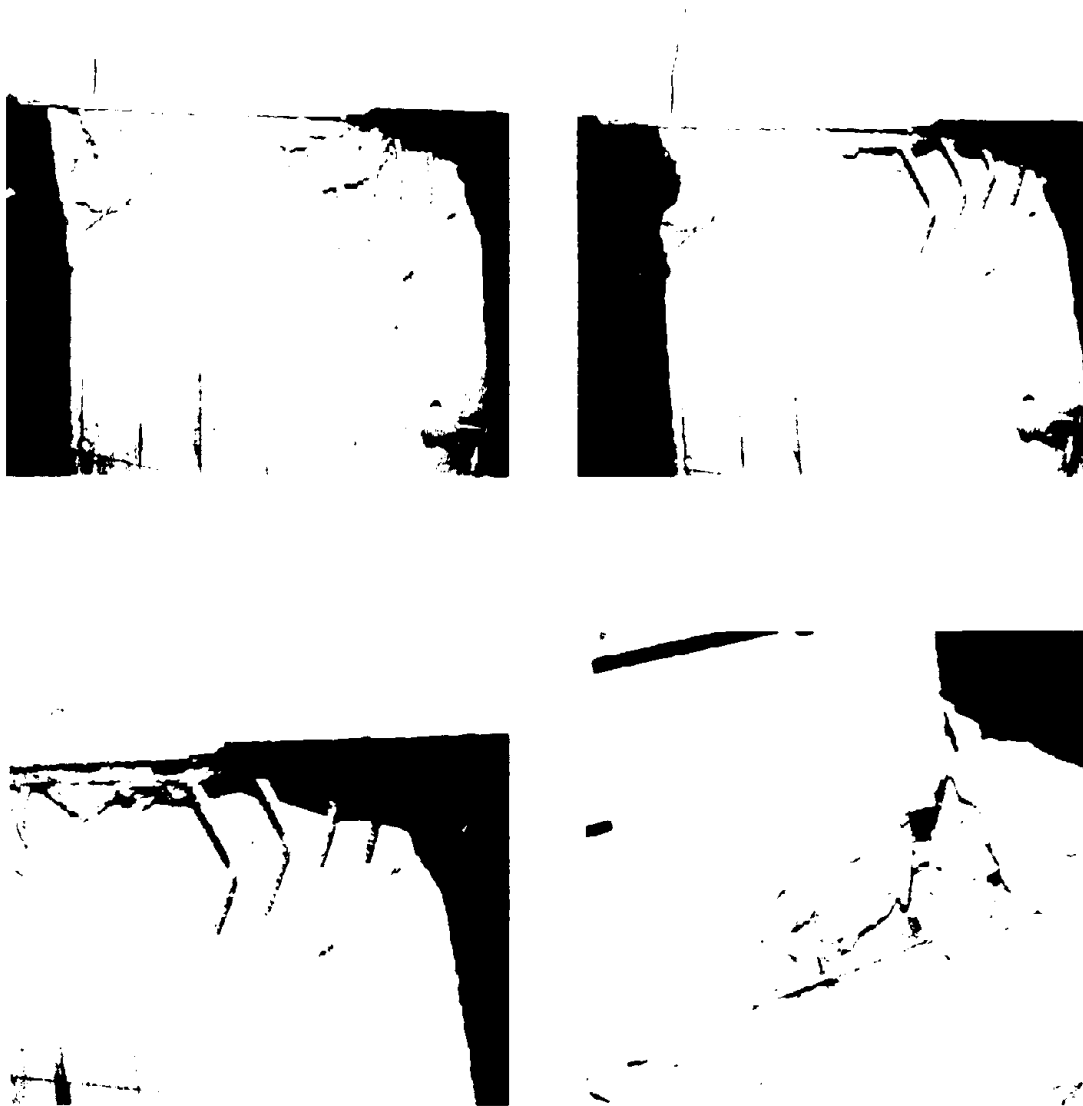
Fig. 3.2   Progressive Damage of the Model during the ±4.0% Drift Amplitude
Loading

3-10

East Face

West Face

Fig. 3.3 Model Pier after the end of Testing

QUASI STATIC LOADING

QUASI DYNAMIC LOADING
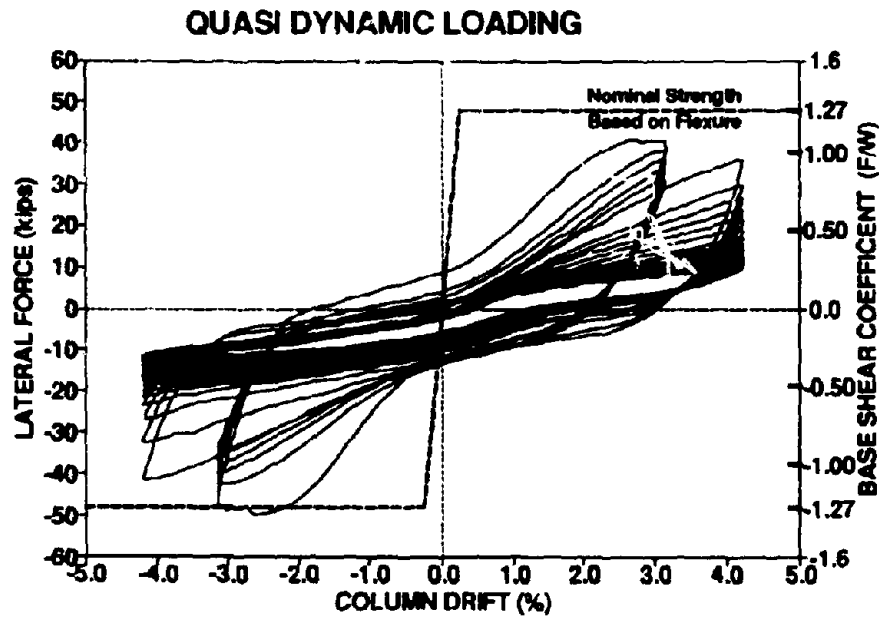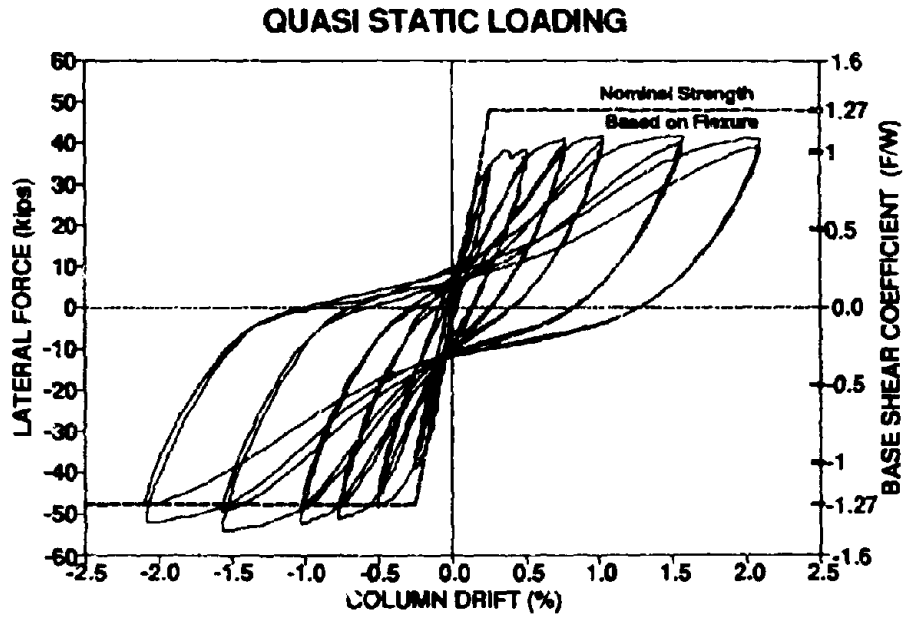
Fig. 3.4   Experimental Lateral Force - Column Drift Relationship
for the Model Pier

3-12

LOWER PLASTIC HINGE

UPPER PLASTIC HINGE
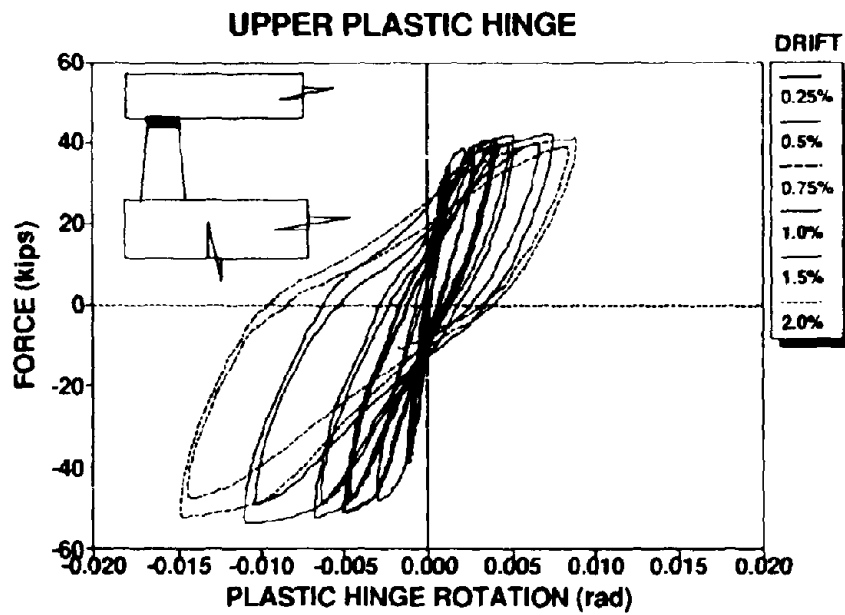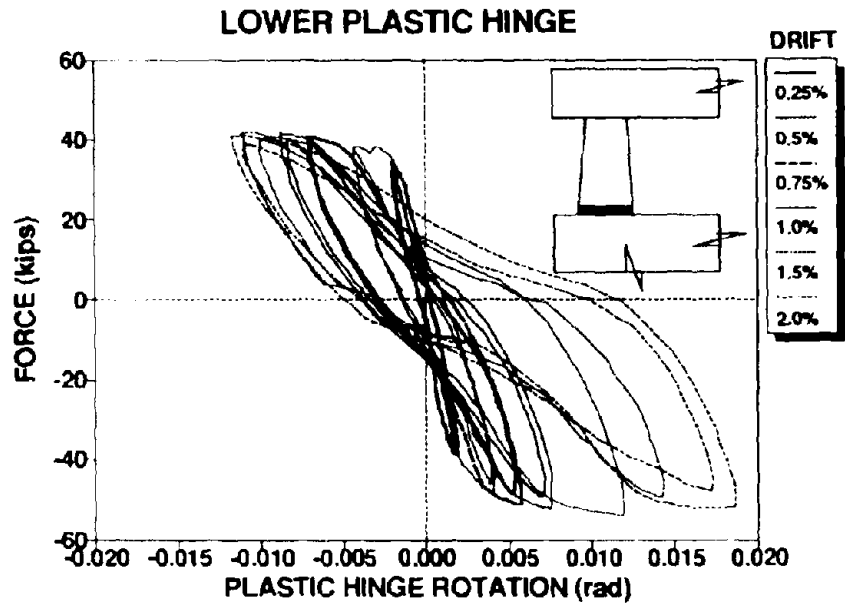
Fig. 3.5 Experimental Force - Plastic Hinge Rotation Relationship for the Model Pier

3-13

Fig. 3.6 Experimental Force Curvature Relationship for the Model

GAUGE LENGTH ADJACENT TO THE BOTTOM

GAUGE LENGTH ADJACENT TO THE TOP
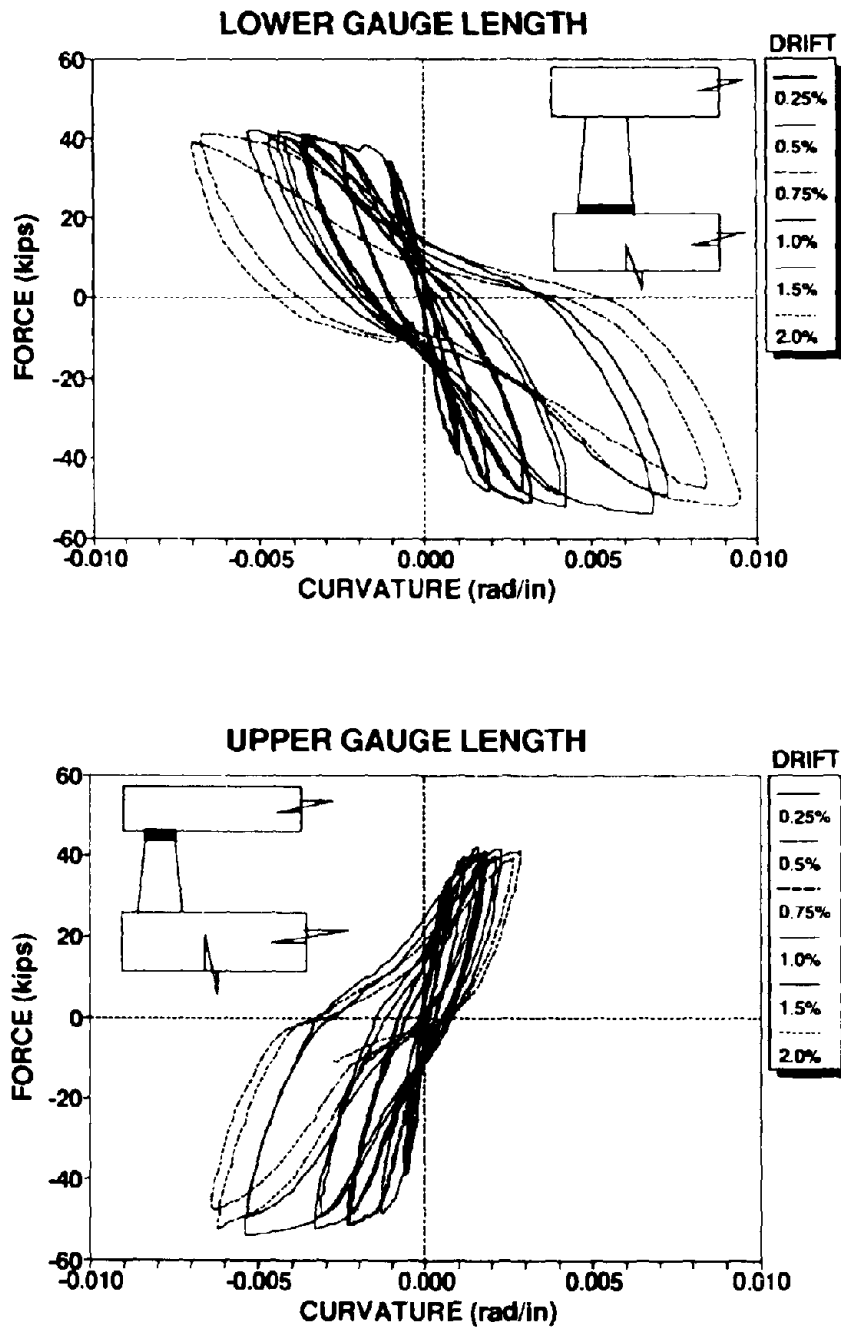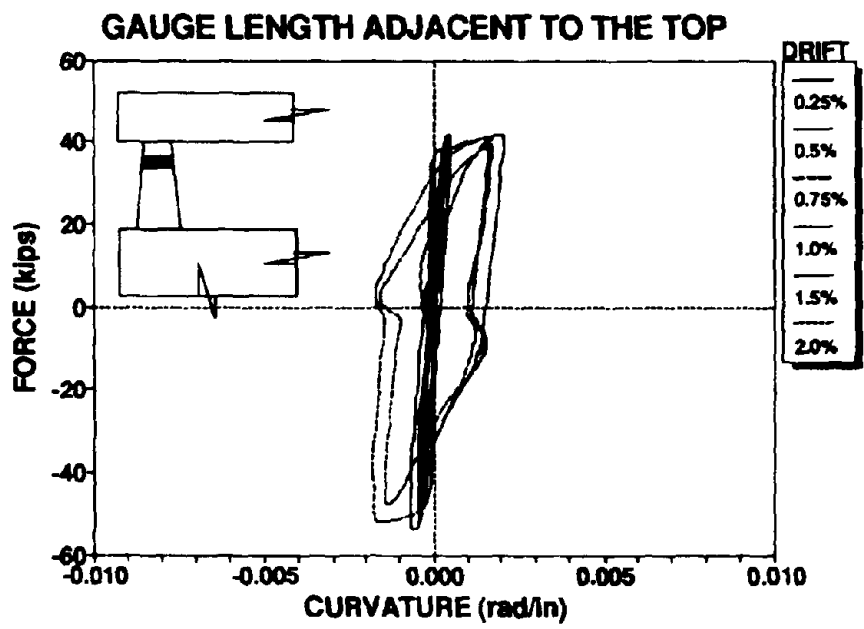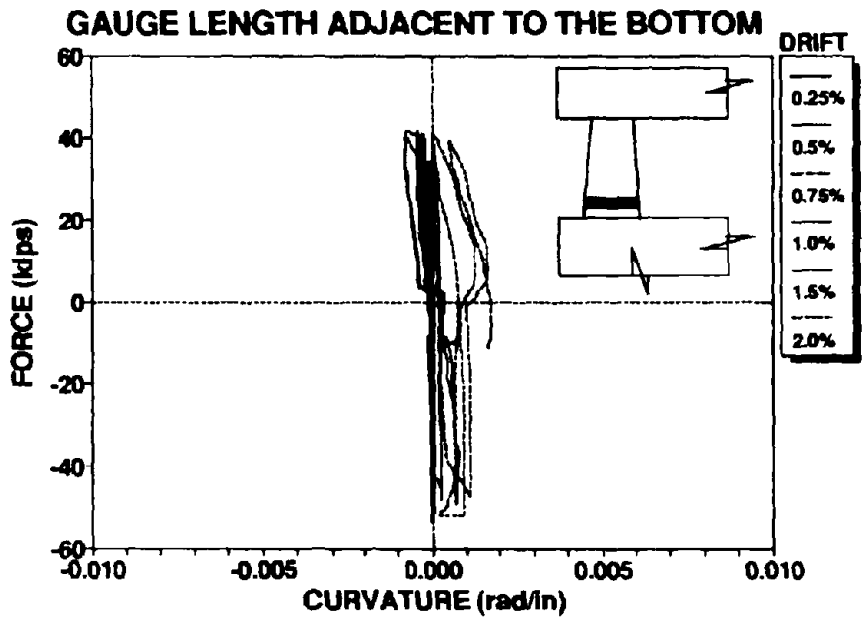
Fig. 3.7 Experimental Force Curvature Relationship for the Model

FORWARD LOADING

REVERSE LOADING

Fig. 3.8 Strain Profiles for Lower Gauge Length

FORWARD LOADING

REVERSE LOADING
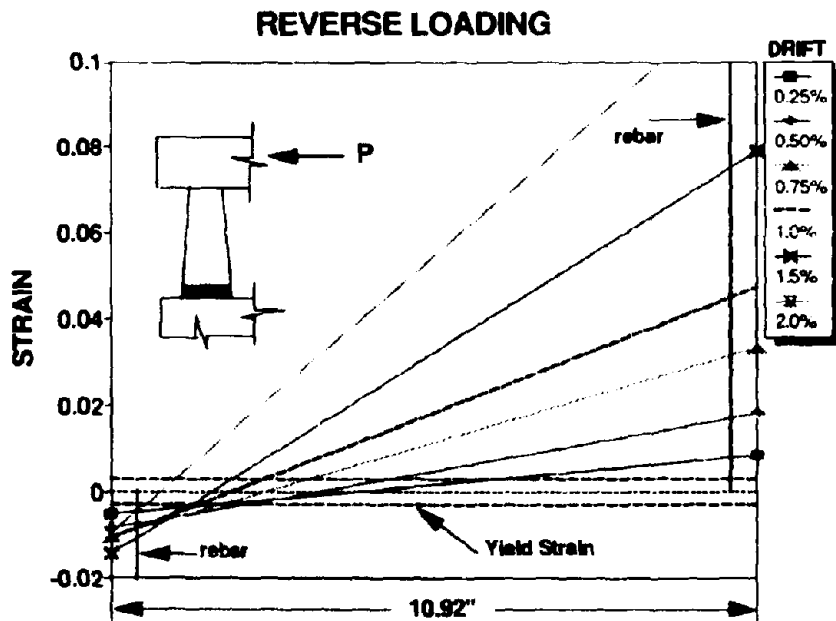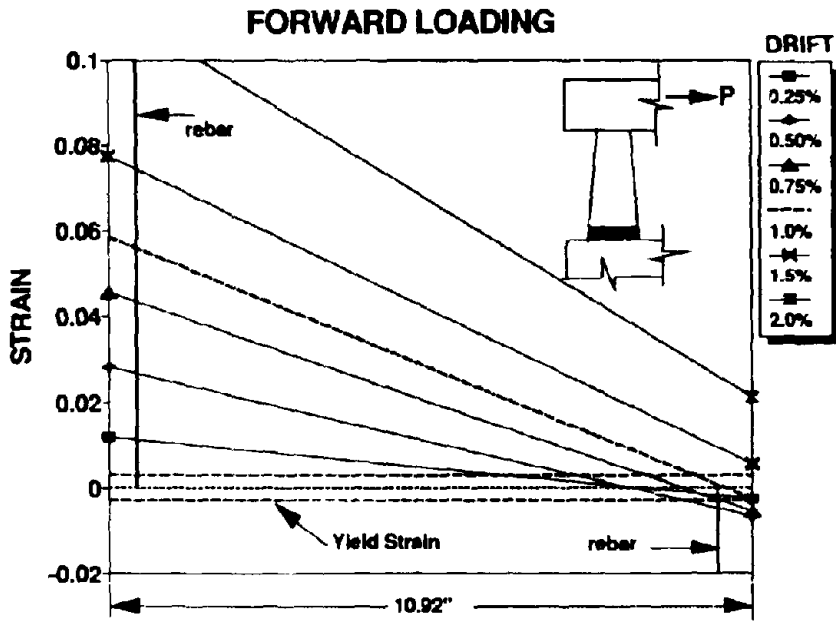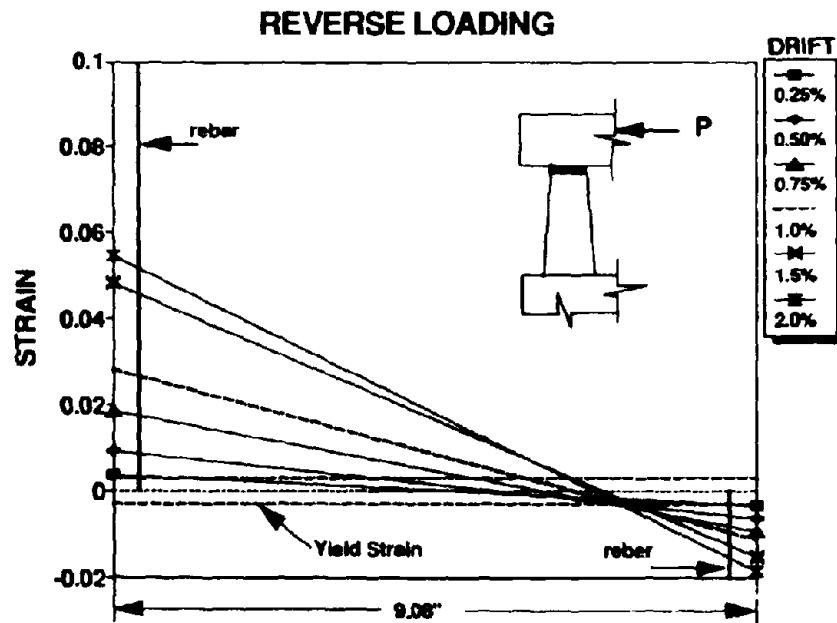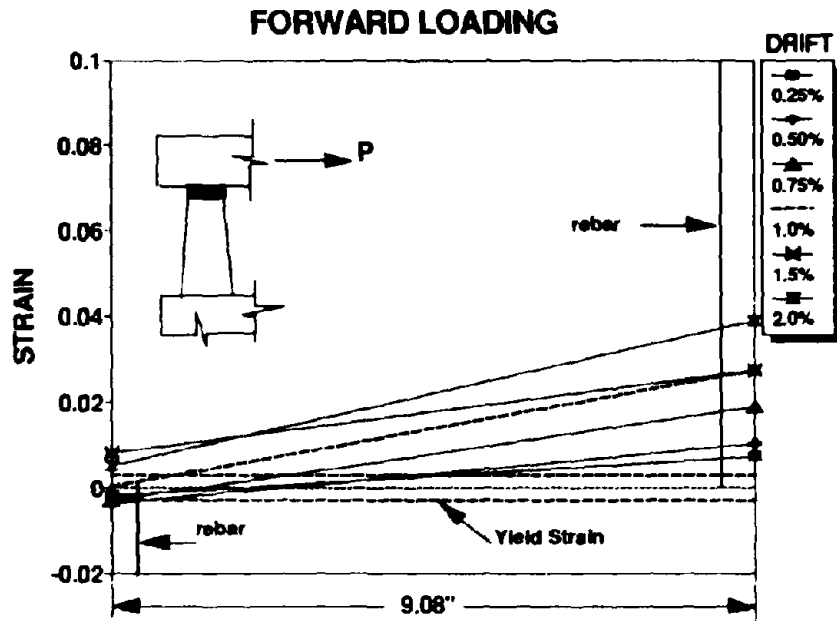
Fig. 3.9 Strain Profiles for Upper Gauge Length

FORWARD LOADING

REVERSE LOADING
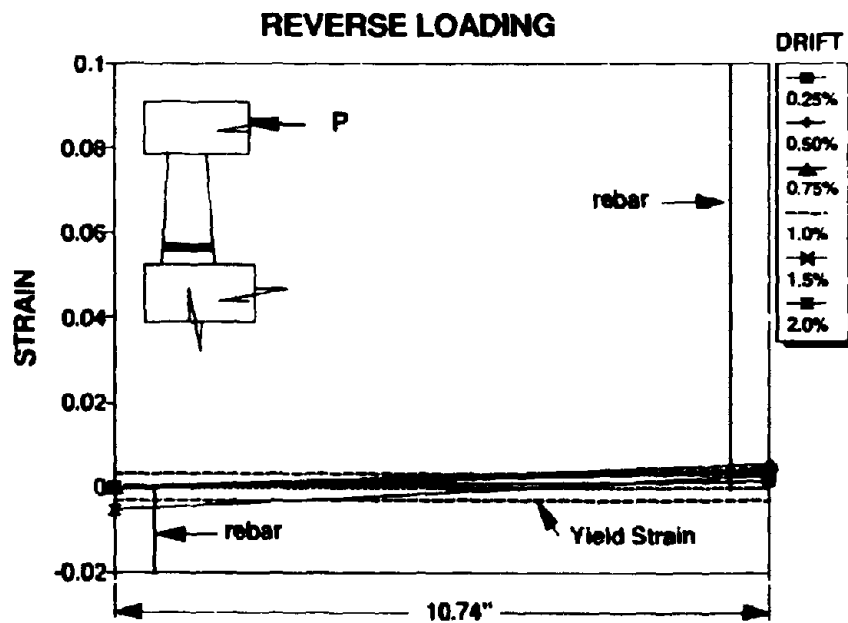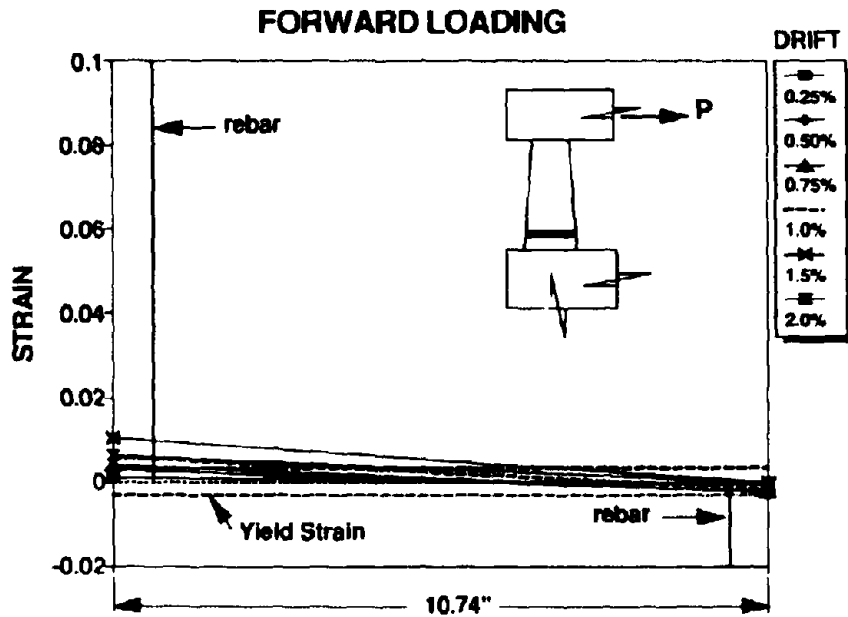
Fig. 3.10 Strain Profiles for Gauge Length adjacent to the Bottom

FORWARD LOADING

REVERSE LOADING
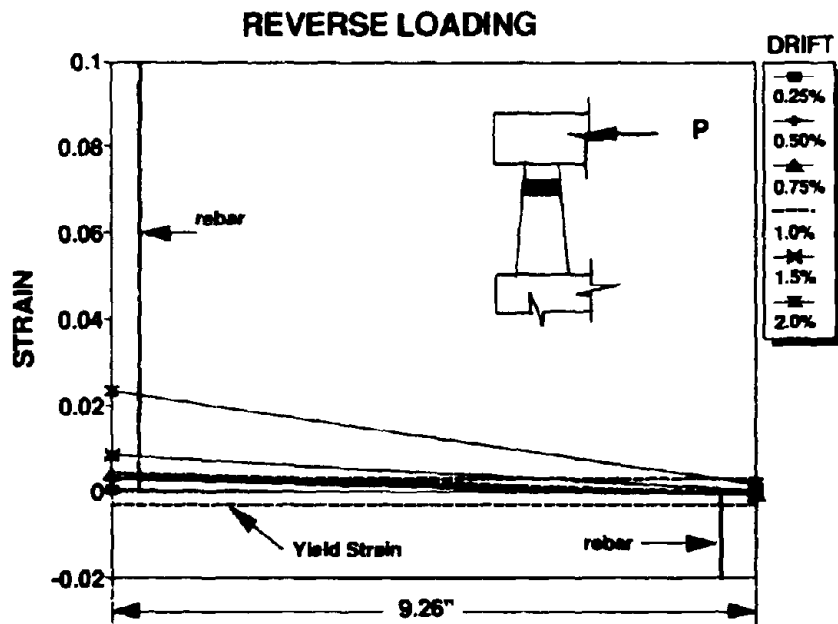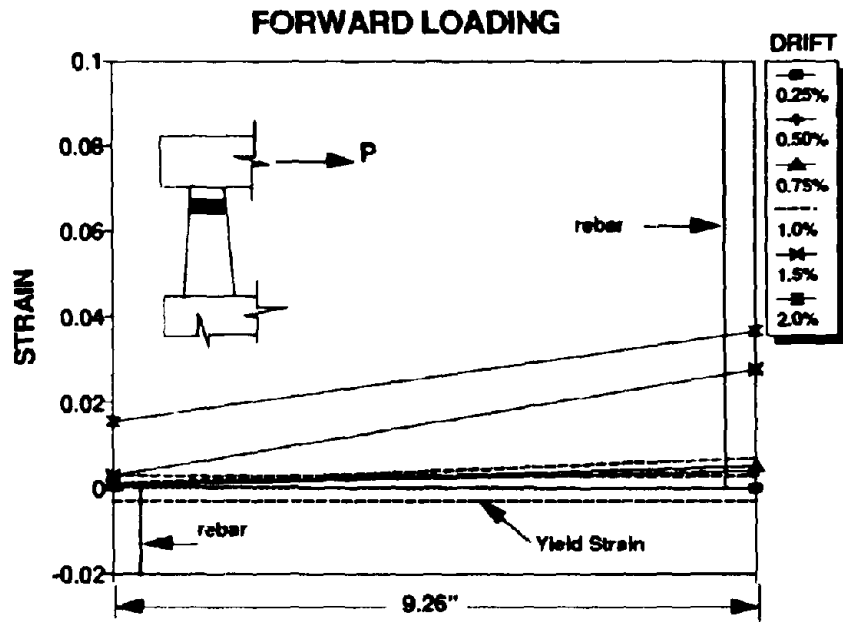
Fig. 3.11 Strain Profiles for Gauge Length adjacent to the Top

3-19
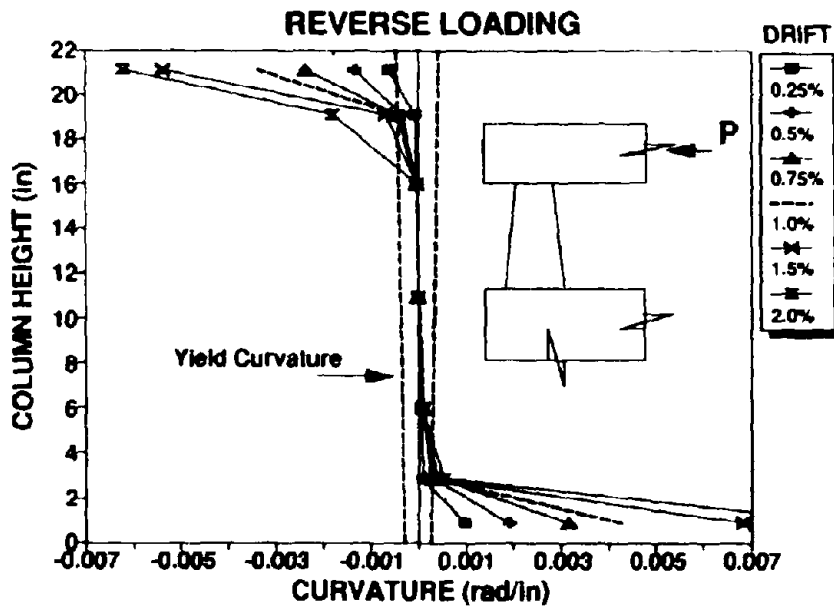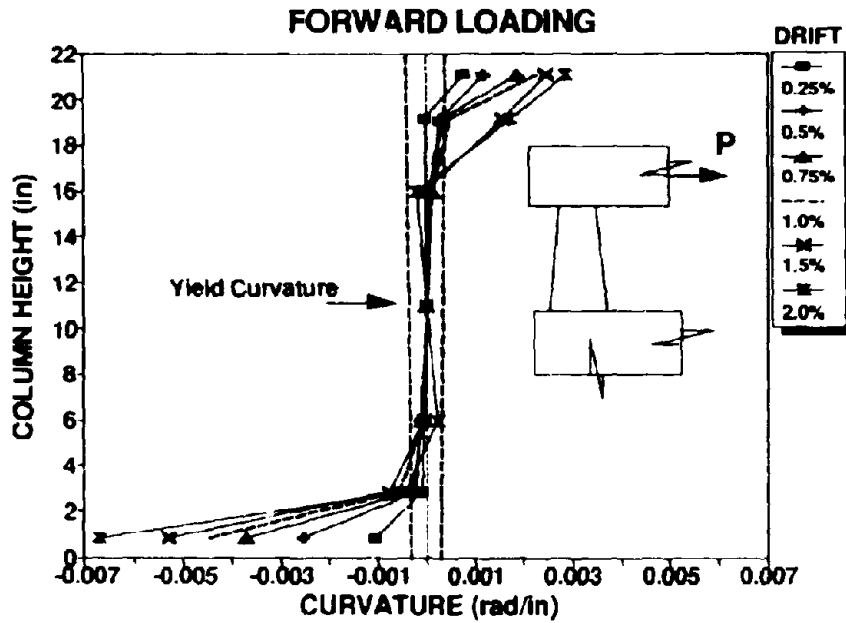
Fig. 3.12 Distribution of Curvatures along Column Height
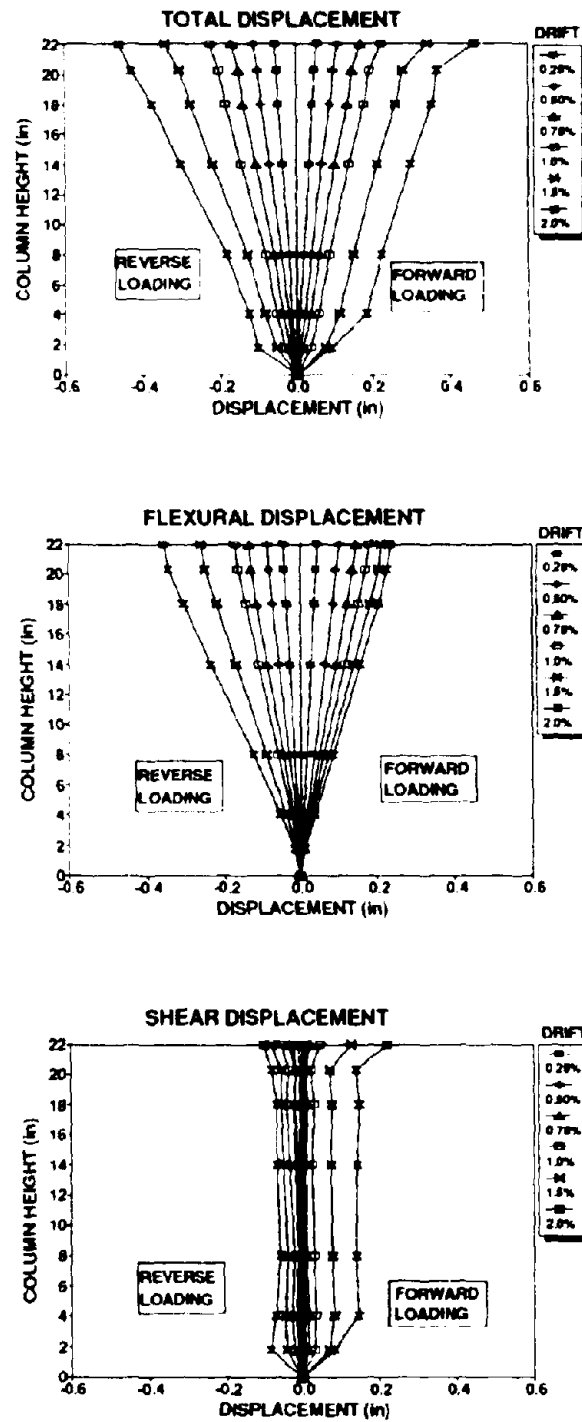
Fig. 3.13 (a) Synthesis of Total, Flexural and Shear Displacement along Column Height
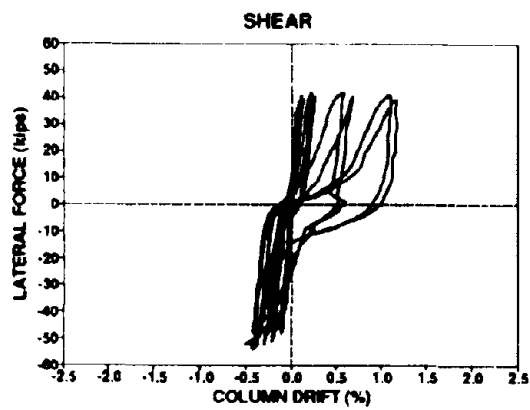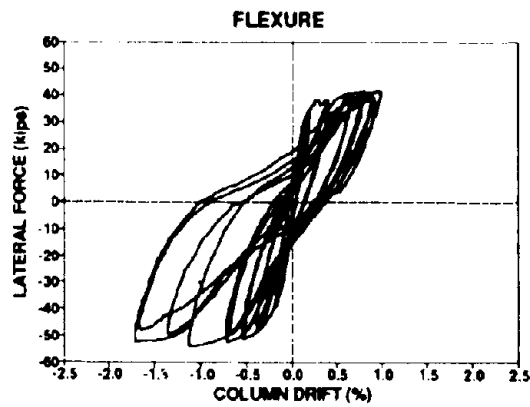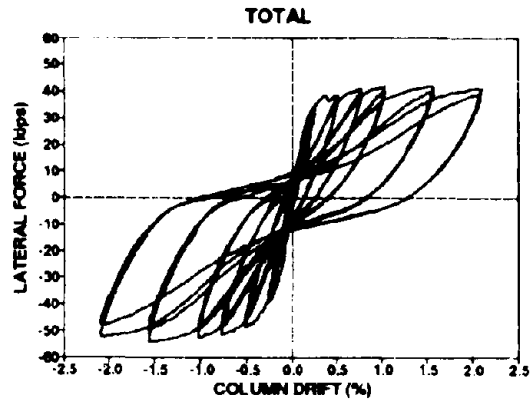
Fig. 3.13 (b) Synthesis of Total, Flexural and Shear Component of Drift

Loading diagram   Deformed Shape   Observed Curvature diagram
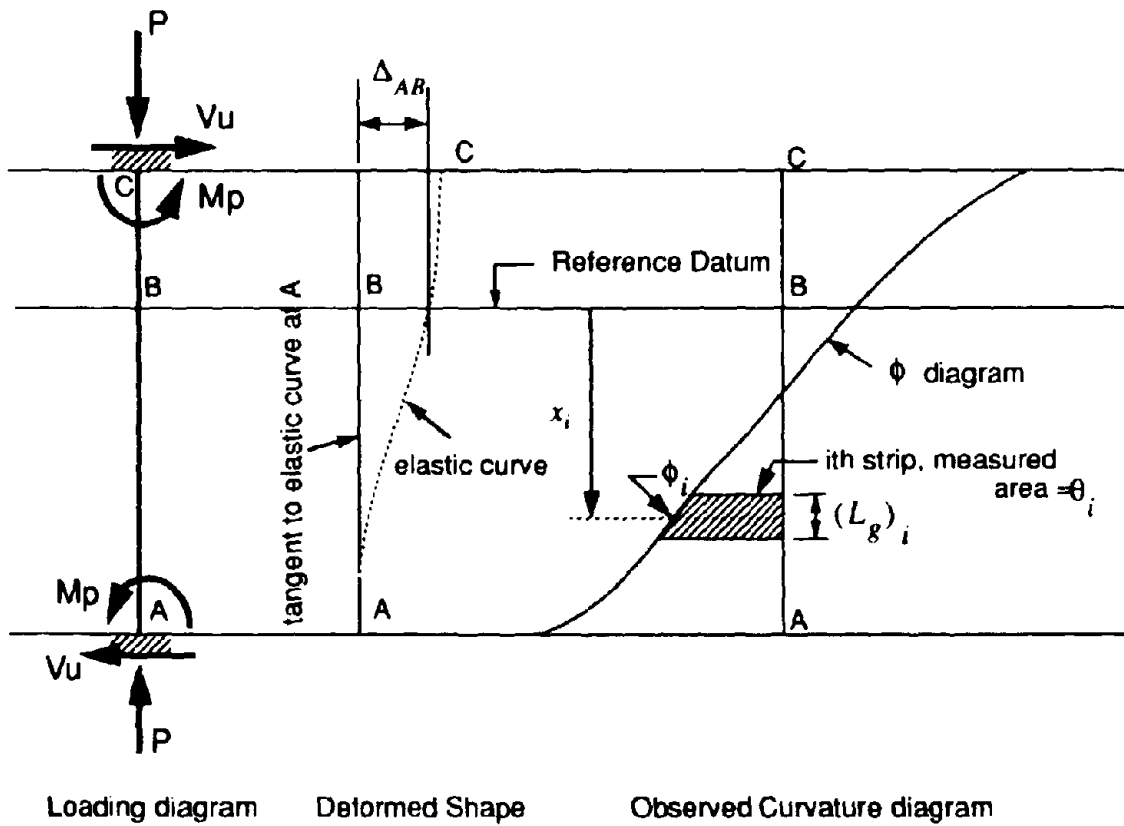
Fig. 3.14 Determination of Deflection using Second Moment-Area Theorem

PEAK FORCE vs LOADING CYCLES
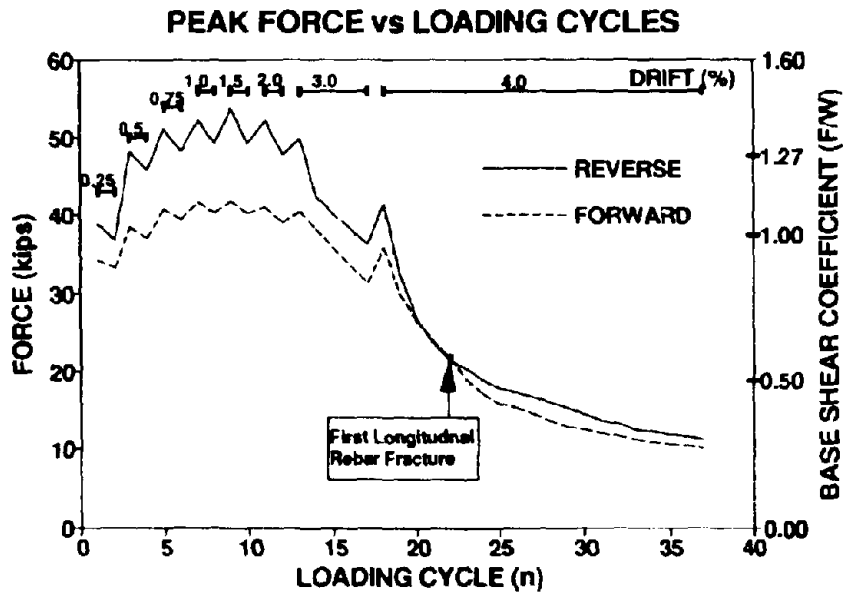
Fig. 3.15 Peak Lateral Force in Each Loading Cycle

ENERGY ABSORBED IN EACH LOADING CYCLE
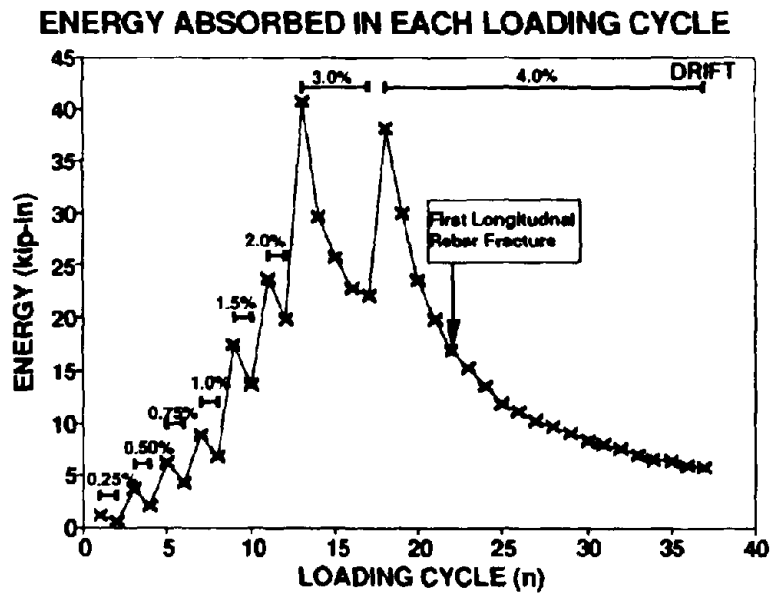
Fig. 3.16 Energy Absorbed in Each Loading Cycle

3-24

CUMULATIVE ENERGY vs CUMULATIVE DRIFT
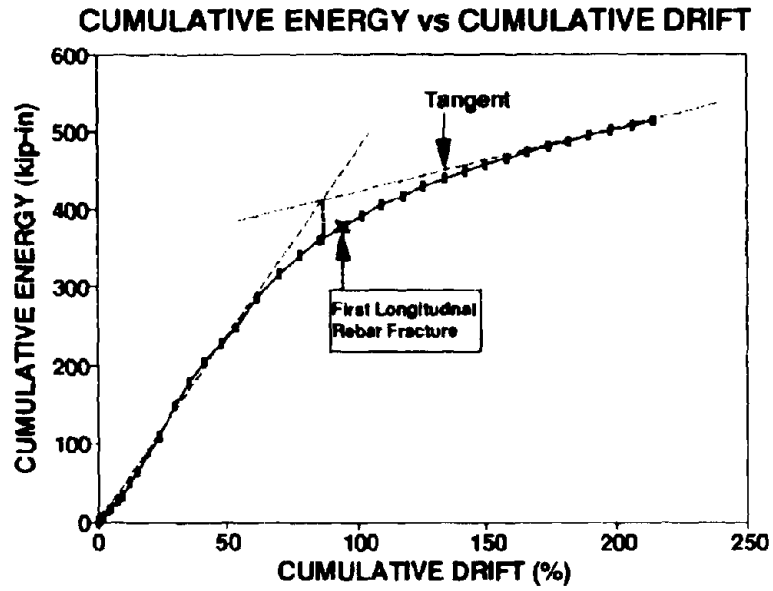
Fig. 3.17 Cumulative Energy vs Cumulative Drift Relationship

PEAK FORCE vs CUMULATIVE DRIFT
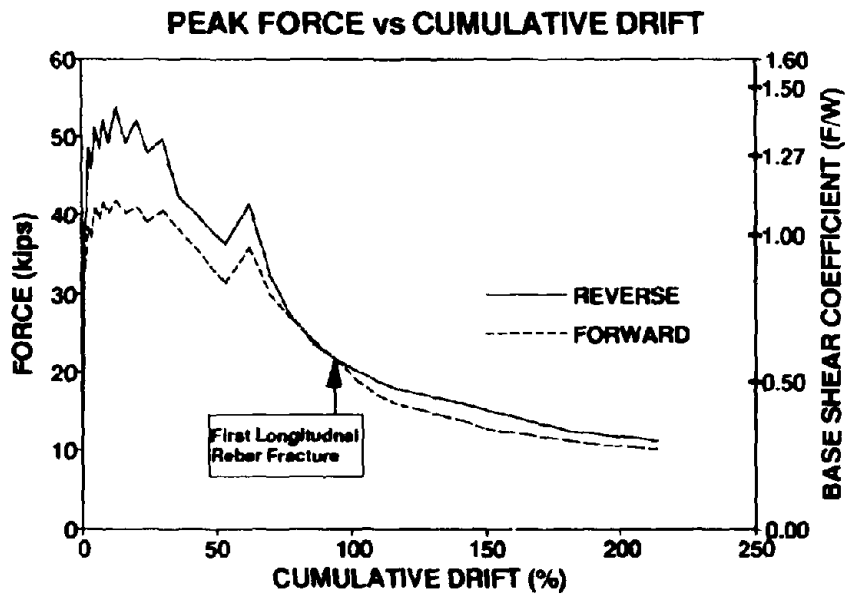
Fig. 3.18 Peak Force vs Cumulative Drift Relationship

SECTION 4
CONSTRUCTION AND INSTRUMENTATION
FOR THE PROTOTYPE SPECIMEN

4.1 Testing Arrangements

Due to the high strength of the specimen and the large magnitude of gravity load and lateral forces necessary to induce a column failure, it was not possible to use the laboratory's existing strong-floor and wall testing systems in the experiment. A self-reacting reaction frame was therefore designed to provide both gravity and lateral forces to the specimen. Figs. 4.1 to 4.5 show different views of these arrangements. Details of the reaction frame and testing setup are presented in the following sub-sections.

4.1.1 Lateral Force

Reaction Frame: Figs. 4.1 and 4.2 show this frame which consisted of two W14X145 beams and four 12" x 1" plates, referred as Beams 1 and 2 respectively, along with their connecting arrangements to the capping beam and to one another. Beams 1 and 2 were respectively inclined at 32° and 24° with the horizontal.

Beam 1 was connected at the bottom of the specimen through a series of connecting plates, fabricated as Beam 3 (as shown in Fig. 4.2), to the horizontal reinforcement of the capping beam. Beam 3 consisted of a 48" x 20" x 1" plate at the northern face of the capping beam which was welded to a 48" x 10" x 1" plate (thus making a T-Section). The 10" wide plate was welded to the reinforcing bars. The T-Connection was stiffened by five triangular plates which also helped in providing an increased weld area.

The four plates of Beam 2 were welded to Beam 1 (the two W14X145 beams) and to a series of connecting plates which formed Beam 4. Beam 4 consisted of a 48" x 16" x 1" plate at the northern face of the capping beam which was welded to two

4.1.2 Dead Load

The total load on the western pier of the bridge was calculated to be 538 kips. Therefore a constant vertical load of 269 kips was required at column top during the test. This load was provided through a system consisting of two W10X77 lever beams and an actuator of 55 kips capacity as shown in Figs. 4.4 and 4.5. The load of 269 kips was achieved as a support reaction for the top beam. The support consisted of one of the high bolster bearings taken from the bridge on top of the column placed at it's center. The bearing's sole plate was welded to the upper W10X77 beam. The tension anchorage connecting the two W10X77 lever beams consisted of three # 8 high strength (Dywidag) threadbars passing through holes in the beams aligned at a distance of 24" from the center of the specimen's column and the bearing seat. These bars were anchored at the top and bottom beams by Dywidag couplers. The beams were stiffened by vertical side plates in the regions of high shear. The actuator was attached to each beam through four 1" diameter bolts. The actuator's centerline was at a distance of 98" from the column's center. In this manner the actuator force was magnified 5.08 times to give the required gravity load to the specimen. Thus, a force of 53 kips through the actuator resulted in a reaction of 269 kips applied at the top of the column. A large amount of fresh concrete was poured at the top in order to ensure that the vertical load was evenly distributed over the entire column section in the lower portions of the specimen starting from the location of application of the lateral load. To achieve this, a 26" long x 14" wide x 10" high steel box was fabricated and filled with concrete to increase the column depth, and spread the bolster bearing load which was welded directly onto the top of this box.

4.1.3 Construction Sequence

The pier was initially lying in the laboratory in such a manner that the column was parallel to the floor. The preparation sequence consisted of a series of steps as listed below:

(1)   The concrete was chipped off using pneumatic jack hammers in the zones where the reinforcing bars needed to be exposed for welding to Beams 3 and 4.

(2)   The plates forming Beams 3 and 4 were prefabricated and welded together.

(3)   Beams 3 and 4 were then welded to their respective reinforcing bars on the capping beam.

(4)   Fresh concrete, as shown in Fig. 4.2, was poured in the vicinity of Beams 3 and 4.

(5)   The 60" x 16" x 0.5" plate was welded to the reinforcing bars of the column and a frame designed for lifting operation of the pier was welded to this plate. This A-shaped lifting frame had a plate welded at its apex which had a hole drilled in it for the crane's hook.

(6)   The pier was then lifted and placed in an upright position, the position in which it was tested.

(7)   The remaining fabrication of the reaction frame was then completed. Beams 1 and 2 were fillet welded to the capping beam and to one another.

(8)   A 3" x 3" x 0.25" angle section was then attached to the column with 0.5" concrete anchor bolts. Its purpose was to hold the 16" x 1" plate, behind Beam 5, in position and at exactly 24° from the vertical.

(9)   Beams 5 and 6 were then placed in position and connected together with 4 # 11 high strength (Dywidag) threadbars.

(10) The three 14" x 10" x 1" plates were then welded to both 16" x 1" and 16" x 0.5" cross-section plates on the northern face at the top of the specimen's column.

(11) The steel box shown in Fig. 4.3 was welded to the steel plates at the north and the south faces at the top of the column.

(12) The fresh concrete at the column top was poured in three different stages, the last one being in the steel box after welding the bearing at its top.

(13) The two 250 kip actuators were placed in position.

(14) The two W10X77 lever beams were placed at top and bottom of the pier. These beams were held in position by three # 8 high strength (Dywidag) threadbars.

(15) A rich cement-sand mixture was then poured onto the top face of the lower lever beam to provide a uniform seat area in contact with the capping beam of the specimen.

(16) The 55 kip actuator was attached to the two lever beams.

(17)   Finally, the instrumentation was attached to the specimen as shown in Figs. 4.6 and 4.7, and described in Subsection 4.2.

Figs. 4.8 to 4.11 include the photographs of various features of the pier specimen during and after its construction. The photographs in Fig. 4.8 show the specimen reaction frame during its construction. Fig. 4.9 shows the concrete core drilling operation being carried out at the column top. The bolster bearing used for transferring the dead (axial) load is shown in Fig. 4.10. Fig. 4.11 shows the instrumentation details and a view of the entire test setup.

4.2   Instrumentation and Data Acquisition

Instrumentation was provided for the test in order to monitor displacements, rotations and forces as follows.

Displacements: A series of sonic (Tempersonic^{TM}) transducers were provided on the southern end of the pier in order to monitor the displacements over the height of the column. As shown in the Fig. 4.6, these transducers were mounted onto a Unistrut^{TM} frame which was attached to the capping beam through concrete anchor bolts. One instrument was provided down the centerline of the column at each level. At the top control level (level 7), two additional sonic transducers were provided, near the east and the west sides of the column to check for column torsion. The control level was at a height of 53" from the column base at the southern end. It represented the level at the point of intersection of the actuator force and column center-line.

The experiment was performed in *Drift Control*. This required the use of sonic transducer 7C, located 53" above the column base to provide the external displacement (Δ_{7C}) control signal during testing. Thus, the specimen drift is defined as:

$$\theta = \frac{\Delta_{7C}}{L_c} \tag{4-1}$$

where L_c = 53"

Curvatures: Fig. 4.7 shows the arrangement of linear potentiometers on the column face. These instruments were mounted in a similar fashion on northern and southern face. The gauge lengths for these instruments were fixed in such a way that some movement would be detected at each section. These instruments were attached to 1/4" wide aluminum strips epoxied to the concrete. Their other ends were restrained from movement through striking plates at those ends, the movement being made possible through springs during testing. These instruments were provided to measure displacements which were used to compute strains, rotations, curvatures and flexural displacements. It should be noted that these instruments could be relied upon as long as concrete did not start spalling.

Loads: The forces were monitored through load cells connected in series to their respective actuators.

Data Acquisition: During the active period of the test, the output voltages of all the instruments were recorded using an Optim Megadec 5533A Data Acquisition System. From these records the force-displacement (drift) and other relations were established.

N ◄—

C̶L Column/Bearing

C̶L Lateral Force

2.25

1

2-250 Kip Actuators

4.167 %

53"

5.165 %

36"

55 Kip Actuator

Reaction Frame

FreshConcrete

Timber Supports

12 0 12 24 36"
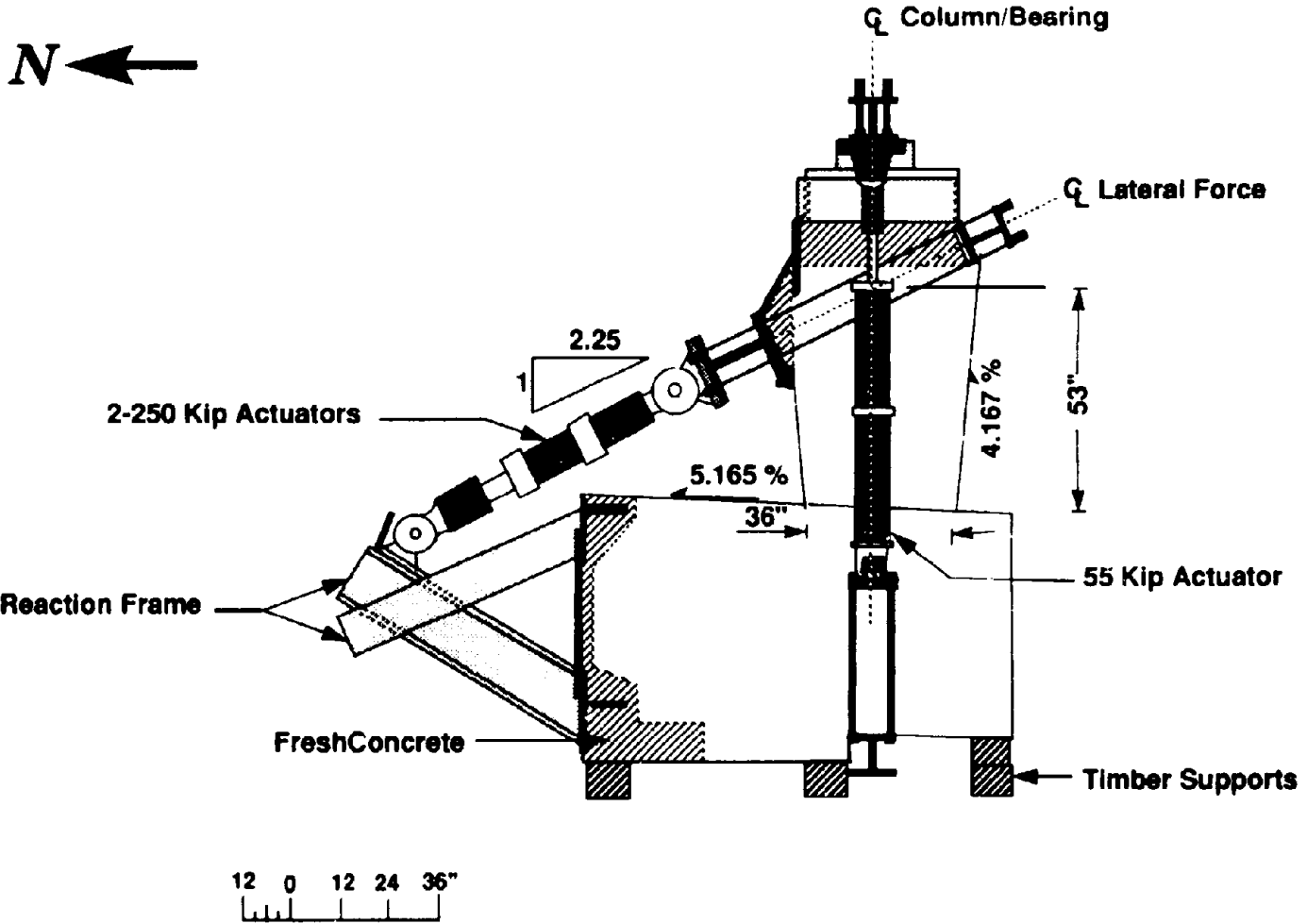
Fig. 4.1 Schematic Elevation of Test Specimen
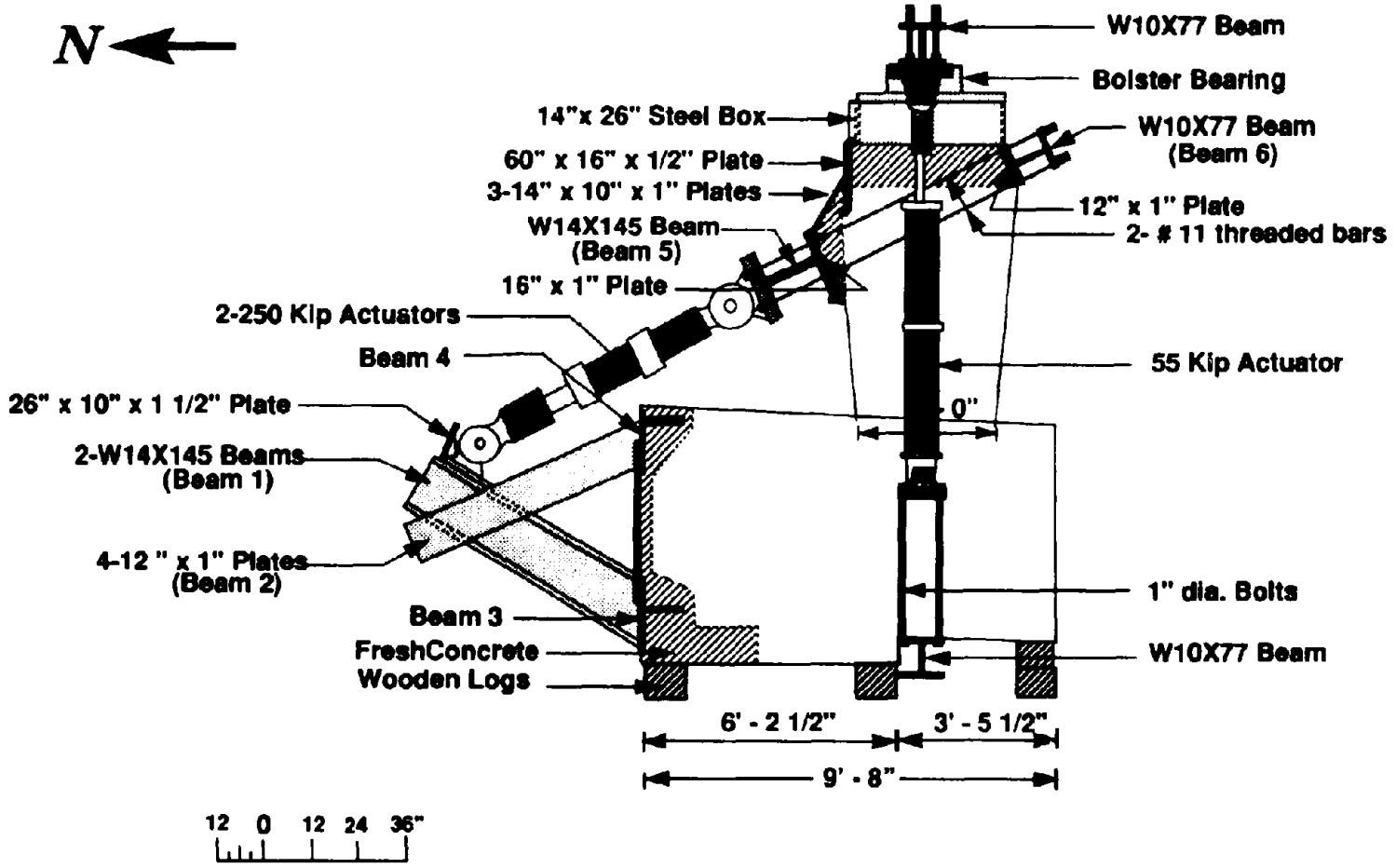
Fig. 4.2 West Elevation Showing Construction Details

55"

41"

39"

N

W10X77 (Beam 6)

Column Top

W10X77

55 kip Actuator

Bolster Bearing

Steel Box

W14X145 (Beam 5)

11 High Strength bar

Capping Beam

2-250 kip Actuators

2- W14X145 Beams
(Beam 1)

4-1" x 12" Plates
(Beam 2)

12   0   12   24"
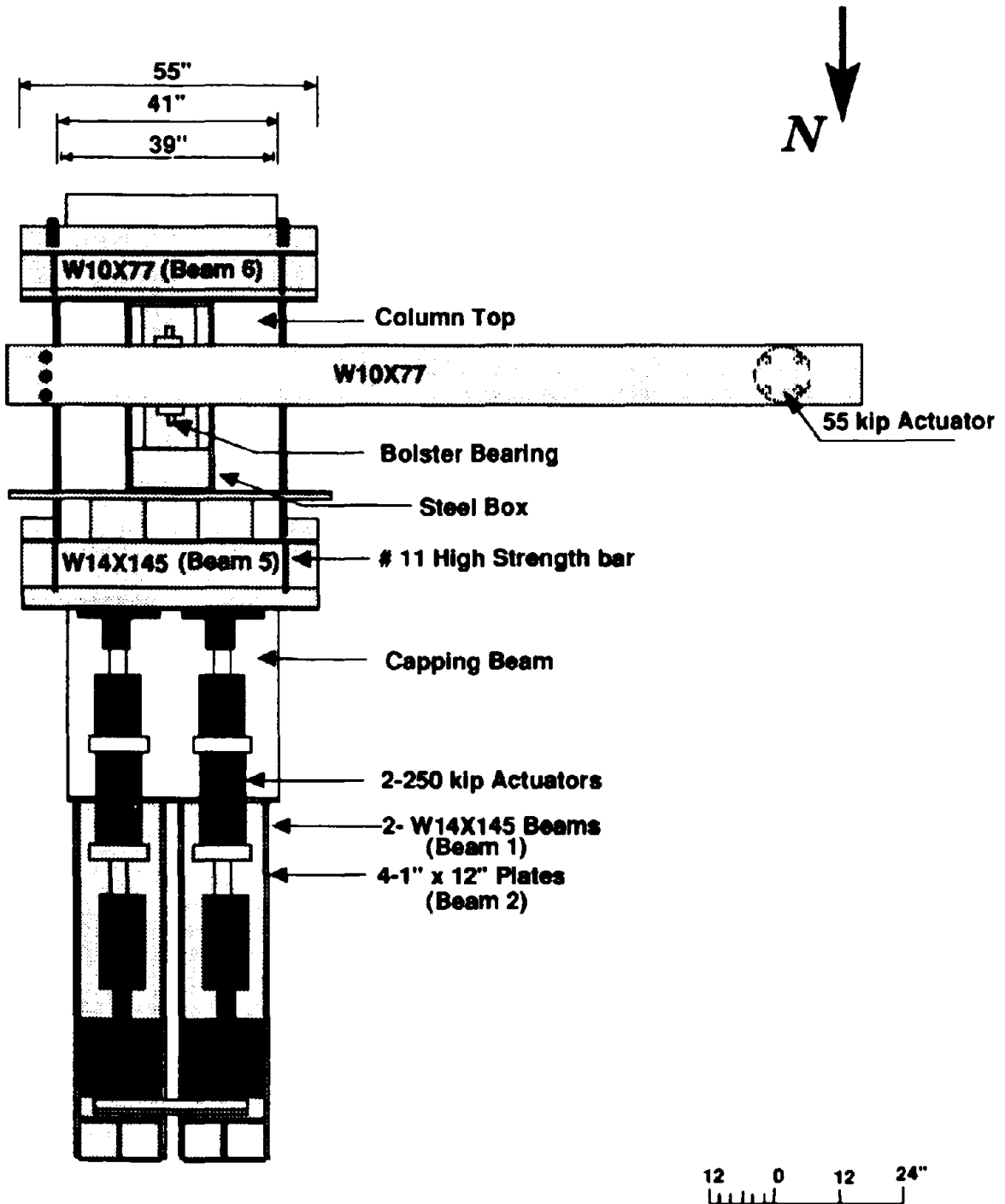
Fig. 4.3 Plan View of Test Setup

E

24" 98"

W10X77

W10X77

2- # 11 H.S.
threadedbars

W14X145

55 kip

3- # 8 H.S.
threaded bars

2-250 kip
Actuators

3- #9 rebars

W10X77

12   0   12   24   36"

Fig. 4.4 North Elevation

W

98" 24"

W10X77

W10X77

W14X145

3- # 8 H.S.
threadbars

55 kip Actuator

3- # 9 rebars

W10X77

Couplers

12 0 12 24 36"

Fig. 4.5 South Elevation

N

Unistrut Reference Frame

Sonic Transducers

7W/E&C

20"

8

7"

6

5

6"

4

5"

3

4"
3"
2

2"

Concrete Anchor Bolts
for Fixity to the Specimen

12   0   12   24"
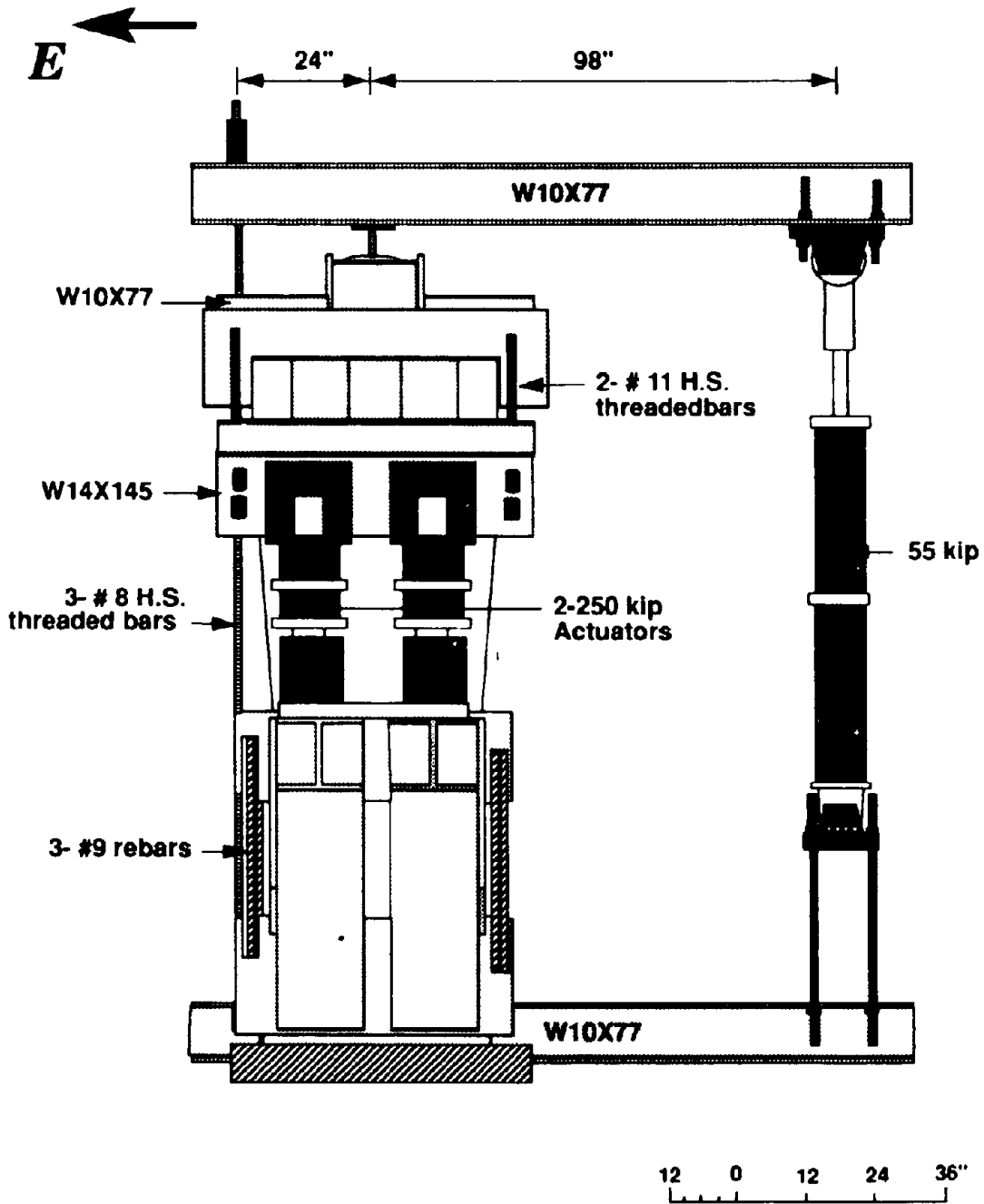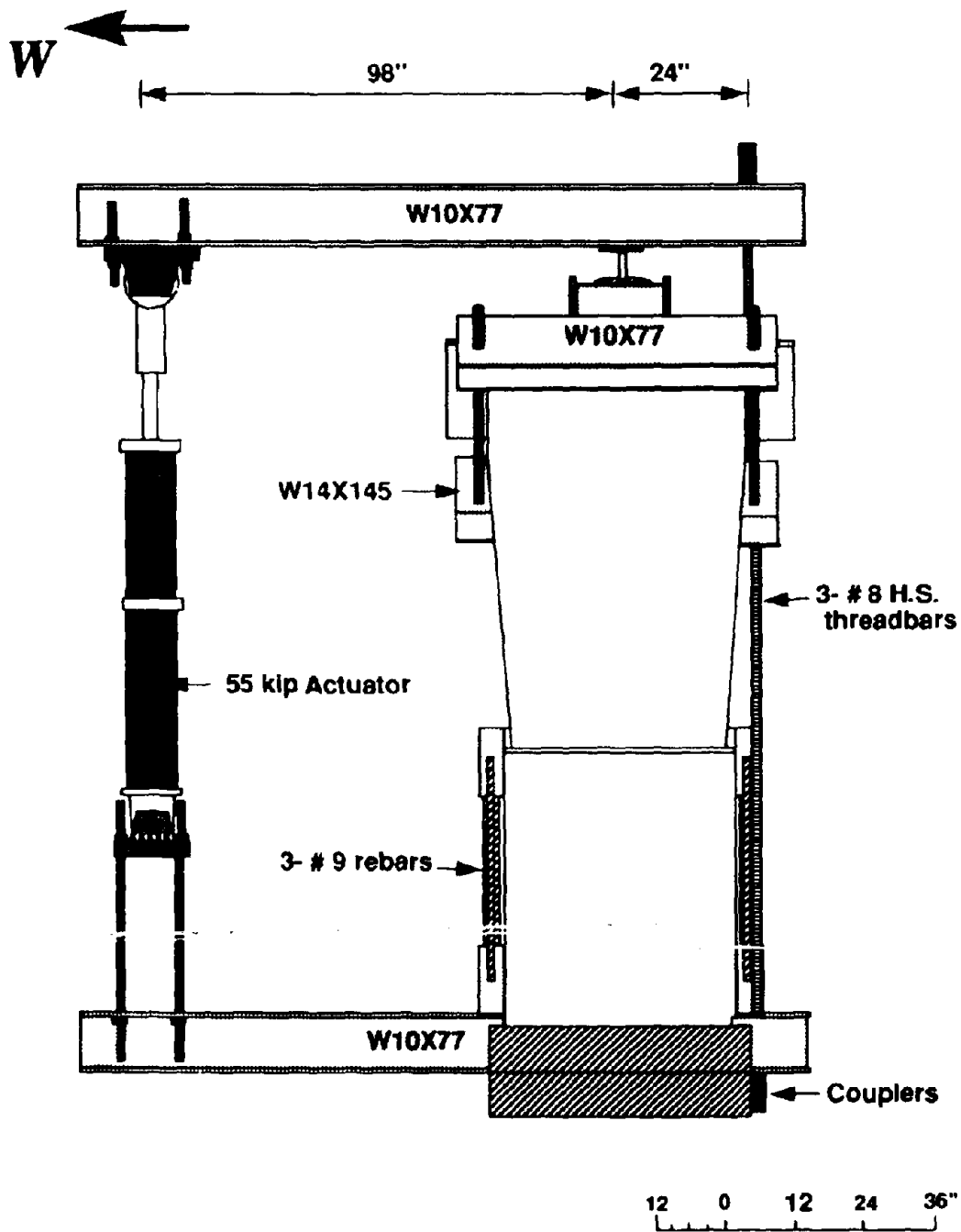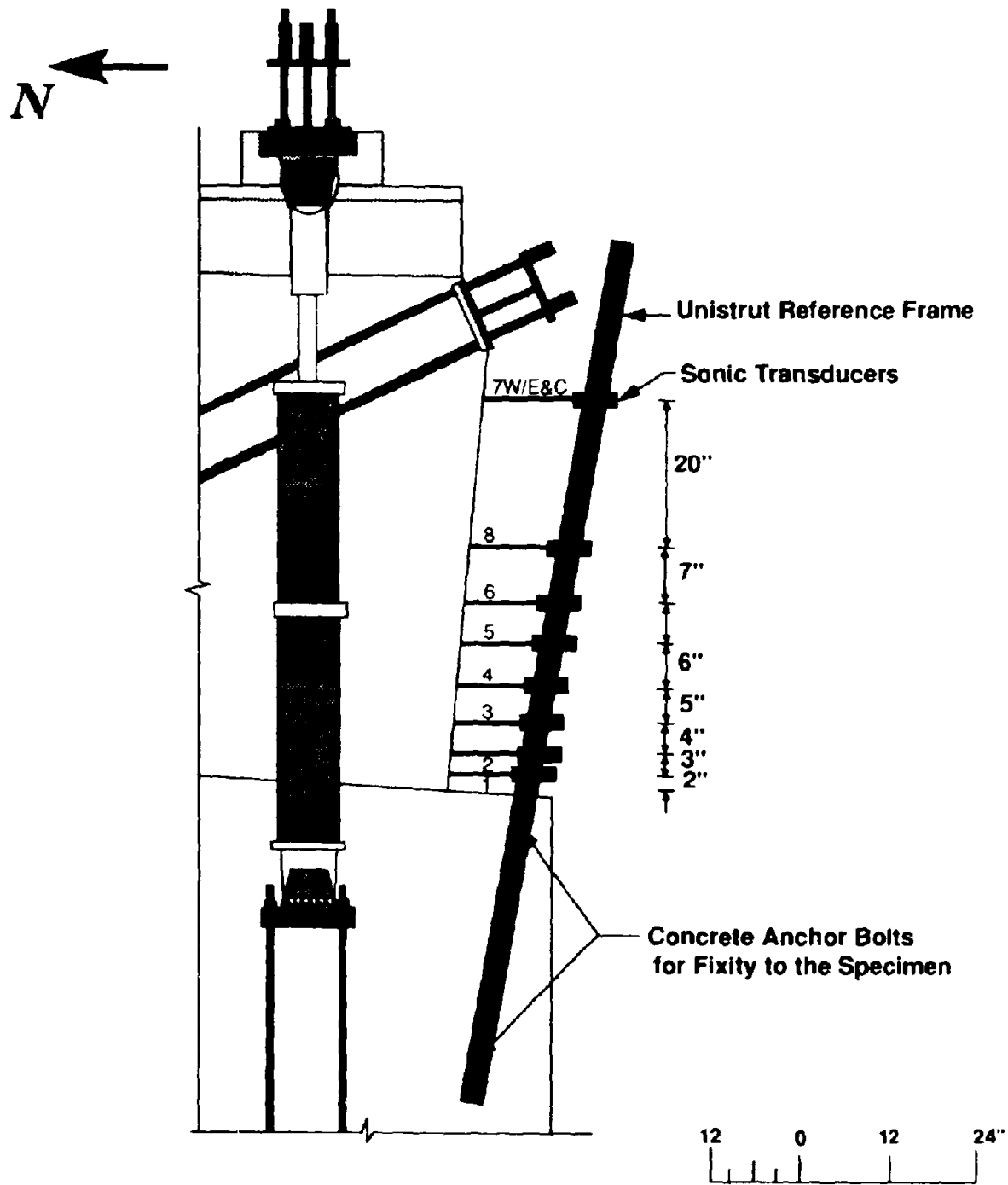
Fig. 4.6 Instrumentation Details: Arrangement of Sonic Transducers
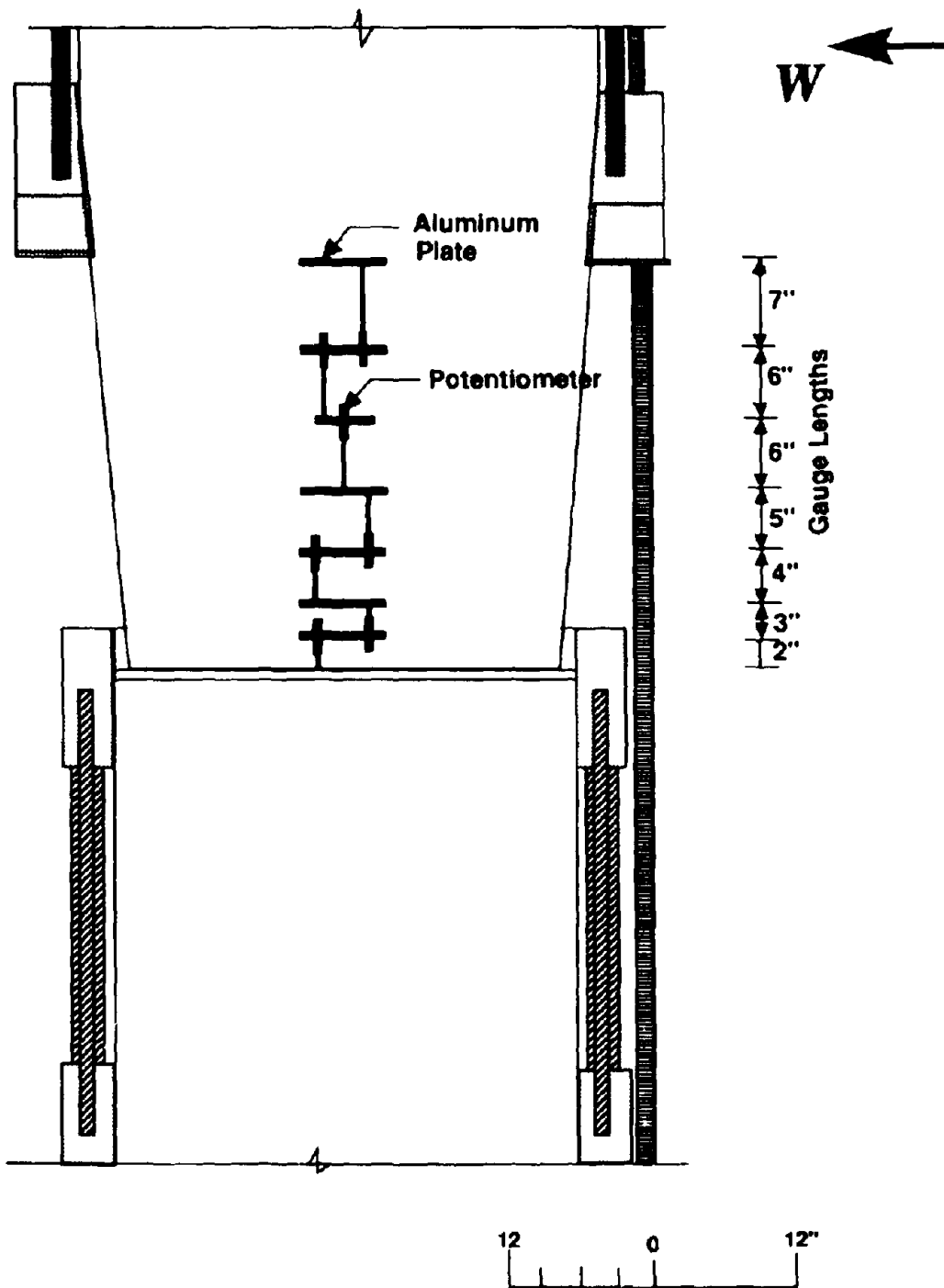
Fig. 4.7 Instrumentation Details: Arrangement of Linear Potentiometers

4-13
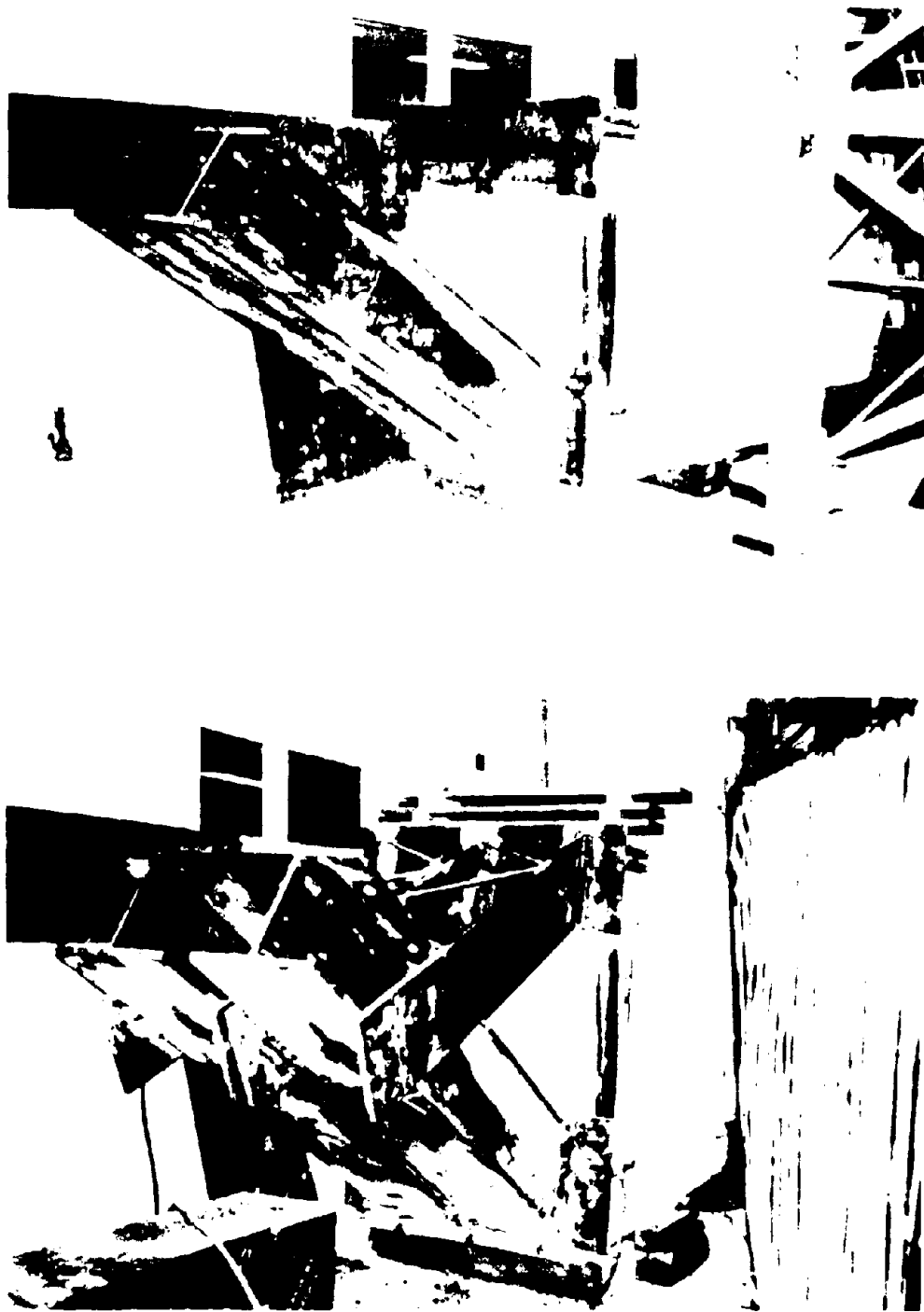
Fig. 4.8 Construction of Reaction Frame
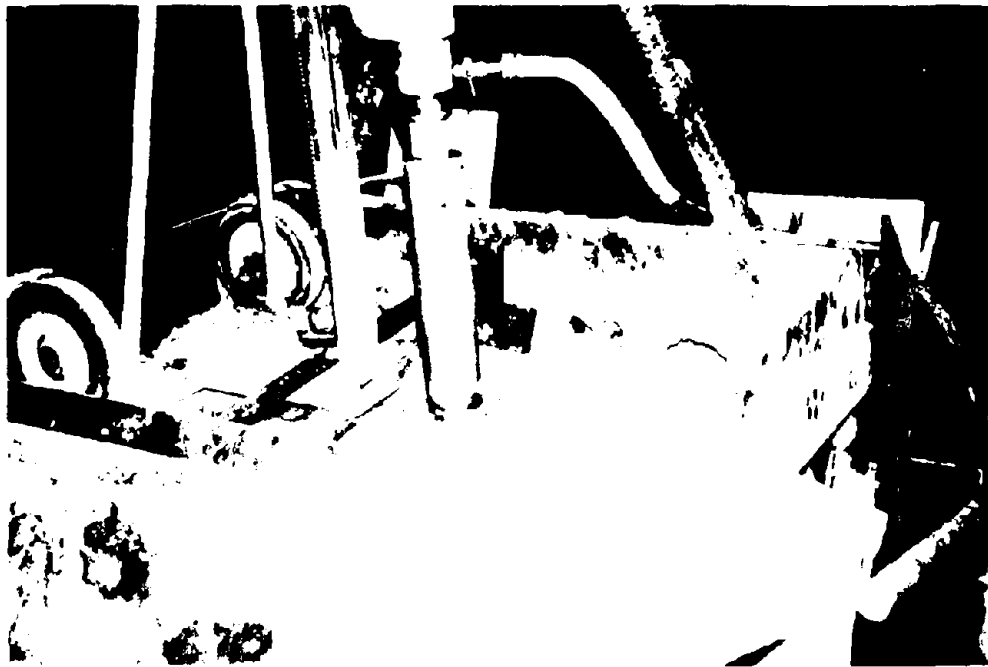
Fig. 4.9 Concrete Core Drilling Operation

Fig. 4.10 Bolster Bearing over the Concrete Filled Steel Box
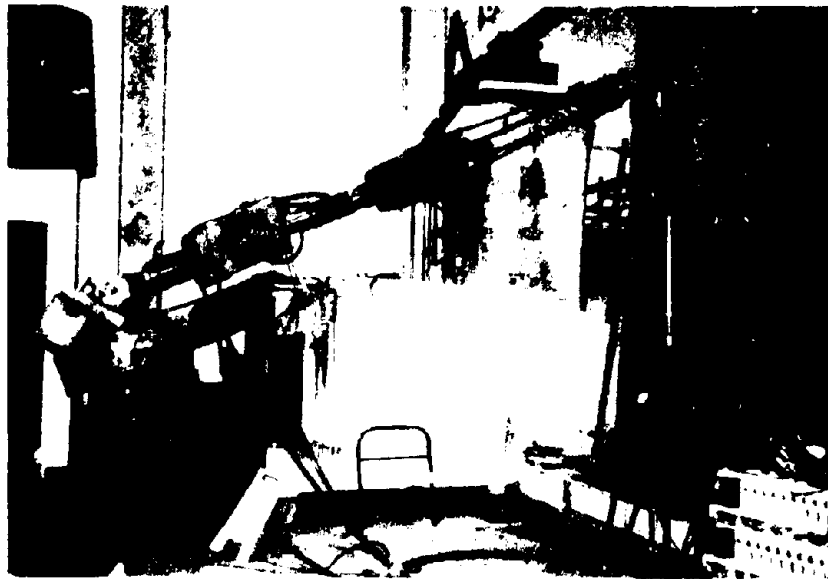
Fig. 4.11 Experimental Setup after Instrumentation

SECTION 5
EXPERIMENTAL RESULTS AND OBSERVATION
FOR THE PROTOTYPE

5.1 Introduction

In this section, the testing procedure, observations during the test and the results from the data reduction are presented. It also includes a brief explanation of the data reduction procedures.

5.2 Testing Procedure

The specimen was tested in two stages with different loading frequencies. The first and second stages are referred to as Quasi Static and Quasi Dynamic loading, respectively.

The Quasi Static stage consisted of a series of loading cycles at different drift or force levels. In order to ensure the proper functioning of the transducers and potentiometers, an elastic *Force Control* cycle with an amplitude of ± 90 kips was firstly applied. The results from all instruments were checked following this initial cycle. As the lateral force was to be provided through two actuators, it was necessary to ensure that an equal amount of force/drift would be provided by each of them during the *Drift Control* cycles in order to avoid torsion. A cycle with 0.1 % drift amplitude was provided after the ± 90 kips cycle with two separate instruments i.e. transducers 7E and 7W working as the controls for east and west sides actuators respectively. The forces in the two actuators did not remain equal during this cycle, therefore another *Force Control* cycle of ± 200 kips amplitude was then applied. For the remaining part of the testing, the control scheme shown in Fig. 5.1 was adopted. The transducer 7C controlled the movement of the east-side actuator. Feedback from this actuator was used to control the displacements of the west-side actuator. In this manner, equal displacements, and similar but not identical forces, were achieved through both actuators. After the ± 200 kips force

5-1

amplitude cycle, all the tests were controlled by drift levels which included one cycle with ± 0.25 % drift amplitude which was followed by two cycles each with ± 0.5 %, ± 0.75 %, ± 1.0 %, ± 1.5 % and ± 2.0 % drift amplitudes. The lateral displacements were applied as sine wave cycles with a frequency of 0.00277 Hz (Period = 360 seconds) during this stage of loading.

The Quasi Dynamic Stage consisted of 5 and 17 loading cycles with ± 3.0 % and ± 4.0 % drift amplitudes respectively. The cyclic frequency was 0.0167 Hz (Period = 60 seconds) during this stage.

A constant vertical (gravity) force of 269 kips was applied at the column's top during both stages of loadings. However, the actual vertical force varied during the tests because of the vertical component of the lateral force which was about 41 % of the actuator loads.

The records of all instruments were logged using the Megadac Data Acquisition System during the experiment. The data sampling rates for Quasi Static and Quasi Dynamic Stages were 1 and 3 Hz respectively.

5.3 Observations During the Test

Due to the slow Quasi Static Loading rate, it was possible to closely observe the specimen during the test for the appearance of cracks. The test was filmed through video cameras and photographs were taken during most of the stages. Cracks at the various drift levels were marked in different colors in order to get a better picture of their formation sequence as follows:

Drift Levels	Color/Pattern
0.25 % and before	green
0.50 %	blue
0.75 %	black
1.00 %	red
1.50 %	dashed green
2.00 %	white

Figs. 5.2 to 5.6 show the extent of damage and cracking at different stages of testing. A description of the visual observations during the tests is presented below.

During the ±90 kips force amplitude cycle, only two hairline cracks were observed in the capping beam. One of them was at the north-western corner of the beam-column joint and it extended down to a few inches into the capping beam. The other crack was observed on the western face of the capping beam near the centerline of the column/bearing. No additional cracking was observed during the ±0.1 % drift level cycle.

Many new cracks appeared during the ±200 kips force amplitude cycle. They included a crack in the capping beam similar to the previous corner crack which extended in length during this cycle. Some cracking occurred at the northern and southern faces of the column, both above and at the beam-column interfaces.

No new crack was observed during the ±0.25 % drift amplitude cycle, but some of the already present cracks extended in length.

At ±0.5 % drift amplitude, the cracks in the capping beam extended down to its bottom in somewhat diagonal direction. There was some lengthening of the column cracks as well. New diagonal shear cracks were also observed at the centers of the eastern and western faces of the column. These cracks did not penetrate up to the edges of the column at this stage. Fig. 5.2 includes the photographs of the specimen during these initial stages of testing.

As it is evident from Fig. 5.3, the diagonal shear cracks became continuous on both eastern and western faces at ±0.75 % drift amplitude. An increase in continuity was noticed in other previously occurred cracks also. Some penetration of the capping beam's cracks was observed in a horizontal direction. The level at which this penetration occurred varied from 4" to 6" below the beam-column joint. The widening of the interface's cracks at the peak levels of the cycles revealed that this penetration resulted because of separation of the beam and column concrete at the construction joint, as those cracks were penetrating vertically downwards.

Photographs during the later stages of the Quasi Static loading are presented in

Fig. 5.4. At the ± 1.0 % drift amplitude, more cracking occurred and most of it was near the centerline of the column. This might have taken place due to the weakening of the section in that zone because of the diagonal cracking. At ± 1.5 % and ± 2.0 % drift amplitudes, fresh cracks did not appear. However, the already present cracks either widened or extended in length during these cycles. The crack at the construction joint became continuous at ± 1.5 % drift amplitude and separation of a small piece of concrete from this location at ± 2.0 % drift amplitude exposed the joint. The two different colors of concrete could be easily observed above and below the joint.

Although significant amount of tension and shear cracking occurred, there was no spalling of concrete due to high compression strains during the Quasi Static stage of loading. The only wide cracks which appeared, were at the beam-column interfaces at the peak levels of the loading cycles.

Figs. 5.5 and 5.6 respectively include photographs of the specimen taken during and after the Quasi Dynamic stage of loading. The concrete started spalling during the ± 3.0 % drift amplitude cycles. However, it was only observed at the northern face of the column at this level. i.e. the face which was under tension in case of positive loading. The potentiometers which were mounted at this face detached and fell down during the loading cycles. At the southern face, a wide crack appeared near the top of the column as a result of extension of an existing diagonal crack. The reinforcing bars were exposed at the northern face and some plastification was observed in them during these cycles. The exposed hoops started opening and the thin tie wires which joined their ends were seen broken at this stage of loading. Most of the concrete spalling took place from the region between the two intersecting diagonal cracks. After the ± 3.0 % drift level cycles, all the instruments except the controlling transducer were taken off the specimen.

At the ± 4.0 % drift amplitude, the specimen became increasingly damaged as the cycling progressed. The spalling of concrete at the southern face began in the first cycle at this level. The exposed stirrups opened out completely, the concrete at the base of the column was damaged entirely and significant shortening of the column was also observed

5-4

along with buckling of longitudinal reinforcing bars. The vertical load of 269 kips was sustained by the column up to the end of the testing. The column remained plastic throughout this loading phase and all the reinforcing bars remained intact. Although the column concrete adjacent to the joint was crushed entirely during this test, yet there was no significant damage in the capping beam.

5.4 Data Analysis

Forces and Total Displacements/Drifts: The force and displacement data was retrieved directly during the test through the actuators' load cells and the sonic transducers respectively. The drifts were calculated from the displacements using the method described in the previous section.

Strains: The strains were calculated by the relation,

$$\epsilon_i = \frac{\Delta_i}{L_{gi}} \tag{5-1}$$

in which i = level of the gauge length, L_{gi} = gauge length and Δ_i = displacement from the potentiometer data.

The first gauge length was taken as 6.25" which included the depth of the construction joint which was 4.25" below the column base.

Curvatures and Rotations: The rotations over a given gauge length are calculated as:

$$\alpha_i = \frac{\Delta_{pi}}{L_{pi}} \tag{5-2}$$

and the curvatures are calculated as:

$$\phi_i = \frac{\alpha_i}{L_g} = \frac{\Delta_{pi}}{L_p L_{gi}} \tag{5-3}$$

in which Δ_{pi} = algebraic difference of the potentiometer readings, and L_{pi} = center to center distance between the potentiometer pairs.

The plastic hinge rotation was taken as the sum of the rotations of the first four

gauge lengths as most of the plastification took place in that region, that is,

$$\alpha = \alpha_1 + \alpha_2 + \alpha_3 + \alpha_4 \qquad (5\text{-}4)$$

Flexural and Shear Displacements: The flexural and shear components of the displacements were calculated by the method explained in Subsection 3.4.

Energy Absorption: The hysteretic energy absorbed by the pier was determined through Eq. 3-7.

5.5 Experimental Results

As the potentiometer data was not available for the Quasi Dynamic Stage of testing, the synthesis of the total displacements into flexural and shear displacements and evaluation of strains, rotations and curvatures was possible only for the Quasi Static Stage.

5.5.1 Forces and Total Displacements

Hysteretic Performance: The Lateral force versus Column drift relationships of the pier for both Quasi Static and Quasi Dynamic loadings are shown in Fig. 5.7. In the Quasi Static Stage, all the tests before the ± 0.5 % drift amplitude cycle are referred to as the *initial tests.*

The pier behaved elastically during the ±90 kip force amplitude, and ±0.1 % drift level loading cycles. During the second half of the ±200 kip force amplitude cycle, the pier started entering the plastic range. The actuator force versus drift curve for ±0.25 % drift amplitude cycle was almost linear in nature. But, it also revealed that some damage had been done to the specimen in the preceding cycle, as a smaller force was used to attain a higher drift under the negative loading. The plastification continued to increase in the cycles at higher drift levels which followed.

On the whole, the pier behaved in a ductile fashion and the Force versus Drift

curves show good energy dissipation characteristics. No fracture of the reinforcing bars was observed but their plastic buckling deformations were obvious once the concrete cover had spalled off.

Flexural and Shear Displacements: The Force versus Drift curves for total, flexural and shear components of the drifts are shown in Fig. 5.8. It should be noted that these graphs are respectively based on direct measurement, Eq. 5.6 and Eq. 5.7. It may be interesting to note that the hysteresis loops for the flexural component of the drift are more elliptic in nature, while sharp pinching of the curves for the shear component occurred with each change in direction of the force. The variation of the peak values of the total and synthesized, flexural and shear displacements along the column height is shown in Fig. 5.9. It was noticed that the peak shear displacements were more than the flexural displacements under the negative (heavier axial load) loading, but smaller in case of the positive loading. Figs. 5.14, 5.15 and 5.16 show the variation of flexural and shear displacements at peak drift levels, as percent of the total displacements, with loading cycles, drift levels and the cumulative drift respectively. The percentage of the shear displacement was high during the initial test, then became smaller, and increased once again.

5.5.2 Curvatures and Strains

The rotations, strains and curvatures were evaluated for the Quasi Static Stage with Force versus the Plastic Hinge Rotation relationship presented in Fig. 5.10. It is evident from the figure that the flexural rotations under the positive loading are larger when compared to those under the negative loading. Again, this difference is attributed to the different relative magnitudes of flexural and shear displacements under forward and reverse loadings.

The Force versus Curvature relationships for all the gauge lengths are presented in Fig. 5.12. The curvatures at the second and third gauge lengths locations were very small as compared with the ones at the fourth and fifth gauge lengths. Fig. 5.11 shows the variation of peak curvatures along the column height as well as the pattern of

cracking on the column. It is evident from this figure that almost no cracking took place in the second and third gauge lengths. As most of the cracking occurred in the fourth and fifth gauge lengths, the evaluated curvatures were larger in those zones.

The strain profiles at the bottom gauge lengths under both positive and negative loadings are shown in Fig. 5.13.

5.5.3 Strength Degradation and Energy Absorption

The degradation in strength of the pier in each loading cycle can be seen in Fig. 5.17. In Fig. 5.18, the peak forces are plotted versus cumulative peak drifts provided during the test. It is evident from the figures that the degradation in strength during the Quasi Static Stage was quite small as compared to the Quasi Dynamic Stage. Almost no degradation was observed during the first stage under the positive loadings. It increased with the drift amplitudes until the specimen was severely damaged under the ± 4.0 % drift amplitude loading cycles. Evidently, there was little degradation of the pier strength between the successive cycles near the end of the testing. The jump in the force magnitude in the hysteretic loop was due to the obstruction to displacement because of broken pieces of concrete, and not because of an increased strength.

The peak forces for the negative loads remained more than those for the positive loadings throughout the Quasi Static Stage. As it is evident from the photographs in Fig. 5.5, there was little damage in the concrete at the column's southern face during the ± 3.0 % drift amplitude loading. Therefore concrete provided enough resistance in compression at this face until it became severely damaged during the first cycle at the ± 4.0 % drift amplitude loading when the peak force for the negative loading became larger once again, although this was for only one cycle. The difference between the shapes of the degradation curves for the negative and positive loadings as shown in Fig. 5.17 is an interesting feature to note.

The energy absorption plotted against the loading cycle is shown in Fig. 5.19. From this graph, it can be seen that the maximum energy was absorbed during the first ± 3.0 % drift amplitude cycle when crushing of the cover concrete occurred. It can also

be noted that the absorption became constant near the end of testing, when all the concrete at the column's base was damaged and the energy was mostly absorbed by reinforcing bar slippage. This is also evident in Fig. 5.20 where cumulative energy is plotted against cumulative drift.

5.6 Summary

1. The experimental technique permitted the decomposition of total force displacement response into flexural and shear components. The shear component contributed 40 to 70 percent of the overall displacement, the higher value being for when the larger axial load was present.

2. Significant strength degradation under repeated cyclic loading took place when the drift limit exceeded 2 percent.

3. After 9 cycles at the 4 percent drift level, a constant lateral resistance was encountered and a constant energy absorption occurred after the 4th cycle. This was observed to be due to frictional slippage resistance of the column reinforcing bar anchorages in the capping beam.

4. The strength degradation was more abrupt under the negative (heavier axial load) loading as compared to the positive (lighter axial load) loading.
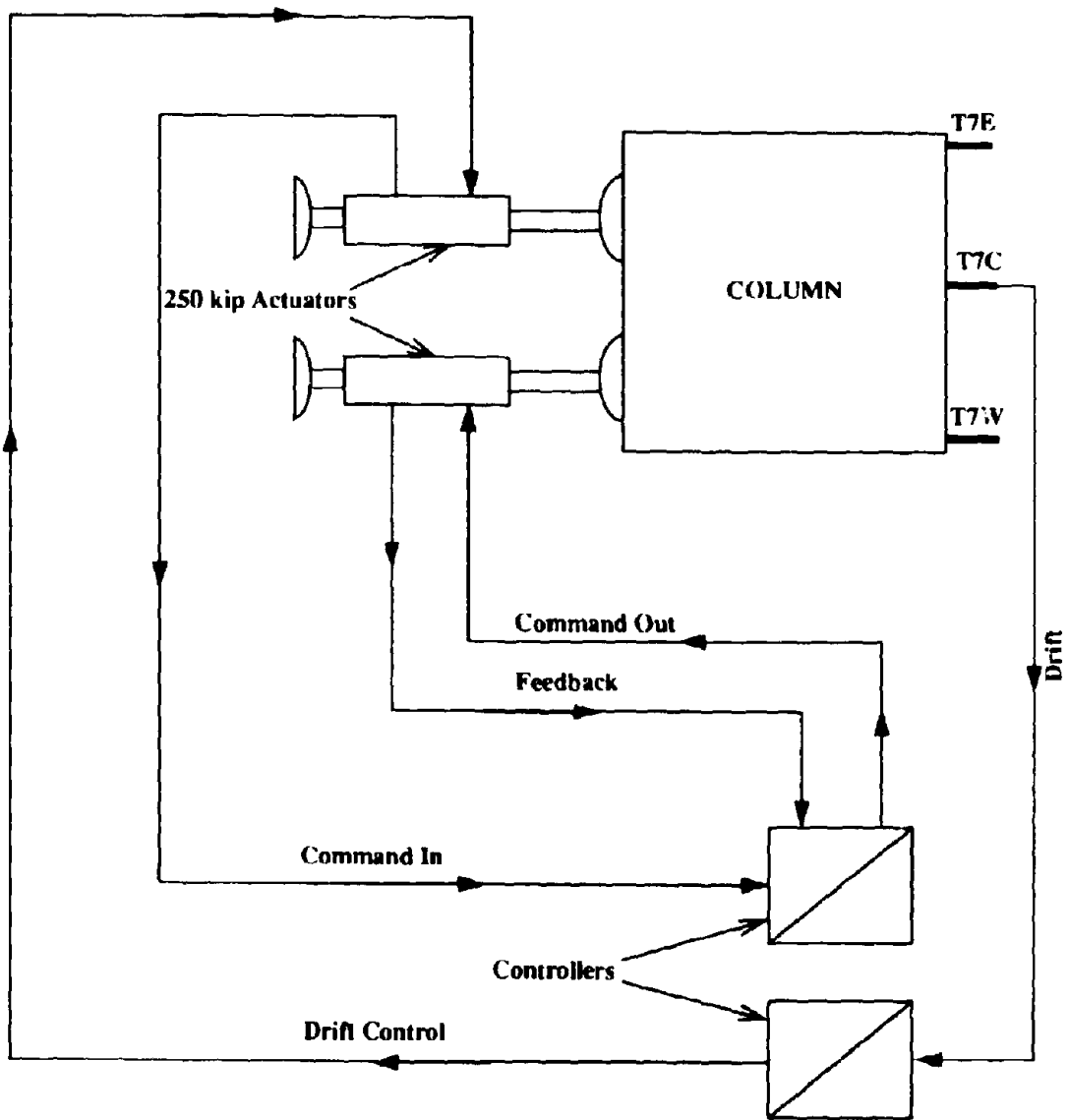
Fig. 5.1 Control Schematic for the Prototype
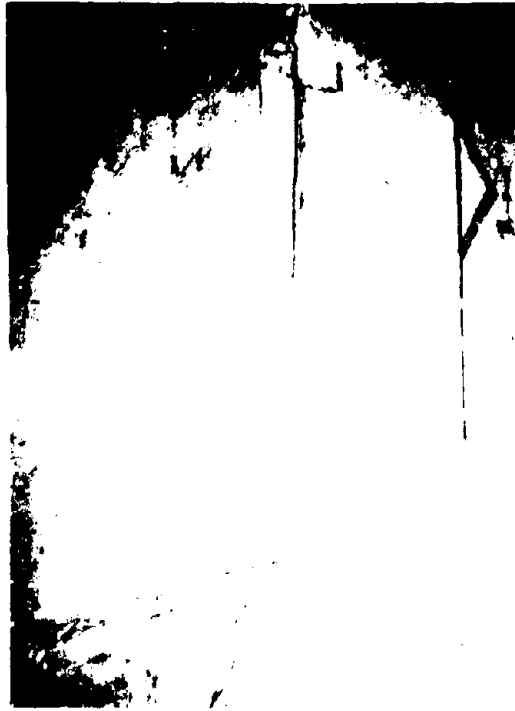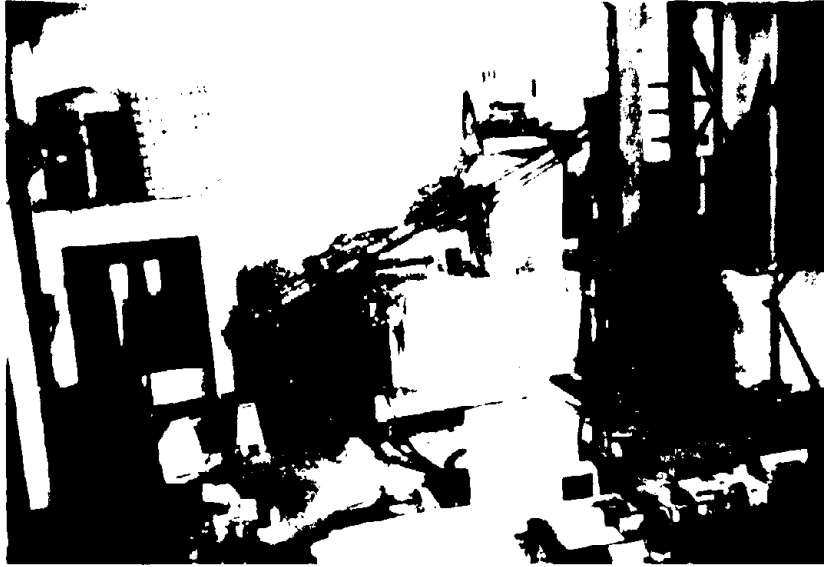
Fig. 5.2 Specimen during Initial Stages of Testing

Fig. 5.3 Specimen after 0.75 % Drift Amplitude Cycles
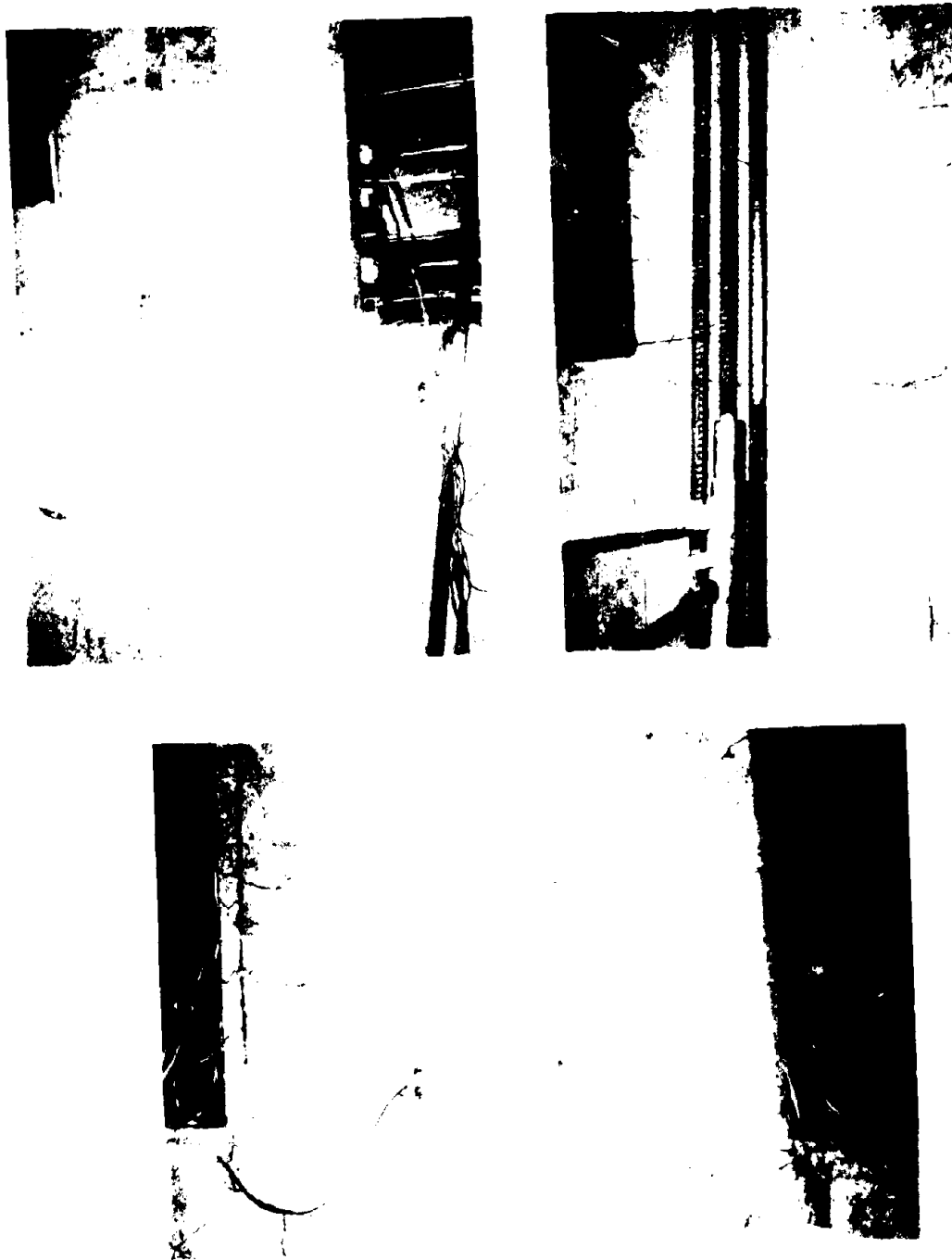
Fig. 5.4 Specimen during Later Stages of Quasi-Static Loading

5-13

Fig. 5.5 Specimen after 3.0 % Drift Amplitude Cycles
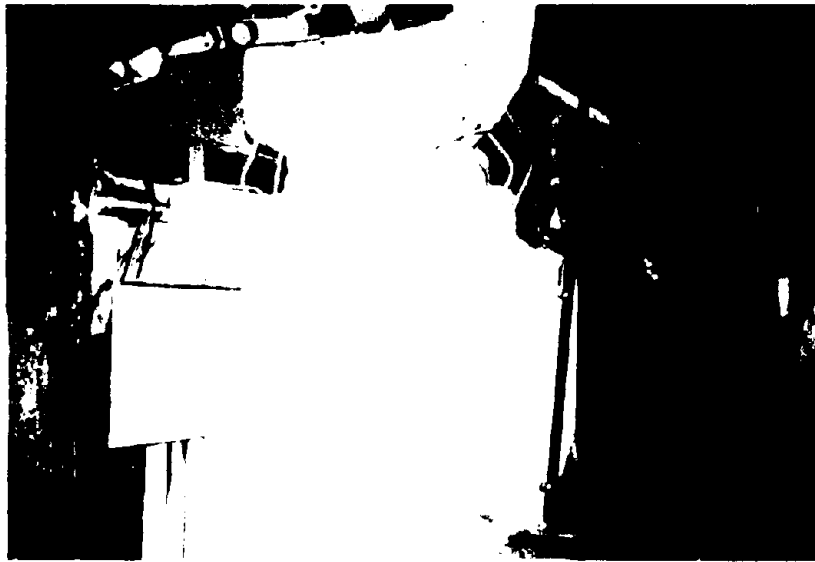
Fig. 5.6 Specimen after Quasi-Dynamic Stage of Loading
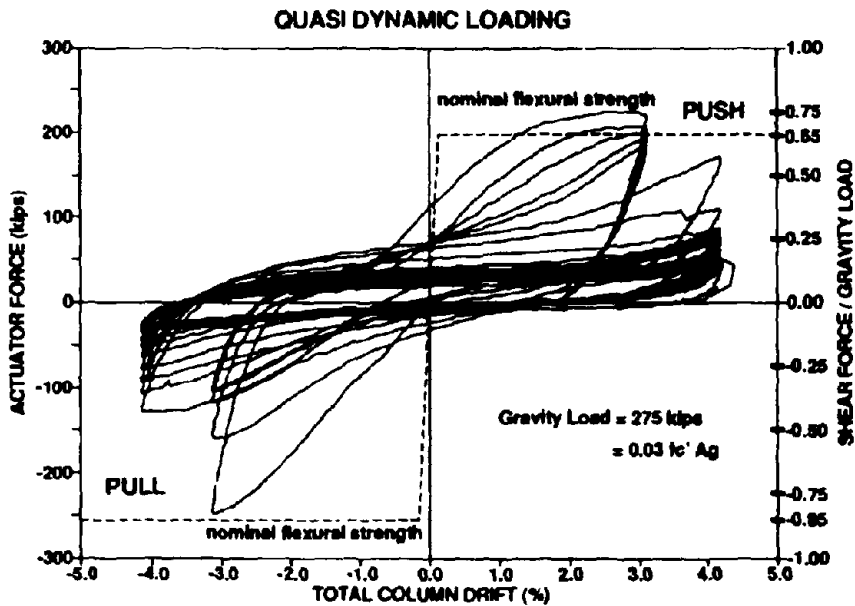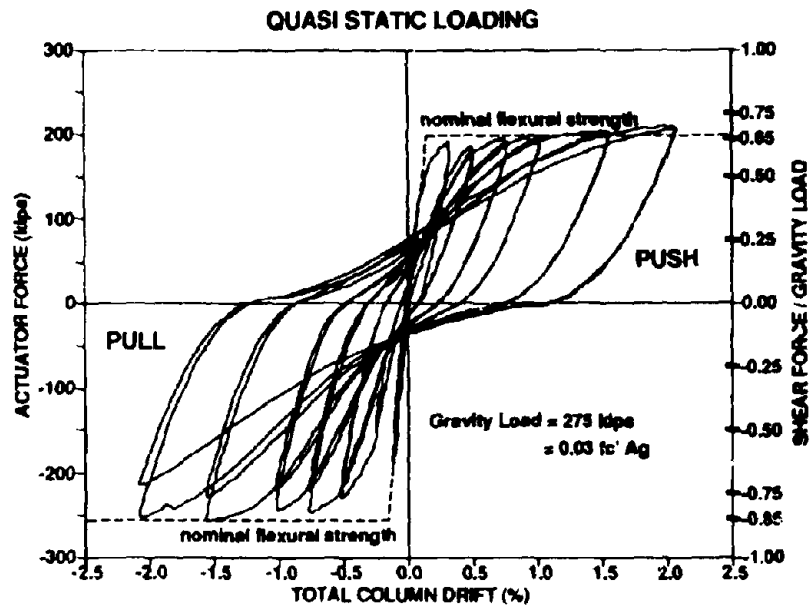
Fig. 5.7 Experimental Lateral Actuator Force - Column Drift Relationship
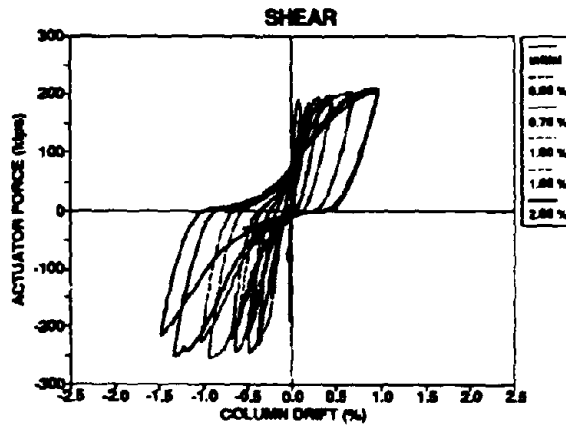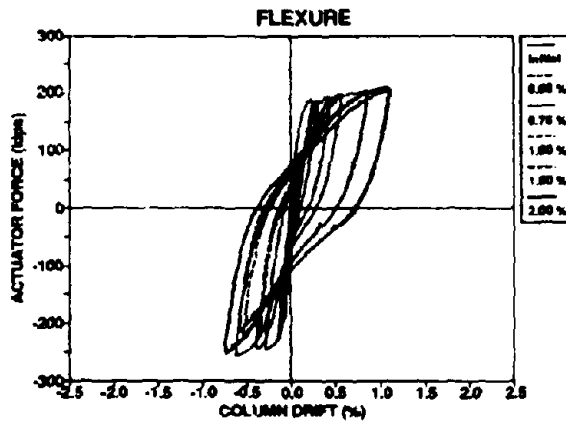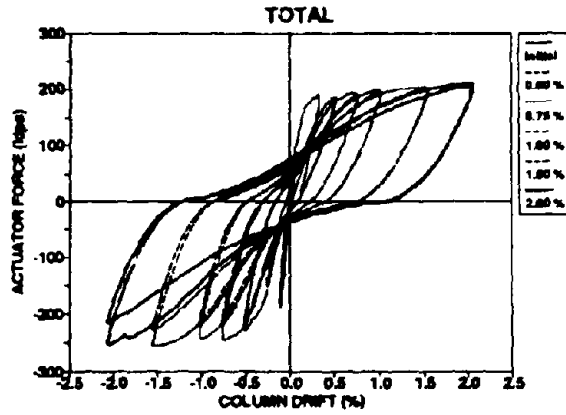
Fig. 5.8 Force vs Synthesised Total, Flexural and Shear Drifts

5-17
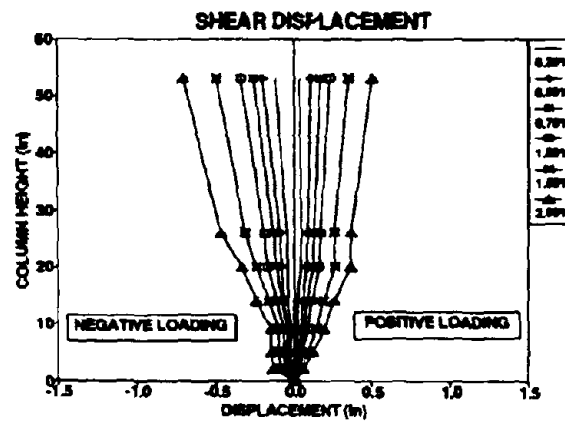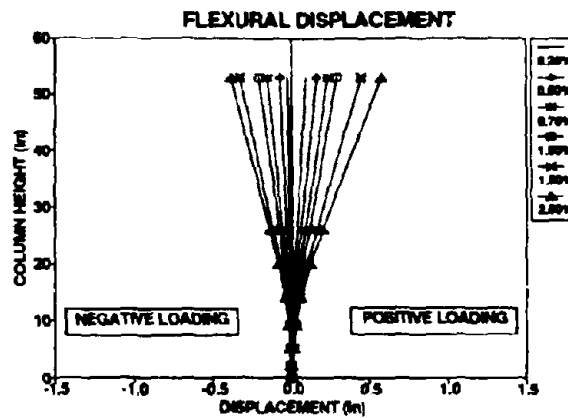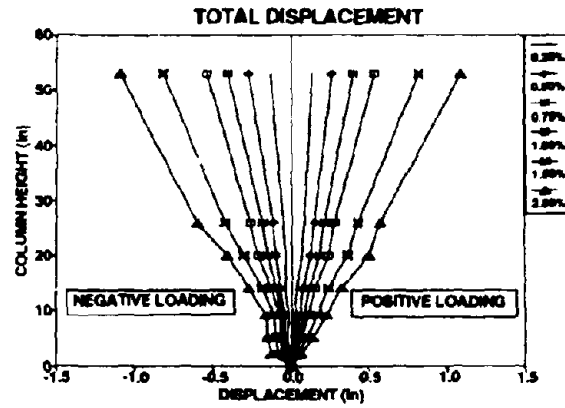
Fig. 5.9 Synthesis of Total, Flexural and Shear Displacements along Column Height
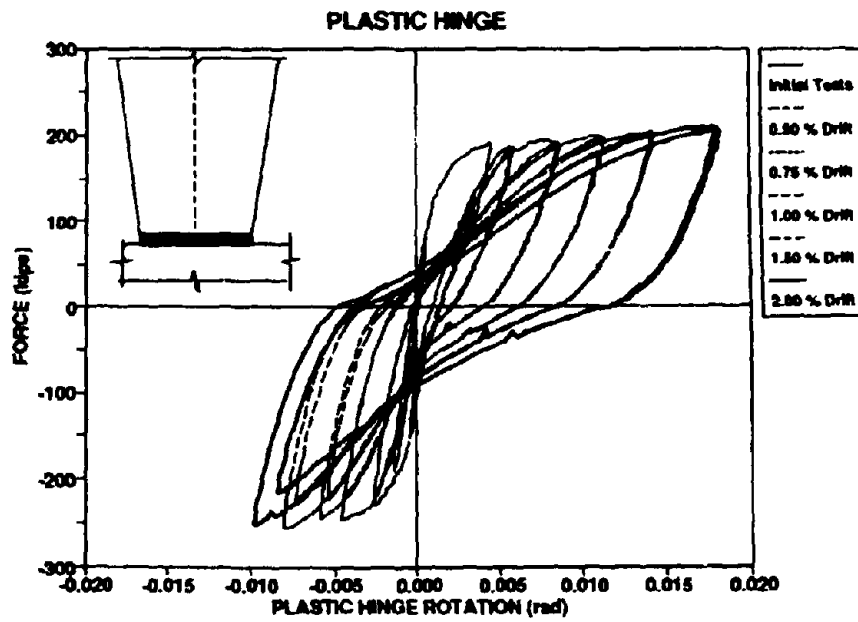
Fig. 5.10 Experimental Force - Plastic Hinge Rotation Relationship
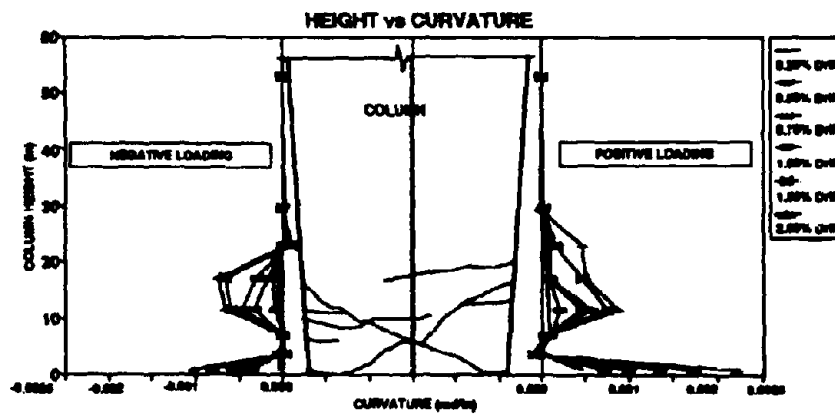
Fig. 5.11 Distribution of Curvatures along Column Height
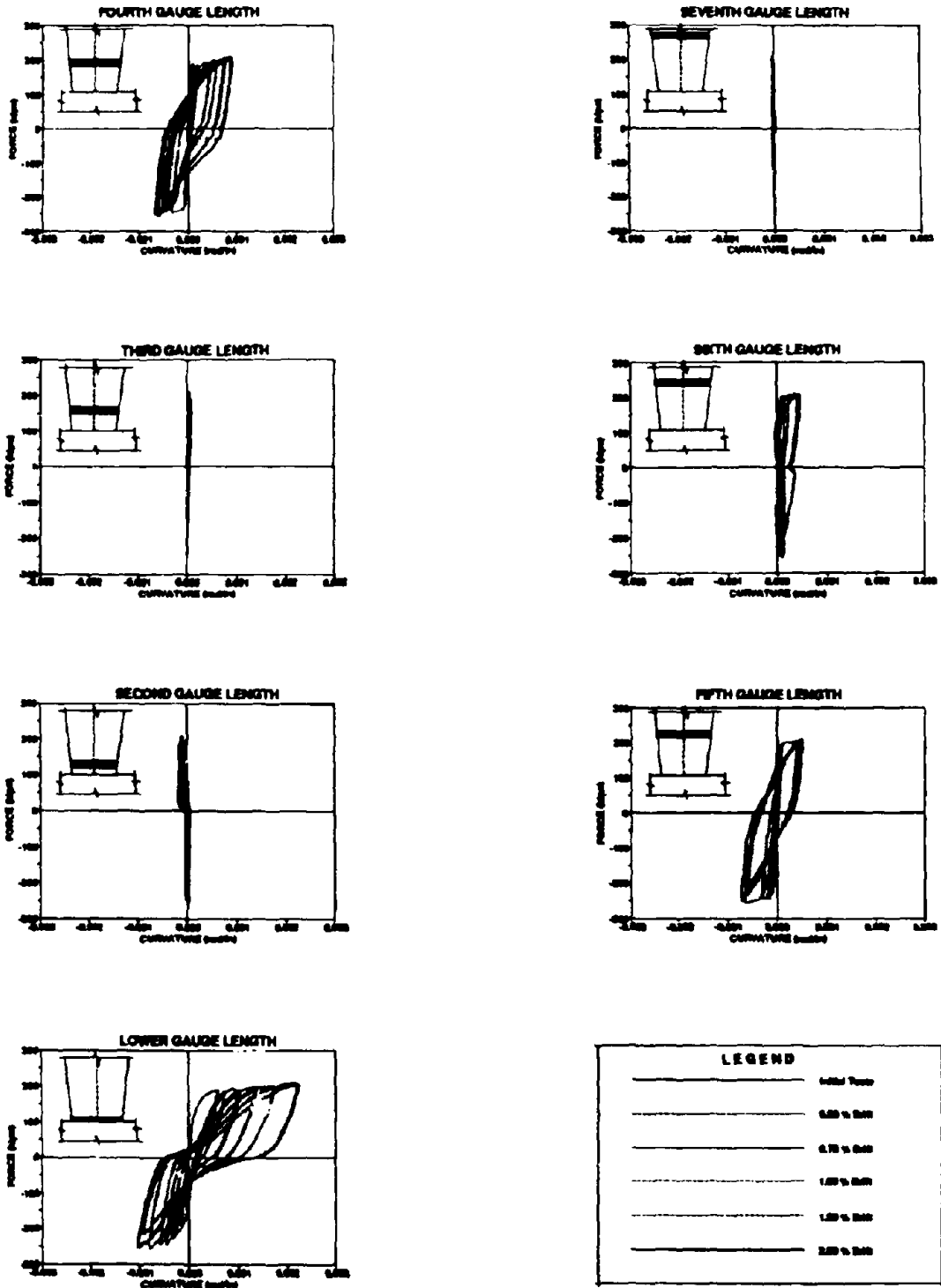
Fig. 5.12 Experimental Force - Curvature Relationships
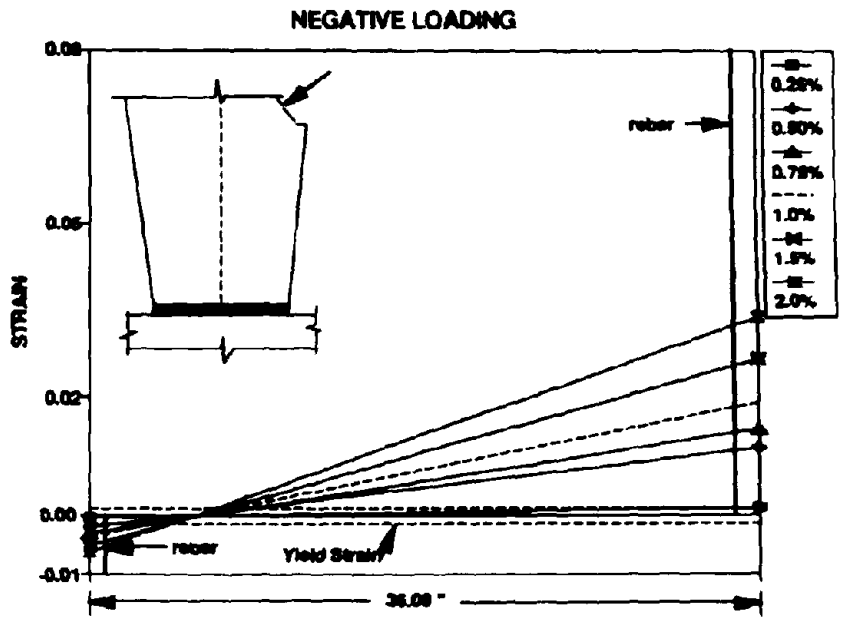
Fig. 5.13 Strain Profiles for Lower Gauge Length
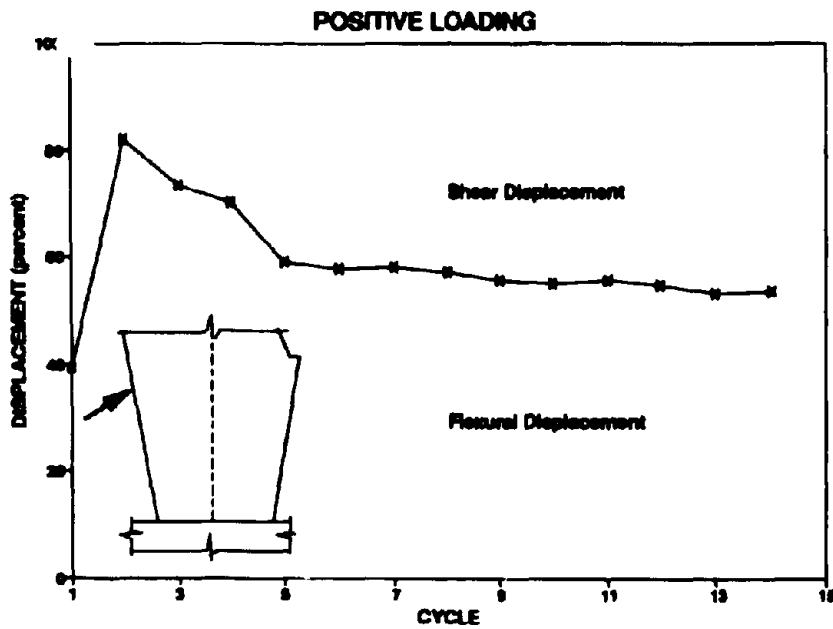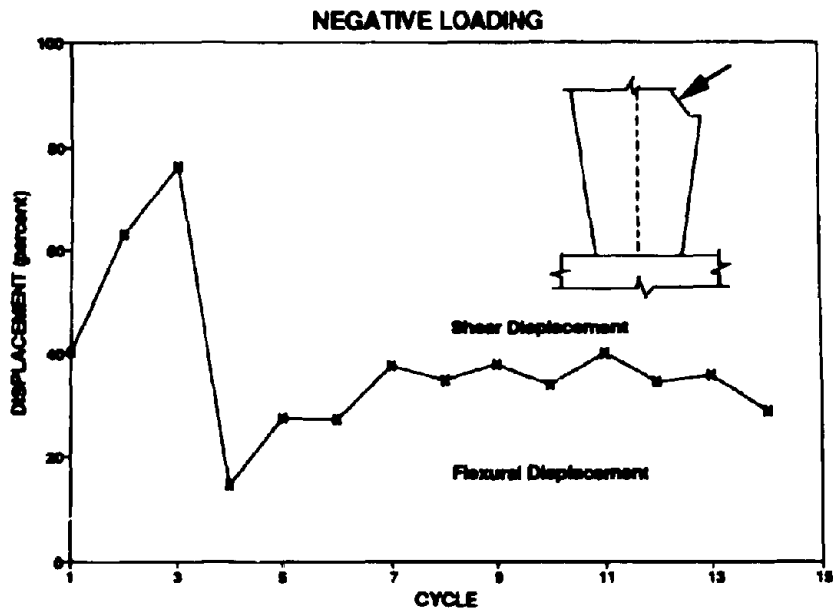
Fig. 5.14 Flexural and Shear Displacement in Each Loading Cycle
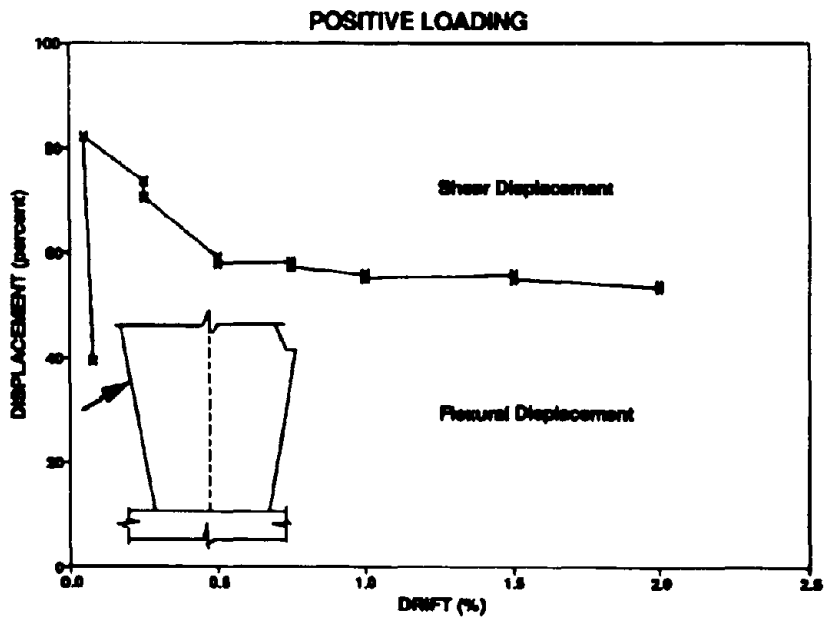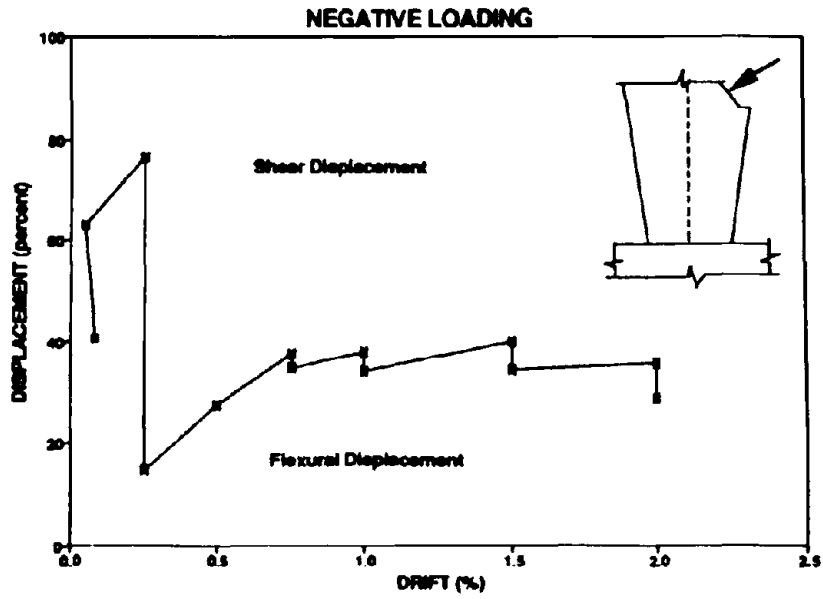
Fig. 5.15 Flexural and Shear Displacement vs Drift
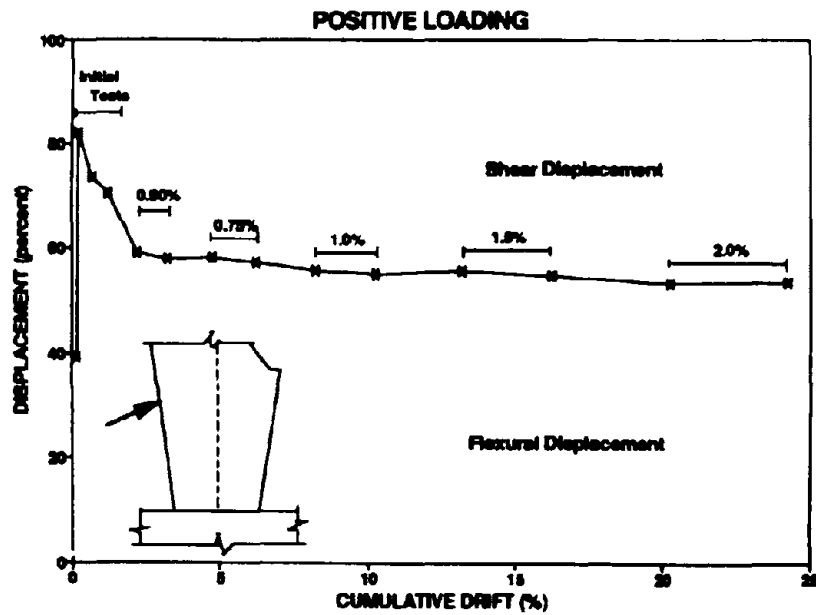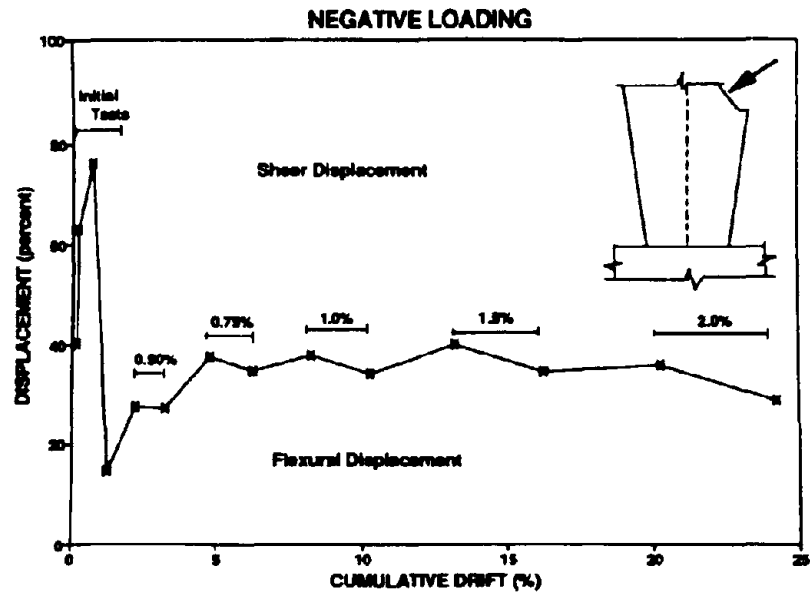
Fig. 5.16 Flexural and Shear Displacement vs Cumulative Drift

PEAK FORCE vs LOADING CYCLES
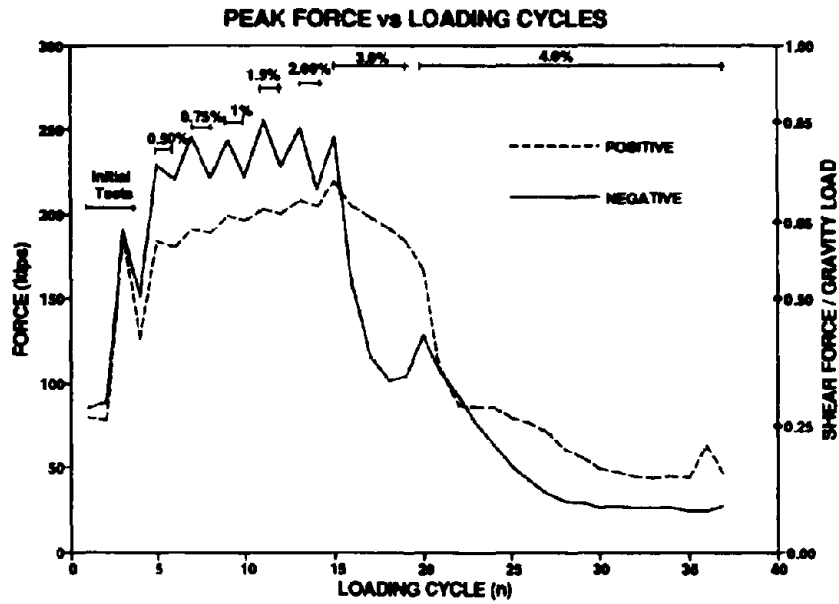
Fig. 5.17 Peak Lateral Actuator Force in Each Loading Cycle

PEAK FORCE vs CUMULATIVE DRIFT
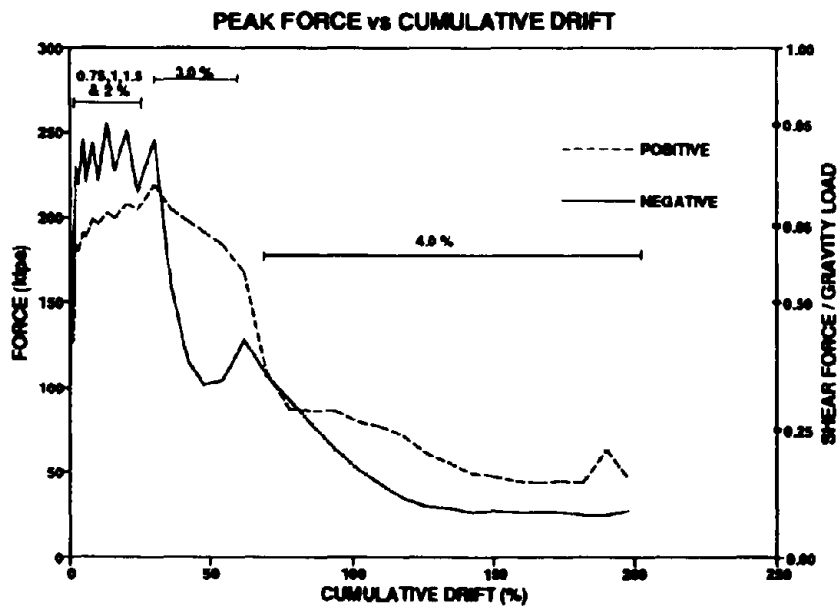
Fig. 5.18 Peak Lateral Actuator Force vs Cumulative Drift Relationship
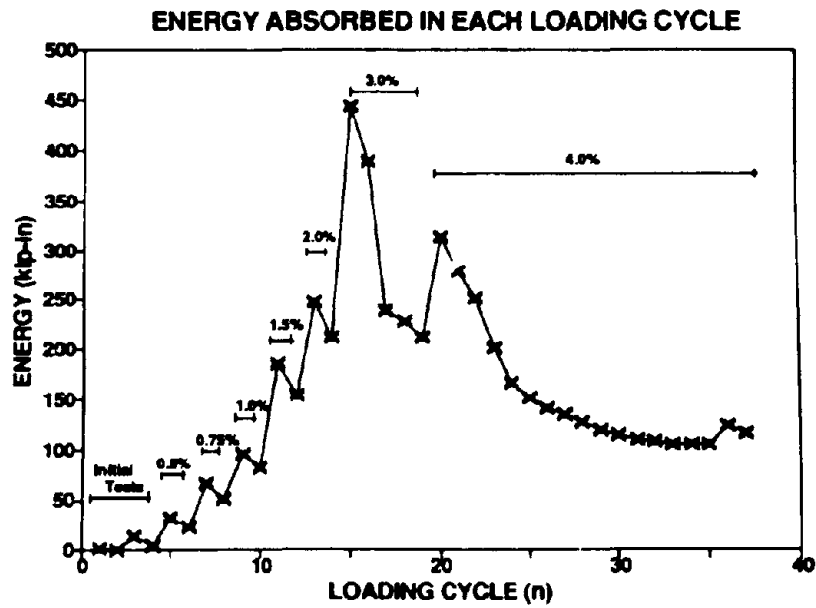
Fig. 5.19 Energy Absorbed in Each Loading Cycle
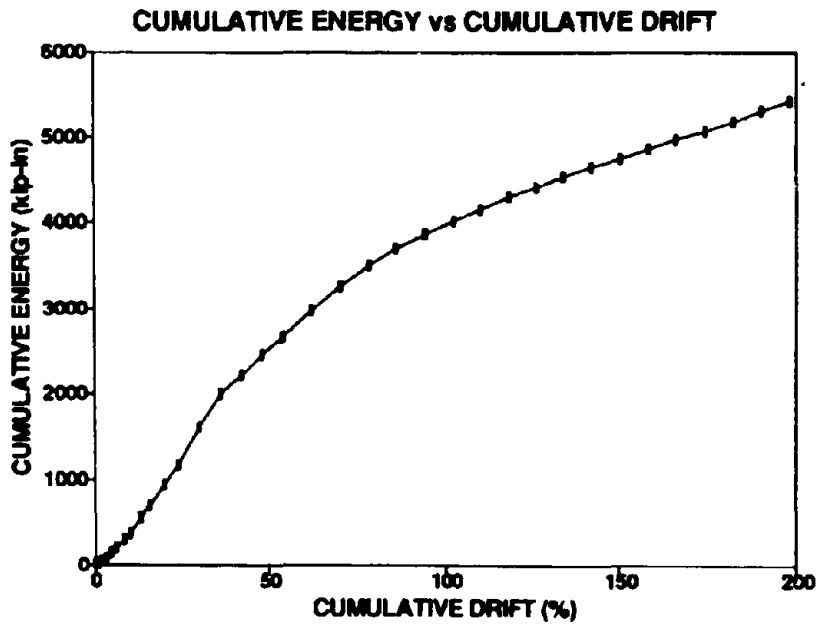
Fig. 5.20 Cumulative Energy vs Cumulative Drift Relationship

5-26

SECTION 6

STRENGTH AND DEFORMATION ANALYSIS

6.1 Introduction

In this section, a theoretical analysis for strength prediction and deformation behavior is presented for both the model pier and the prototype column to cap specimen. A comparison is made between code based formulations and the experimental results. Finally, a seismic vulnerability analysis of such bridge piers is presented.

6.2 Flexural Strength and Deformation

6.2.1 Model Pier Strength

The ultimate flexural strength of the pier was found by carrying out a plastic analysis of the bent with hinges forming in the columns as shown in Fig. 6.1a. Employing the virtual work method of plastic analysis,

$$F_p = \frac{M_{p1} + M_{p2} + M_{p3} + M_{p4}}{L_c} \tag{6-1}$$

in which M_{p1} to M_{p4} are the plastic hinge moment capacities shown in Fig. 6.1 and L_c is the clear height of the column. The plastic moment capacity at each hinge location was found from the column interaction diagram shown in Fig. 6.1b. The calculations were based on the usual ACI 318 assumptions, namely; an ultimate compression strain $\epsilon_{cu} = 0.003$, an average concrete stress across the stress block of $0.85 f_c'$ with a depth of $a = \beta_1 c$ where c is the neutral axis depth and

$$\beta_1 = 0.85 - 0.05 \left(\frac{f_c' - 4000}{1000} \right) \tag{6-2}$$

and employing the measured material properties described in Section 2.4. Note that no capacity reduction factor was used in the analysis ($i.e$ $\phi = 1.0$). At locations 1 and 4 the column cross-section is 11"x11" while at locations 2 and 3 it is 9"x9". Determination

of F in Eq. 6-1 is of an iterative nature as M_p is a function of axial load. The changes in the axial load are found by determining the overturning reactions (T and C) by taking moments about the base:

$$F_p \times L_c = M_1 + M_4 + T \times L_b$$

$$T = C = \frac{F_p \times L_c - M_1 - M_4}{L_b} \tag{6-3}$$

These overturning reactions are added (C) or subtracted (T) from the gravity reactions and the moment capacity at each hinge is found by iteratively solving Eqs. 6-1 and 6-3.

6.2.2 The Prototype Column to Cap Specimen Strength

The total actuator force F, is used to determine the horizontal and vertical components of force that affect the flexural and shear strength capacities and are given by:

$$F_v = F \cos 24° \tag{6-4 a}$$

$$F_h = F \sin 24° = V \tag{6-4 b}$$

in which F_h = the horizontal force component and is equal to the column shear force V, and F_v = the vertical force component that adds to the column axial load. In Eq. 6-4 the 24° angle is the inclination above the horizontal of the 250 kip actuators. The applied axial load at the top of the column was 269 kip and when combined with the column's self weight gives a constant vertical load of 275 kip. Thus, the total vertical load is given by:

$$P = 275 - F \sin 24° = 275 - 0.407 F \tag{6-5}$$

where, P = compression positive, and reverse loading (negative F) will increase the axial compression in the column. The maximum column bending moment is given by

$$M = 53 F \cos 24° = 48.4 F \quad (in-kips) \tag{6-6}$$

Thus, the jack loads (in kips) in terms of nominal moment capacity and ultimate shear

are:

$$F_n = 0.0207 M_n \qquad (6\text{-}7)$$

$$F_n = 1.095 V_n \qquad (6\text{-}8)$$

The cracking, yield and nominal ultimate flexural strengths of the pier are presented in Table 6.1 for positive (forward) and negative (reversed) loading and the corresponding axial load vs moment interaction diagram is presented in Fig. 6.2.

In the analysis of the cracking strength, a concrete tensile strength of $7.5\sqrt{f_c'}$ was adopted. The yield forces were determined using straight line elastic theory, with no tension capacity of concrete contributing to the strength.

TABLE 6.1: Prototype Column Flexural Strength Capacities

		Negative Loading	Positive Loading
Cracking Force	(kips)	-172	155
Yield Force	(kips)	-202	161
Nominal Ultimate Jacking Force	(kips)	-256	197
Nominal Moment Capacity	(ft-kips)	-1034	794
Axial Load at Nominal Ultimate	(kips)	380	194

6.2.3 Ultimate Flexural Curvature and Displacement Ductility

The ultimate curvature and displacement were calculated using a plastic hinge concept. The equivalent plastic hinge length L_p was calculated by the relation suggested by Priestley and Park (1987):

$$L_p = 0.08L + 6d_b \qquad (6\text{-}9)$$

where L = length of the column from base to the point of contraflexure and d_b =

diameter of the main longitudinal reinforcing bars.

The nominal yield curvature ϕ_y is given by:

$$\phi_y = \phi_y' \frac{M_n}{M_y} \qquad (6\text{-}10)$$

where M_n = nominal ultimate moment, M_y = moment at first yield of the tension steel

with ϕ_y' = corresponding curvature given by:

$$\phi_y' = \frac{\epsilon_y}{d - kd} \qquad (6\text{-}11)$$

in which, kd = the neutral axis depth at first yield from the extreme compression fiber

and ϵ_y = yield strain of the tension reinforcement.

The ultimate curvature is calculated as:

$$\phi_u = \frac{\epsilon_{cu}}{c} \qquad (6\text{-}12)$$

where c = the neutral axis depth at the nominal ultimate moment, and ϵ_{cu} = ultimate

compression strain taken herein as 0.008 which is roughly equal to the spalling strain.

Finally, the ultimate flexural drift is calculated by the relation:

$$\theta_u = \theta_y + L_p \left(1 - \frac{0.5 L_p}{L} \right) (\phi_u - \phi_y) \qquad (6\text{-}13)$$

where θ_y = the drift at yield. Herein θ_y was taken as the experimentally observed value.

The ultimate ductilities for curvature μ_ϕ and displacement (drift) μ_Δ respectively, are

given by the following relationships:

$$\mu_\phi = \phi_u / \phi_y \qquad (6\text{-}14)$$

$$\mu_\Delta = \Delta_u / \Delta_y = \theta_u / \theta_y \qquad (6\text{-}15)$$

The results of the above calculations for the four hinge locations of the model pier and

the prototype column to cap specimen are presented in Tables 6.2 and 6.3 respectively.

TABLE 6.2: Determination of the Theoretical Ultimate Drift Angle for the Model Pier

Quantity		Hinge 1	Hinge 2	Hinge 3	Hinge 4
M_y	(in-kip)	227	176	214	272
M_u	(in-kip)	267	213	264	332
L	(inches)	12.22	9.78	9.75	12.25
L_p	(inches)	2.33	2.13	2.13	2.33
k		0.206	0.240	0.274	0.234
ϕ_y'	(rad/in)	0.000266	0.000342	0.000359	0.000276
ϕ_y	(rad/in)	0.000313	0.000415	0.000443	0.000337
ϕ_u	(rad/in)	0.011299	0.010256	0.006612	0.008122
θ_y	(percent)	0.25	0.25	0.25	0.25
θ_u	(percent)	2.56	2.12	1.42	1.89
μ_ϕ		36	25	15	24
μ_Δ		11	9	6	8

TABLE 6.3: Determination of the Theoretical Ultimate Drift Angle for the Prototype

Quantity		Positive Loading	Negative Loading
M_y	(in-kip)	7798	9793
M_u	(in-kip)	9526	12410
L_p	(inches)	9.49	9.49
k		0.258	0.295
ϕ_y'	(rad/in)	0.000055	0.000058
ϕ_y	(rad/in)	0.000067	0.000074
ϕ_u	(rad/in)	0.0021	0.0027
θ_y	(percent)	0.15	0.15
θ_u	(percent)	1.91	2.42
μ_ϕ		31	36
μ_Δ		13	16

6.2.4 Experimentally Observed Equivalent Plastic Hinge Length

Using the data obtained from the experiment, it is possible to evaluate the observed equivalent plastic hinge length at different drift levels. Eq. 6-13 can also be written as:

$$\theta_p = \frac{\Delta_u - \Delta_y}{L_c} = L_p (\phi_u - \phi_y)(1 - 0.5 \frac{L_p}{L}) \tag{6-16}$$

where θ_p = plastic hinge rotation (and drift) and $(\phi_u - \phi_y) = \phi_p$ = plastic curvature.

From this the ratio of plastic hinge length to the column height is calculated by:

$$\frac{L_p}{L} = 1 - \sqrt{1 - \frac{2\theta_p}{\phi_r L}} \qquad (6\text{-}17)$$

The results of this analysis are discussed below:

(a) Model Pier

The results of the experimentally observed plastic hinge lengths for the four hinge locations in the model pier are presented in Table 6.4. Yield drift for the model was found to be 0.25% from the experiment. As only one column was instrumented during the test, therefore calculations for hinges 1 & 2 (lighter column) and hinges 3 & 4 (heavier column) are performed corresponding to the Reverse and Forward loading cycle data respectively, assuming that the behavior of the model is symmetric in both directions.

(b) Prototype

The curvature and drift at yield were found to be 0.000085 and 0.0015 respectively, through the experimental results. Equivalent plastic hinge lengths at increasing drift amplitudes are given in Table 6.5.

It is evident from the results that the experimentally observed equivalent plastic hinge lengths increase with increasing drift amplitude, and are larger for the greater axial load under negative loading. It should also be noted that the pier experienced its peak force levels under 1.5 % and 3.0 % drift amplitudes for negative and positive loadings respectively. It therefore appears that an equivalent plastic hinge length of 7.5" could be taken for both the forward and reverse direction. It is of interest to note that this is 20 percent lower than the theoretical value of 9.49" given by Eq. 6-13. The difference between the theoretical and observed values appears to be due to the tapered nature of the column.

6-7

TABLE 6.4: Experimental Observed Plastic Hinge Lengths for the Model

Hinge #	Drift	ϕ_p	θ_p	L_p/L	L_p*
1	0.50%	0.002227	0.002159	0.083	1.0
	0.75%	0.003407	0.004168	0.106	1.3
	1.00%	0.004137	0.005714	0.122	1.5
	1.50%	0.004977	0.007209	0.127	1.5
	2.00%	0.006407	0.008377	0.113	1.4
2	0.50%	0.000788	0.002159	0.336	3.3
	0.75%	0.001451	0.004168	0.358	3.5
	1.00%	0.001884	0.005714	0.384	3.8
	1.50%	0.002035	0.007209	0.475	4.6
	2.00%	0.002445	0.008377	0.453	4.4
3	0.50%	0.000867	0.001450	0.190	1.8
	0.75%	0.001897	0.003726	0.227	2.2
	1.00%	0.002897	0.005302	0.210	2.0
	1.50%	0.004927	0.009347	0.218	2.1
	2.00%	0.005747	0.013811	0.288	2.8
4	0.50%	0.001659	0.001450	0.074	0.9
	0.75%	0.002912	0.003726	0.110	1.4
	1.00%	0.003979	0.005302	0.115	1.4
	1.50%	0.006565	0.009347	0.123	1.5
	2.00%	0.009170	0.013811	0.131	1.6

* According to Eq. 6-9, L_p = 2.33, 2.13, 2.13 and 2.33" for hinges 1 to 4 respectively.

6-8

TABLE 6.5: **Experimental Observed Equivalent Plastic Hinge Lengths for the Prototype**

Drift Level	ϕ_p	θ_p	L_p/L	L_p^*
0.50 %	0.000615	0.0014	0.044	2.3
0.75 %	0.000915	0.0030	0.064	3.4
1.00 %	0.001245	0.0043	0.067	3.6
1.50 %	0.001625	0.0073	0.089	4.7
2.00 %	0.002095	0.0102	0.097	5.1
-0.50 %	0.000235	0.0001	0.008	0.4
-0.75 %	0.000345	0.0013	0.074	3.9
-1.00 %	0.000445	0.0023	0.103	5.4
-1.50 %	0.000665	0.0046	0.140	7.4
-2.00 %	0.000815	0.0057	0.142	7.5

* According to Eq. 6-9, $L_p = 9.49"$.

6.3 Shear Strength Determination

6.3.1 Code Comparison

One of the principal focuses of this study was to examine the shear strength capacity predicted using various different code and rational methods. Generally, codes determine the nominal shear strength of reinforced concrete columns by combining the shear carried by concrete V_c and the transverse reinforcement V_s as follows:

$$V_n = V_c + V_s \qquad (6-18)$$

where the steel contribution is given by:

$$V_s = A_{sh} f_{yh} \frac{d}{s} \cot\theta \qquad (6-19)$$

in which, A_{sh} = area of transverse reinforcement, f_{yh} = yield stress of transverse

6-9

reinforcement, d = effective depth, s = center to center spacing of transverse hoops and θ is the orientation of the shear cracks, normally taken as $45°$.

The equations for the shear strength provided by the concrete have been revised from time to time based on recent research in this regard, in order to relax the conservatism. As a realistic evaluation of the strength was sought, four different approaches were adopted for comparison and are described below.

ACI 318-89 / AASHTO (1989)

The ACI 318-89 concrete design code and the AASHTO (1989) bridge design code both require that the shear carried by concrete shall not exceed a basic shear force

$$V_c = 2\sqrt{f_c'}\, b_w d \qquad (6\text{-}20)$$

unless a more rigorous analysis is used as described below. In Eq. 6-20, b_w = width of column and d = effective depth of the section and f_c' is in psi units.

For column members subjected to axial compression,

$$V_c = 2\left(1 + \frac{N_u}{2000 A_g}\right)\sqrt{f_c'}\, b_w d \qquad (6\text{-}21)$$

where, N_u = axial load on column, A_g = gross cross-sectional area of column, and b_w = column width. A more detailed analysis can be obtained from the following relationship,

$$V_c = \left(1.7\sqrt{f_c'} + 2500\, \rho_w \frac{V_u d}{M_u}\right) b_w d \quad \leq 3.5\sqrt{f_c'}\, b_w d \qquad (6\text{-}22)$$

where, $V_u d / M_u \leq 1$, ρ_w = volumetric longitudinal steel ratio, V_u = shear force at the section, and M_u = bending moment at the section. Eq. 6-22 can be used for members subjected to axial compression with $M_m = M_u - N_u(4h - d)/8$ substituted for M_u and $V_u d/M_u$ not limited to 1.0.

However, in any case V_c should not exceed,

$$V_c = 3.5 \sqrt{f_c} \sqrt{1 + \frac{N_u}{500 A_g}} \, b_w d \qquad (6\text{-}23)$$

In this study the initial and final shear strengths are taken as V_{ci} and V_{cf} where $V_{ci} = V_c$ given by the appropriate value in Eqs. 6-20 to 6-23, and $V_{cf} = 0$. The latter is for plastic hinge zones in accordance with ACI 318 seismic provisions when $N_u < 0.05 f_c' A_g$.

NZS 3101 (1982)/ ACI-ASCE Committee 426 (1979)

The New Zealand concrete code NZS 3101 (1982) has adopted the ACI-ASCE Committee 426 (1979) recommendations where the concrete contribution outside the plastic hinge zone is given as:

$$V_c = v_b \left(1 + 3\frac{P}{f_c' A_g}\right) b_w d \qquad (6\text{-}24)$$

where, P = axial load on the column, v_b is the basic shear stress given by

$$v_b = \left(0.85 + 120 \, \rho_w\right) \sqrt{f_c'} \le 2.4 \sqrt{f_c'} \qquad (6\text{-}25)$$

In the plastic hinge zone, the concrete shear strength can be taken as

$$V_c = 4 v_b \sqrt{\frac{P}{f_c' A_g}} \, b_w d \qquad (6\text{-}26)$$

In this study, Eqs. 6-24 and 6-26 were adopted for the evaluation of V_{ci} and V_{cf} respectively. It should be noted that Eq. 6-26 is normally used only if $P \ge 0.1 f_c' A_g$.

CAN3-23.3-M84

Canadian National Standard (1984) for design of structures is based on the

Compression Field Theory which is referred to in that code as the "General Method".
It gives the following relation for the evaluation of shear resistance:

$$V_r = A_v f_y \frac{d_v}{s} \cot\theta \qquad (6\text{-}27)$$

where d_v = effective shear depth and θ = crack inclination to the longitudinal axis and
taken greater than or equal to $15°$ for non-seismic design and $30°$ for the seismic design.
The diagonal compressive stress f_2 is to be checked to ensure that web crushing does not
take place , where

$$f_2 = (\tan\theta + \cot\theta)\frac{V_r}{b_v d_v} \leq f_{2max} \qquad (6\text{-}28)$$

where b_v = minimum effective width within depth d_v and,

$$f_{2max} = \frac{\alpha f_c'}{(0.80 + 170\epsilon_1)} \qquad (6\text{-}29)$$

in which α is taken as 0.8 and 1.0 respectively, for the seismic and non-seismic design.
The principal tensile strain ϵ_1 is given by,

$$\epsilon_1 = \epsilon_x + \frac{\epsilon_x + 0.002}{\tan^2\theta} \qquad (6\text{-}30)$$

where ϵ_x is the longitudinal strain at the center of the web. In lieu of a more exact
analysis where ϵ_x is determined from curvatures, the code recommends that 0.004 and
0.002 be used for ϵ_x in seismic and non-seismic conditions respectively.

In this study the values of the stress f_2 were found to be much less than f_{2max} for
both seismic and non-seismic conditions which means that the shear strength is governed
by the yielding of transverse reinforcement and resistance is given by Eq. 6-27 with θ
set to $15°$ and $30°$ for V_i and V_f respectively.

Ang, Priestley and Paulay (1989)

Ang et al (1989) tested a number of confined circular bridge pier models and modelled the shear resistance mechanism as dependent on the displacement ductility. The initial concrete shear strength is given by

$$V_{ci} = \left[4.45\, \alpha \left(1 + 3\,\frac{P}{f_c' A_g}\right) \sqrt{f_c'}\right] b_w d \qquad (6\text{-}31)$$

where, $\alpha = \dfrac{2}{M/VD} \geq 1$.

The initial value of the concrete shear strength is applicable up to a displacement ductility of 2. Concrete is assumed to possess a final shear strength V_f at the ultimate ductility. The strength degradation from V_i to V_f is assumed to be linear and:

$$V_f = V_{cf} + V_s \qquad (6\text{-}32)$$

where,

$$V_{cf} = \left(225\, \rho_s \sqrt{f_c'}\right) b_w d \qquad (6\text{-}33)$$

and V_s is given by Eq. 6.19. ρ_s = volumetric transverse reinforcement ratio and the crack inclination to the longitudinal axis θ is given by,

$$\theta = \tan^{-1}\left(\frac{\psi}{\sqrt{1 - \psi}}\right) \geq 25° \qquad (6\text{-}34)$$

where $\psi = \dfrac{\rho_s f_{yh}}{\nu f_c'}$ and $\nu < 1$ is a factor for reduced strength of the diagonal compression strut.

6.3.2 Degradation of Shear Strength

It is well recognized that the concrete contribution to shear resistance degrades with cyclic loading and/or increasing ductility amplitude. ATC 6-2 (1983) suggests a

shear degradation relationship based on an initial capacity V_{ci} which can be sustained until a ductility factor of $\mu = 2$. The shear strength degrades linearly to the final shear capacity V_{cf} at a ductility factor of $\mu = 5$ for an M/VD aspect ratio of 2. This effect is shown in Fig. 6.3. For the model pier, the yielding occurred at a drift amplitude of 0.25% which means that V_{ci} is the shear strength up to a drift amplitude of 0.5% and V_{cf} after 1.25%. For the prototype column, the experimentally obtained drift at yield is 0.15%, which gives initial and final shear capacities ending and commencing at drift amplitudes of 0.3% and 0.75% respectively.

6.3.3 Application of Code Formulations to the present studies

The results of the code equations discussed in 6.3.1 are respectively presented in Tables 6.6 and 6.7 for the model pier and the prototype. The strength degradation of the pier along with the theoretical failure envelopes are presented in Fig. 6.4 for the pier model and in Fig. 6.5 for the prototype beam-column joint. The degradation patterns for ACI 318-89 and NZS 3101 shear strengths were derived as suggested by ATC (1983).

None of the code based methods indicate the measure of ductility observed in the experiments. In fact, in all the cases, according to ATC 6-2 (1983) guidelines, the pier would be defined as shear brittle with no ductility capacity since the initial shear strength is predicted to be less than the nominal flexural strength $(V_i < V_n)$. Only the method by Ang, Priestley and Paulay (1989) shows that the model and prototype are capable of sustaining some inelastic response. According to the ATC 6-2 evaluation procedures, the ductility capacity of a structural element whose final shear capacity is less than the flexural overstrength $(V_f < V_o(d) = 1.3 V_n)$ but initial shear capacity greater than the flexural overstrength $(V_i > 1.3 V_n)$ as shown in Fig. 6.3, is given by

$$\mu = 2 + \left[0.75 \frac{L_c}{b_c} \right] \frac{V_i(c) - V_o(d)}{V_i(c) - V_f(c)} \tag{6-35}$$

in which b_c = width of column in the direction of shear (see subsection 6.6 for details).

6-14

Table 6.6: Code based Shear Strength for Model Pier

Approach	Eq. No.	V_c (kips)	V_s (kips)	V_n (kips)	$F_{np} = 2V_n$ (kips)	Remarks
ACI 318-89	6-20	12.4	2.4	14.8	29.6	Basic
	6-21	15.6	2.4	18.0	36.0	Approx.
	6-22	14.0	2.4	16.4	32.7	Exact
NZS 3101 (1982)	6-24	9.9	2.4	12.3	24.6	Initial
	6-26	7.5	2.4	9.9	19.8	Final
CAN3-A23.3 (1988)	6-27	-	7.8	7.8	15.6	Initial
	6-27	-	3.6	3.6	7.2	Final
Ang et al (1988)	6-31	29.8	2.3	32.1	64.2	Initial
	6-32	1.3	4.8	6.1	12.2	Final

TABLE 6.7: Code based Shear Strength for the Prototype

(a) Negative Loading

Approach	Eq.No.	V_c (kips)	V_s (kips)	V_u (kips)	$F_u = 1.095\, V_u$ (kips)	Remarks
ACI 318-89	6-20	204	23	227	229	Basic
	6-21	236	23	259	284	Approx.
	6-22	196	23	219	241	Exact
NZS 3101 (1982)	6-24	103	23	126	138	Initial
	6-26	75	23	98	108	Final
CAN3-A23.3 (1988)	6-27	-	86	86	94	Initial
	6-27	-	40	40	44	Final
Ang et al (1988)	6-31	693	23	716	784	Initial
	6-32	12	46	58	63	Final

(b) Positive Loading

Approach	Eq.No.	V_c (kips)	V_s (kips)	V_u (kips)	$F_u = 1.095\, V_u$ (kips)	Remarks
ACI 318-89	6-20	204	23	209	229	Basic
	6-21	218	23	241	265	Approx.
	6-22	196	23	219	240	Exact
NZS 3101 (1982)	6-24	100	23	123	135	Initial
	6-26	53	23	76	83	Final
CAN3-A23.3 (1988)	6-27	-	86	86	94	Initial
	6-27	-	40	40	44	Final
Ang et al (1988)	6-31	657	23	680	745	Initial
	6-32	12	46	58	63	Final

This gives ductility capacities of μ = 4 and μ = 15 translating into ultimate drift angles of θ_u = 1.0% and θ_u = 2.25% for the model and prototype specimens, respectively.

The above result, using the recommendations of Ang et al and ATC 6-2 still fall well short of the observed flexural-shear ductility capacity. Based on the flexural capacity alone, the experimentally observed ultimate drift was θ_u = 3% for both model and the prototype.

One possible explanation for this discrepancy is due to the fact that Ang et al (1989) tested their specimens at five completely reversed cycles of loading at drift angles of approximately ±0.75%, ±1.5%, ±2.0%, ±3.0%, ±4.0%..... until the failure occurred. (Each of the shear-critical specimens studied by Ang et al had a yield drift of approximately 1.0%). In the present study however, only two cycles of loading were applied at drift amplitudes of ±0.25%, ±0.5%, ±0.75%, ±1.0%, ±1.5% and ±2.0%, and five cycles at ±3.0% and about 7 cycles at ±4.0% at which time the residual capacity (defined in the next subsection) was obtained.

6.4 Proposed Strength Deterioration Model

From the results it is evident that the failure of the specimen is difficult to define and (or) predict experimentally. This makes analytical predictions even more difficult. Even when the testing was terminated the specimen was still performing its primary function -- supporting the tributary gravity load! In light of this result and in keeping with the ATC 6-2[1] idealization for flexural-shear interaction shown in Fig. 6.3, it is proposed to define a three step strength deterioration model based on (I) an initial shear capacity, (II) a residual strength, and (III) a cumulative drift capacity based on the energy absorption due to repetitive cyclic loading. Each of these steps in the analysis are described below:

(I) Initial Strength Capacity

The initial capacity should be taken as the more critical of the nominal flexural

strength or the theoretical shear strength. A rational assessment of the initial shear capacity can be made using the Modified Compression Field Theory (MCFT). In this study the program *RESPONSE* (details to be found in Collins and Mitchell[11]) was used to apply the MCFT for the determination of the ultimate post-cracking shear capacity.

(II) Final Strength

The final (residual) strength exists after either: (a) the concrete resistance capacity is destroyed due to damage resulting from repetitive cyclic loading; or (b) the longitudinal bars fracture due to low cycle fatigue. Following the final stage the member does not fail, but rather a change in behavior state takes place where the column either slides or rocks on it's foundation as shown in Fig. 6.6.

The final/residual capacity is defined as lesser of: (a) the column rocking lateral strength shown in Fig. 6.6, or (b) the sliding shear capacity of the section, such that

$$F_f = \min \{F_{rocking}, F_{sliding}\} \qquad (6\text{-}36)$$

in which

$$F_{rocking} = Wjd/L_c \qquad (6\text{-}37)$$

$$F_{sliding} = \mu W \qquad (6\text{-}38)$$

where W = tributary gravity weight, L_c = clear height of the column, and jd = the internal lever arm taken as the lesser of

$$jd = (d - d') \qquad (6\text{-}39a)$$

$$jd = h - a \qquad (6\text{-}39b)$$

where h = column width and $a = P/(0.2f_c'b)$ = the residual stress block depth. In Eq. 6-38, μ = the coefficient of sliding friction. A dependable value of $\mu = 0.7$ may be assumed according to Paulay and Priestley (1992). For the specimens in the present study Eq. 6-37 is critical giving F_f = 14 and 75 kips respectively, for the model and the prototype. This difference is attributed to the continued crushing of concrete in the hinge zones which continued to reduce the internal moment arm (jd) progressively. But still

the flexural strength ratios are relatively high which indicate that despite such extensive damage the specimens are capable of withstanding reasonably large lateral loads and sustain their tributary gravity loads without complete collapse.

(III) Concrete Damage Analysis for Determination of Drift Capacity

In what follows is a damage analysis, developed from first principles for unconfined concrete beam-columns which is used to determine drift and history dependant moment capacities. An energy approach is used, similar to that adopted by Mander, Priestley and Park (1988), to assess the cyclic capacity (cumulative drift) of concrete. The external work done (EWD) on the compressed concrete is equal to the internal work or energy absorption capacity (IWD) of the entire concrete section, thus by virtual work

$$EWD = IWD$$

$$2N_c C_c \left(\phi_p \frac{c}{2} \right) = A_g \int_0^{\epsilon_{cm}} f_c d_\epsilon \tag{6-40}$$

in which ϕ_p = the plastic curvature applied to the section, c = depth of the concrete stress block from the extreme compression fiber to the neutral axis, C_c = compression force carried by the concrete, and $2N_c$ = the number of reversals to failure, N_c being the number of completely reversed cycles. The integral $\int_0^{\epsilon_{cm}} f_c d_\epsilon$ is the area beneath the entire concrete stress-strain curve which is equal to the total energy absorption capacity of the plain concrete. In lieu of a more precise analysis, this may be taken as $0.008 f_c'$. Rearranging Eq. 6-40 gives

$$N_c(\phi_p h) = \frac{0.008}{\left(\dfrac{C_c}{f_c' A_g} \right) \left(\dfrac{c}{h} \right)} \tag{6-41}$$

The plastic rotation may be determined from an equivalent plastic hinge length given by

$$\theta_p = \phi_p L_p = (\phi_p h)(L_p / h) \tag{6-42}$$

where L_p = the equivalent plastic hinge length may be determined from the relationship suggested by Paulay and Priestley (1992):

$$L_p = 0.08L + 0.022 f_y d_b \tag{6-43}$$

where L = column length (M/V), f_y = yield stress of the longitudinal steel (MPa) and d_b = diameter of the longitudinal bars. Hence from Eq. 6-41 it may be assumed that the cumulative plastic drift capacity is given by

$$\Sigma \theta_p(c) = \frac{0.016 L_p / h}{\left(\dfrac{C_c}{f'_c A_g}\right)\left(\dfrac{c}{h}\right)} \tag{6-44}$$

Note that the cumulative plastic drift is defined as the sum of all the positive and negative plastic drift amplitudes to a given stage of testing. Thus five cycles at the ± 3 percent drift amplitude contribute a cumulative plastic drift amplitude of 0.0025 radians $[(0.03-0.0025)\times 5 \times 2$, where 0.0025 is the yield drift].

The damage to the concrete for one cycle is thus given by

$$D_{ci} = \frac{2\theta_{pi}}{\Sigma \theta_p(c)} \tag{6-45}$$

where θ_{pi} is the plastic rotation for the ith half-cycle.

Assuming the level of damage is proportional to the loss in moment capacity which is contributed by the concrete, then at the end of the ith cycle, the modified ideal capacity M_i can be evaluated through

$$\frac{M_i}{M_n} = 1 - \frac{M_c}{M_n} \sum D_{ci} = 1 - \frac{M_c}{M_n} \frac{\sum \theta_p}{\sum \theta_p(c)} \tag{6-46}$$

in which ΣD_{ci} = accumulated damage, $\sum \theta_p$ = current cumulative plastic drift, M_n =

6-20

nominal moment capacity, and M_c is the moment generated by the eccentric concrete stress block which may be computed by

$$M_c = 0.5 C_c h \left(1 - \frac{c}{h} \right)$$ (6-47)

where h = total section depth.

The concrete compression force C_c can be determined in terms of the familiar stress block parameters, such that

$$C_c = \alpha \, \beta f_c' c b$$ (6-48)

in which α = average concrete stress ratio, β = depth ratio of the concrete stressed in compression, c = stress block depth, and b = section width. Eq. 6-48 can be normalized for use in Eq. 6-40 such that

$$\frac{C_c}{f_c' A_g} = \alpha \, \beta \left(\frac{c}{h} \right)$$ (6-49)

where $A_g = bh$ = gross section area.

The stress block depth ratio (c/h) in Eq. 6-49 can be found from force equilibrium on the column section that requires

$$P_e = C_c + C_s - T_s$$ (6-50)

where P_e = the applied axial load, and C_s and T_s are the forces provided by the longitudinal compression and tension reinforcement, respectively. Assuming that the total area of longitudinal reinforcement (A_{st}) is equally distributed in each of the four faces of a rectangular column $(0.25 A_{st}$ each side), and that under large curvatures all steel is yielding, then by proportion it can be shown that

$$P_e = C_c - 0.5 A_{st} f_y \left(\frac{1 - 2c/h}{1 - 2d'/h} \right)$$ (6-51)

where d' is the depth from an outer face to the centroid of the adjacent steel layer.

6-21

Solving Eqs. 6-49 and 6-51 for the stress block depth ratio gives

$$\left(\frac{c}{h}\right) = \frac{\left(\frac{P_e}{f'_c A_g}\right) + \left(\frac{0.5\,\rho_t f_y/f'_c}{1 - 2\,d'/h}\right)}{\left(\alpha\,\beta + \frac{\rho_t f_y/f'_c}{1 - 2\,d'/h}\right)} \qquad (6\text{-}52)$$

where ρ_t = volumetric ratio of the longitudinal reinforcement (A_{st}/A_g). Here stress block parameters appropriate for large curvatures should be used. Thus it may be assumed that $\alpha = 0.66$ and $\beta = 1.3 - 0.07 f'_c$ but $0.75 \leq \beta \leq 1.00$.

In summary, the damage analysis proceeds as follows:

1. Determine the neutral axis depth ratio c/h using Eq. 6-52.

2. Determine the concrete compression force ratio $C_c/f'_c A_g$ using Eq. 6-49.

3. Determine the equivalent plastic hinge ratio L_p/h using Eq. 6-43.

4. Determine the cumulative plastic drift capacity $\sum \theta_p(c)$ using Eq. 6-44.

5. Using Eq. 6-47, determine the proportion of the moment capacity that is contributed by the eccentric concrete stress block, M_c/M_n.

6. Finally, by applying the damage model Eq. 6-45, and the model for strength degradation Eq. 6-46, the modified theoretical strength capacity may be determined as a function of the actual (experimental) cumulative plastic drift history.

This simple energy consumption theory will now be applied to the model bridge pier. To simplify the analysis an average column size of $10'' \times 10''$ is assumed, thus $P_e = 0.036 f'_c A_g$, $c/h = 0.11$, $C_c = 0.066 f'_c A_g$ and $L_p/h = 0.36$, therefore $\sum \theta_p(c) = 0.80$ *radians*. Table 6-8 presents a tabulation of the damage analysis. Experimental drifts for the model and prototype at nominal yield of 0.25 and 0.15 percent respectively, have been assumed when calculating the plastic rotations. It will be noted that Table 6-8 also lists the relative strength ratio

6-22

TABLE 6.8: Concrete Damage Analysis

(a) Pier Model

Drift Amplitude in Test (1)	Cycles (2)	Experimental Cumulative Drift (3)	Plastic Rotation θ_p (radian) (4)	Cum. Plastic Drift $\Sigma \theta_{pi}$ (5)	Damage Index ΣD_{ci} (6)	M_i/M_n (7)
0.5%	2	0.03*	0.0025	0.010	0.01	0.99
0.75%	2	0.06	0.0050	0.030	0.04	0.97
1.00%	2	0.10	0.0075	0.060	0.08	0.95
1.50%	2	0.16	0.0125	0.110	0.14	0.91
2.00%	2	0.24	0.0175	0.180	0.22	0.85
3.00%	5	0.54	0.0275	0.454	0.57	0.62
4.00%	4.6**	0.90	0.0375	0.772	1.00	0.34

(b) Prototype

Drift Amplitude in Test (1)	Cycles (2)	Experimental Cumulative Drift (3)	Plastic Rotation θ_p (radian) (4)	Cum. Plastic Drift $\Sigma \theta_{pi}$ (5)	Damage Index ΣD_{ci} (6)	M_i/M_n (7)
0.5%	2	0.03*	0.0035	0.018	0.02	0.99
0.75%	2	0.06	0.0060	0.042	0.04	0.97
1.00%	2	0.10	0.0085	0.076	0.08	0.94
1.50%	2	0.16	0.0135	0.130	0.14	0.90
2.00%	2	0.24	0.0185	0.205	0.22	0.85
3.00%	5	0.54	0.0285	0.489	0.52	0.64
4.00%	6**	1.02	0.0385	0.951	1.00	0.30

*   Includes the effect of previous elastic cycles

**   Number of cycles chosen to give $\sum D_{ci} = 1$.

at the end of each drift amplitude. These modified theoretical strength capacities are plotted in Figs. 6.7 and 6.8 for the model and prototype respectively. It is evident that this energy-based method of analysis provides a more reliable and rational assessment of the strength envelop due to cyclic loading of a poorly detailed reinforced concrete column member.

6.5 Comparison of Prototype and Model Tests

When comparing the model pier and the prototype specimen behavior, it should be noted that the material strengths were slightly different : ie. $f_c' = 5,050$ psi and 7,400 psi, and $f_y = 65,000$ psi and 39,500 psi in the model and prototype, respectively. However, by normalizing the prototype and model behavior with respect to the nominal strength of a plastic flexural mechanism, a direct comparison can be made between the two as shown in Fig. 6.9(a). The force inclination on the pier during laboratory test resulted in different forward and reverse strengths. This difference was overcome by taking the averages of (absolute) normalized forces for positive and negative halves of the cycles. For this reason, only half loops are shown in the comparison.

In Fig. 6.9(b) the normalized cumulative energy absorption versus cumulative plastic drift relationships for the model and the prototype are presented. The cumulative energy was normalized by dividing E (given by Eq. 3-7) by $2 F_n h_c$ where F_n = the nominal ultimate strength (in kips) of the specimen, and h_c = the effective height of the column which is equal to the clear column height (22") for the model and the moment arm (53") for the prototype cap to column specimen. The energy absorbed by an Elasto-Perfectly Plastic (EPP) material is $E_{EPP} = 4 F_n X_{EPP} = 4 F_n h_c \theta_{EPP}$ (the area of a parallelogram) in which X_{EPP} = plastic drift of an EPP material and θ_{EPP} = the rotation corresponding to that plastic drift. The ratio (normalized energy) thus obtained is $= \sum \theta_p / \theta_{EPP}$ where θ_p = the plastic component of the cumulative drift amplitude in one direction which means that it is equal to half of the actual cumulative plastic drift. The straight line in the Fig. 6.9(b) represents the 100% EPP behavior. In this manner,

6-24

the cumulative energy absorption as a fraction of the energy absorbed by an EPP material is obtained e.g. up to a cumulative drift of 0.25 radian, the model and the prototype had energy absorptions of 33% EPP and 39% EPP respectively.

It can be seen that the maximum achieved forces for both model and prototype were similarly close to the nominal flexural strength and there is a considerable resemblance in the shapes of the loops. Similarly the energy absorption pattern was remarkably similar among them. This close comparison gives credence to model studies where the real materials are modeled using scaled deformed reinforcing bars and scaled down aggregate (not to be confused with micro-concrete).

6.6 Seismic Evaluation Using ATC 6-2 Procedures

This subsection applies the ATC 6-2 (1983) seismic evaluation procedures to the pier examined in the present study through the use of capacity/demand ratios. In this analysis it is assumed that the columns are well founded such that a foundation/footing failure will not result. Because the class of bridges represented by the type of pier considered in this study generally possesses simply supported slab-on-girder superstructures, the single-mode spectral method (Procedure 1 in ATC 6-2) can be used for assessing seismic demands for each of the seismic performance categories. Furthermore, the natural period for this class of bridges is generally small enough ($T <$ 0.33 sec.) that the base shear coefficients always lie on the flat top portion of the elastic design spectra. Therefore, the base shear coefficient is given by,

$$C_s = 2.5 A \qquad (6-53)$$

where A = normalized peak ground acceleration coefficient. For this class of bridge pier it can be shown that the natural period is given by

$$T = 2\pi \sqrt{\frac{\theta_y h_c}{C_n(c) g}} \qquad (6-54)$$

in which θ_y = yield drift, h_c = column height, $C_n(c)$ = nominal (yield) strength and g = gravitational acceleration. For the present study T = 0.087 sec. (12 Hz).

6-25

The lateral load corresponding to the elastic moment and shear demands by combining the effects of the loading in the two orthogonal directions (100 % of the elastic value along one axis of the bridge plus 30 % of the value for the perpendicular axis) results in

$$W_l = 1.3 \, C_s \, W_{DL} \qquad (6\text{-}55)$$

in which W_{DL} = dead load on the pier. An elastic base shear demand can thus be defined as

$$C(d) = \frac{W_L}{W_{DL}} = 1.3 \, C_s \qquad (6\text{-}56a)$$

which for the present study gives,

$$C(d) = 3.25 \, A \qquad (6\text{-}56b)$$

Flexure:

A capacity demand (C/D) ratio for the nominal ultimate flexural moment capacity to the elastic moment demand is defined as

$$r_{oc} = \frac{C_n(c)}{C(d)} = \frac{C_n(c)}{3.25 \, A} \qquad (6\text{-}57)$$

in which $C_n(c)$ = the nominal flexural mechanism capacity which is taken as 0.90 for the prototype bridge in this study.

Anchorage:

If the effective development length is insufficient then the C/D ratio for anchorage of the longitudinal reinforcement is given by

$$r_{ca} = \frac{l_a(c)}{l_a(d)} r_{oc} \qquad (6\text{-}58)$$

in which $l_a(c)$ = the actual development length and $l_a(d)$ = required effective

6-26

anchorage length of the longitudinal reinforcement given by

$$l_a(d) = \frac{k_s d_b}{\left(1 + 2.5\frac{c}{d_b} + k_{tr}\right)\sqrt{f_c'}}$$

(6-59)

where k_s = a constant for the steel given by $k_s = 0.2083f_y - 2.292$ (f_y = steel yield stress in psi), d_b = diameter of the longitudinal rebars, c = lesser of the clear cover over the rebars, or half the clear spacing between longitudinal rebars, and

$$k_{tr} = \frac{A_{tr}(c)f_{yt}}{600 s d_b}$$

(6-60)

in which $A_{tr}(c)$ = area of transverse reinforcement normal to splitting cracks, and f_{yt} = yield stress of the transverse reinforcement.

For the present study $l_a(d) = 30 d_b$ and $l_a(c) = 43 d_b$ giving $r_{ca} = 1.43 r_{ac}$, thus anchorage is theoretically not a problem.

Column Shear:

The C/D ratio of the columns subjected to shear is calculated in accordance with the procedures outlined in Fig. 6.10, taken from ATC 6-2 (1983). In that figure the shear demand resulting from flexural overstrength is defined as

$$V_s(d) = 1.3\sum M_u/L_c$$

(6-61)

The initial and final shear capacities, $V_i(c)$ and $V_f(c)$ are calculated in accordance with the AASHTO (1989) provisions previously described in Subsection 6.3.1. In the present study for those situations where $r_{ac} < 1.0$ then a shear capacity will be defined as

$C_v(c) = V_i(c)/W$, thus

$$r_{cv} = \frac{V_i(c)}{V_e(d)} = \frac{C_v(c)}{C(d)} = \frac{C_v(c)}{3.25 A} \qquad (6\text{-}62)$$

Using the ACI/AASHTO procedures to calculate V_i gives Case A (Fig. 6.10) as being critical, ie. $C_v(c) = 219/275 = 0.796$. However, if a more realistic assessment of shear is determined then Case B will apply. Adopting the experimentally observed results or the values given by Ang et al (1989) it is evident that the ductility capacity is $\mu > 5$. Therefore, a dependable shear capacity can conservatively be adopted as $r_{cv} = 5 r_{ec}$.

Confinement:

The C/D ratio for transverse confinement is given by

$$r_{cc} = \mu\, r_{ec} \qquad (6\text{-}63)$$

In the present study specimen pier all of the confining steel requirements were violated that is,

$$s > 6 d_b$$

$$s > 0.2 b_{min}$$

and $\qquad\qquad\qquad\qquad p(c) \approx 0$

Therefore, only a minimum ductility capacity can be assumed, and in accordance with ATC 6-2 this gives $\mu = 2$, and $r_{cc} = 2 r_{ec}$.

Summary of C/D Ratios for Present Study:

From the foregoing discussion ATC 6-2 based C/D ratios for the present bridge pier are:

$r_{ec} = 0.278/A$ for elastic response

$r_{cv} = 0.245/A$ for theoretical shear capacity

$r_{cv} = 5\,r_{ec}$ for shear capacity based on experimental observations

$r_{ec} = 2\,r_{cc}$ theoretical ductile flexural capacity

From these relationships if the C/D ratios are set to 1.0, then it is possible to identify the peak ground acceleration ratio A at which incipient failure is expected. Thus, elastic response is probable when A < 0.28, except that the ATC 6-2 analysis shows that theoretically the pier should fail prematurely in brittle shear when A <0.245. If however, a more realistic assessment of shear capacity is used in the analysis, then a ductile flexural response will result when 0.28 < A < 0.56. The results of the aforementioned C/D ratios are plotted in Fig. 6.11. In this figure the various Seismic Performance Categories for the United States are also shown. Based on a dependable ductile mechanism (μ = 2) it is evident that a "safe" performance can be assured for all Seismic Performance Categories in the United States. However, it should again be emphasized that the ATC 6-2 procedures for assessing shear strength paint a false picture indicating "unsafe" shear-brittle behavior in categories C and D.

(a)Plastic Collapse Mechanism
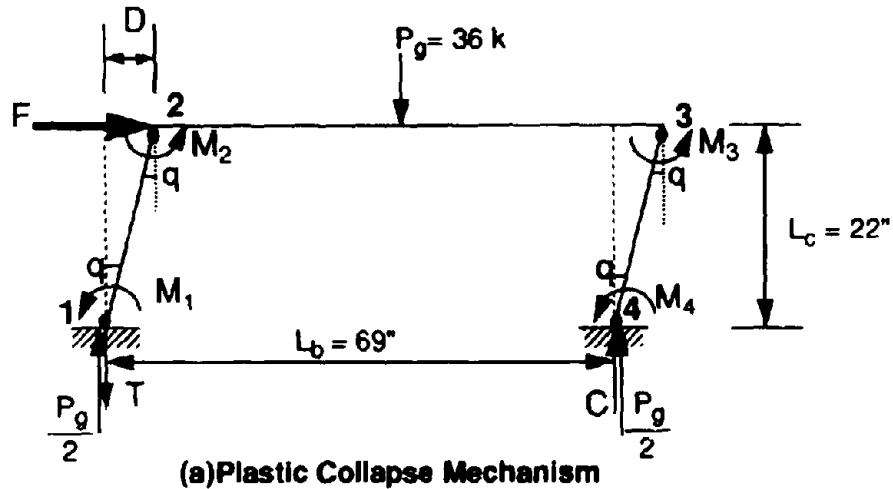
(b) COLUMN INTERACTION DIAGRAM
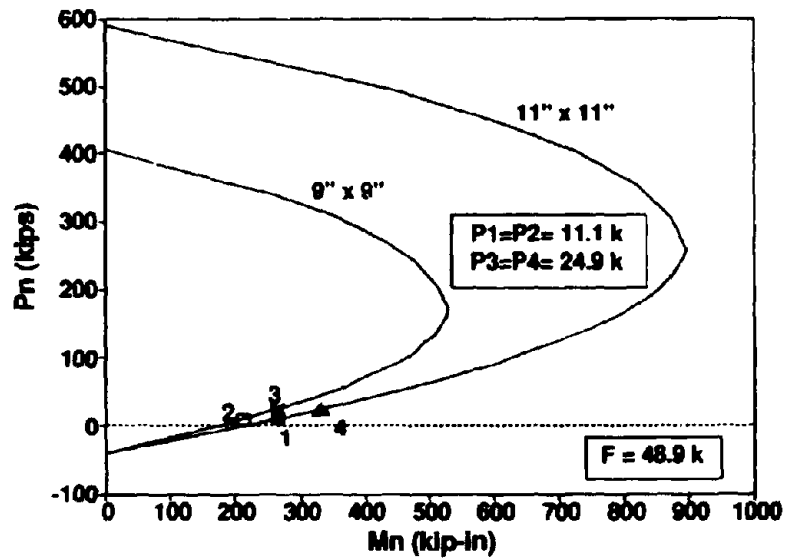
(c) Summary:

P_1 & P_2 (kips)	P_3 & P_4 (kips)	M_1 (kip-in)	M_2 (kip-in)	M_3 (kip-in)	M_4 (kip-in)	T=C (kips)	F (kips)
11.1	24.9	266.6	213.3	264.4	332.1	6.9	48.9

Fig. 6.1 Plastic Collapse Mechanism and Collapse Load Determination for the Model Pier

6-30
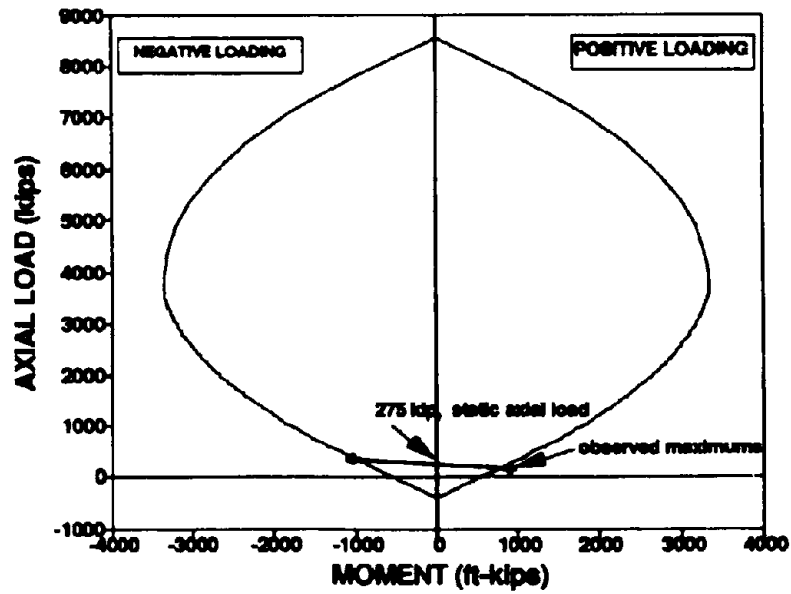
Fig. 6.2 Theoretical and Experimental Strengths of the Prototype Column
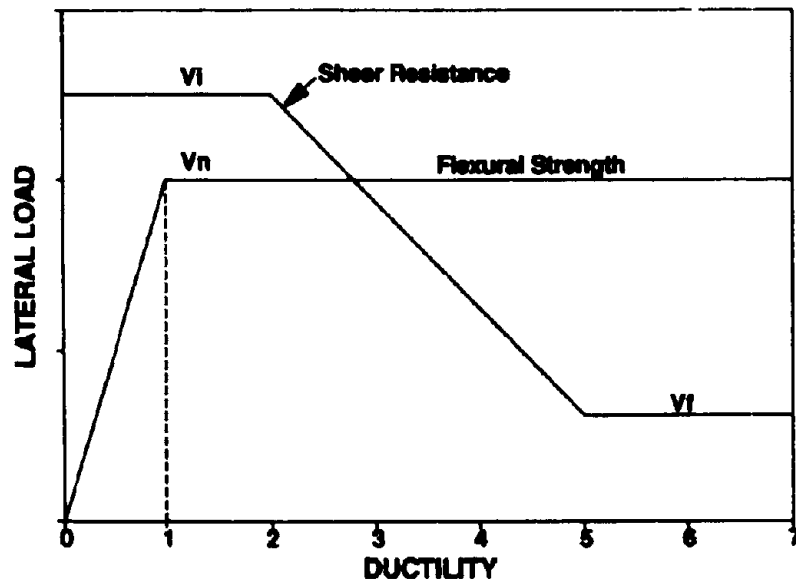
Fig. 6.3 Shear Strength Degradation Pattern Assumed in ATC 6-2

6-31
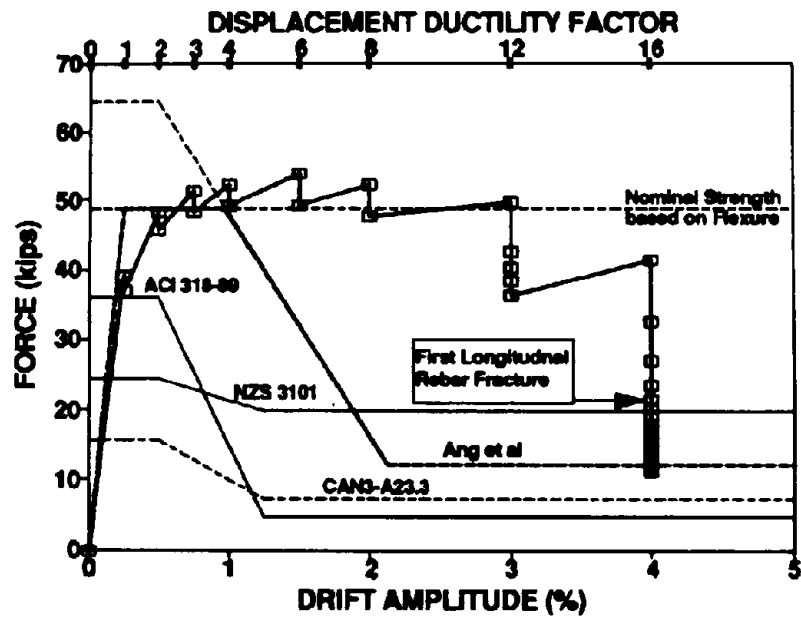
Fig. 6.4 Theoretical and Experimental Model Pier Strength

NEGATIVE LOADING

DISPLACEMENT DUCTILITY FACTOR

POSITIVE LOADING

DISPLACEMENT DUCTILITY FACTOR
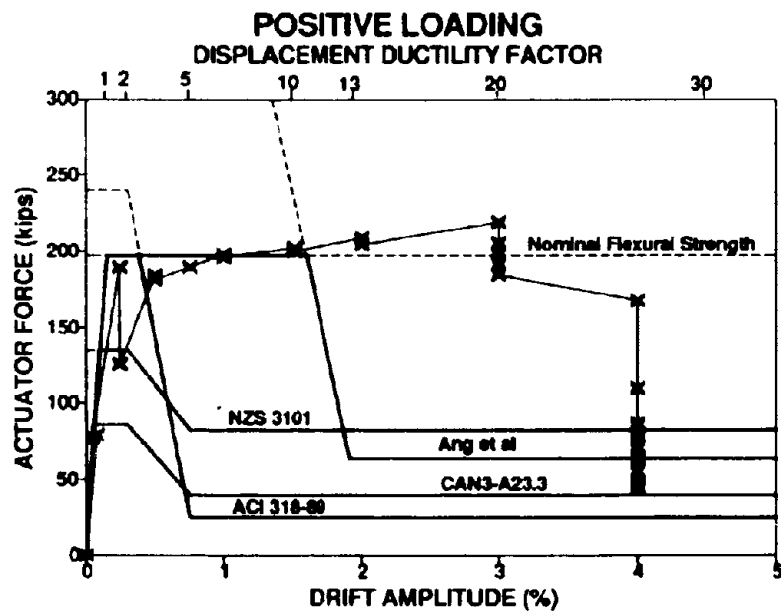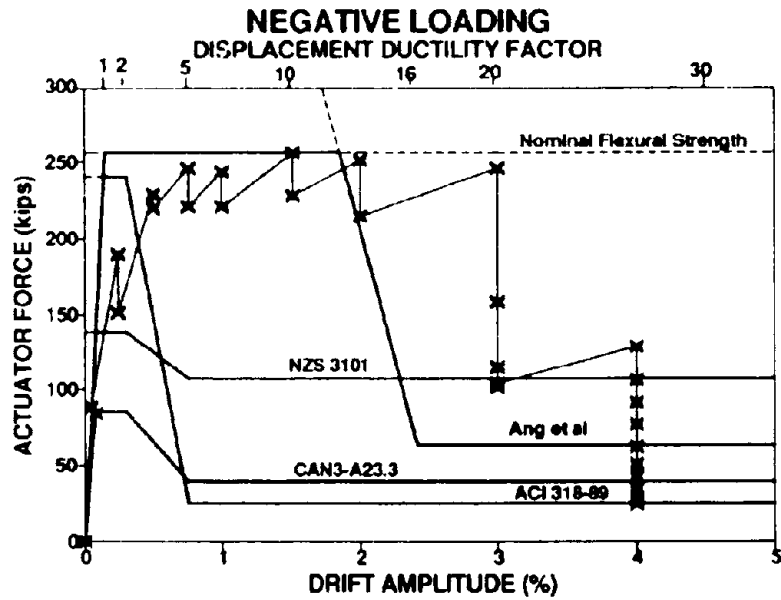
Fig. 6.5 Theoretical and Experimental Column Strength (Prototype)

6-33
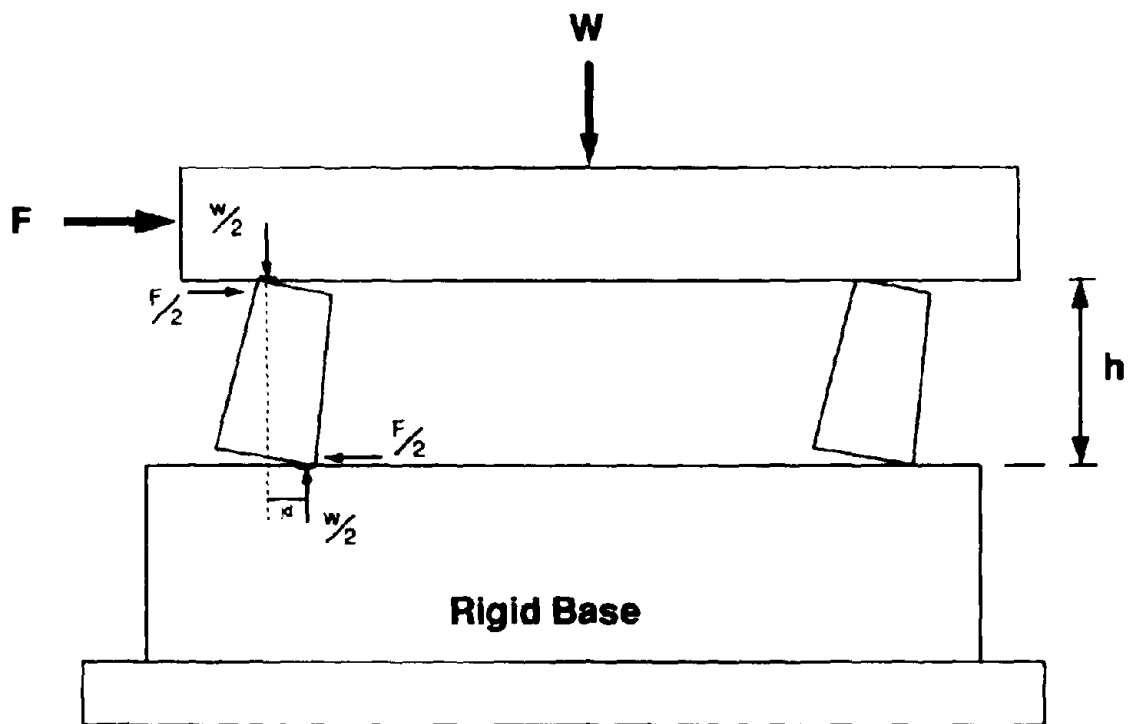
Fig. 6.6 Column Rocking Model for calculating residual lateral Strength
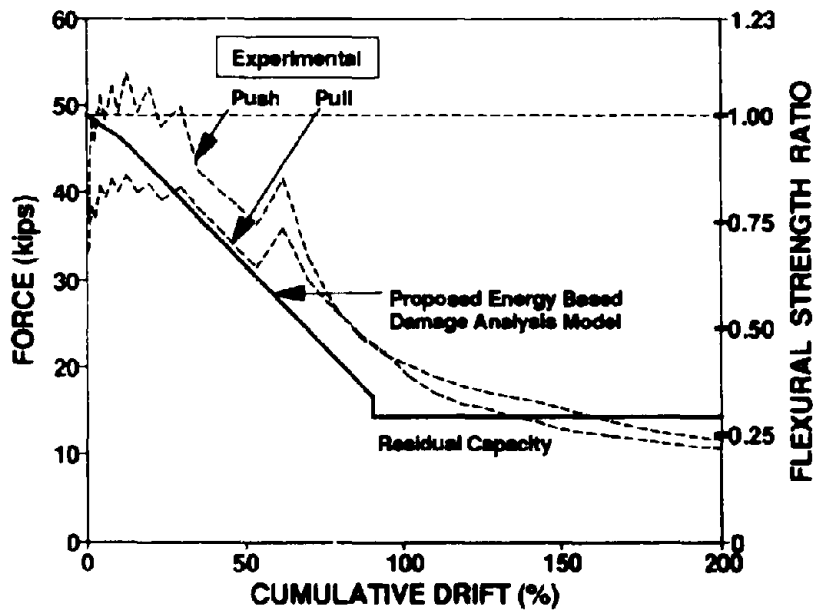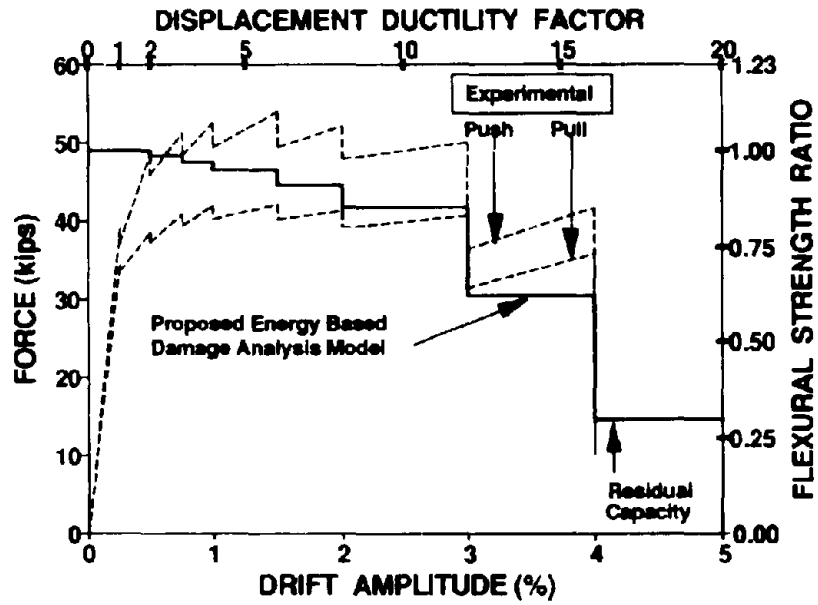
Fig. 6.7 Proposed Strength Degradation Model based on Cumulative Drift (For the Model)
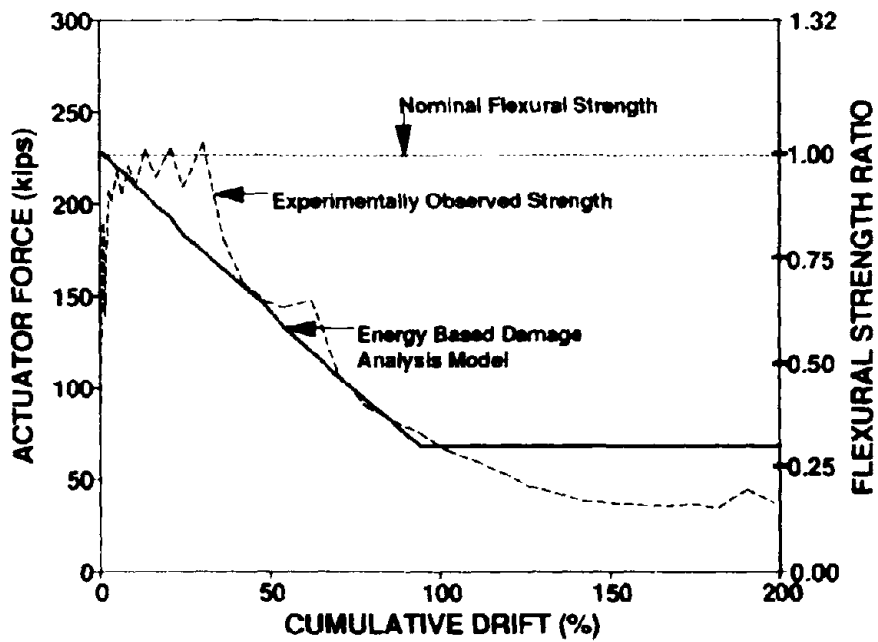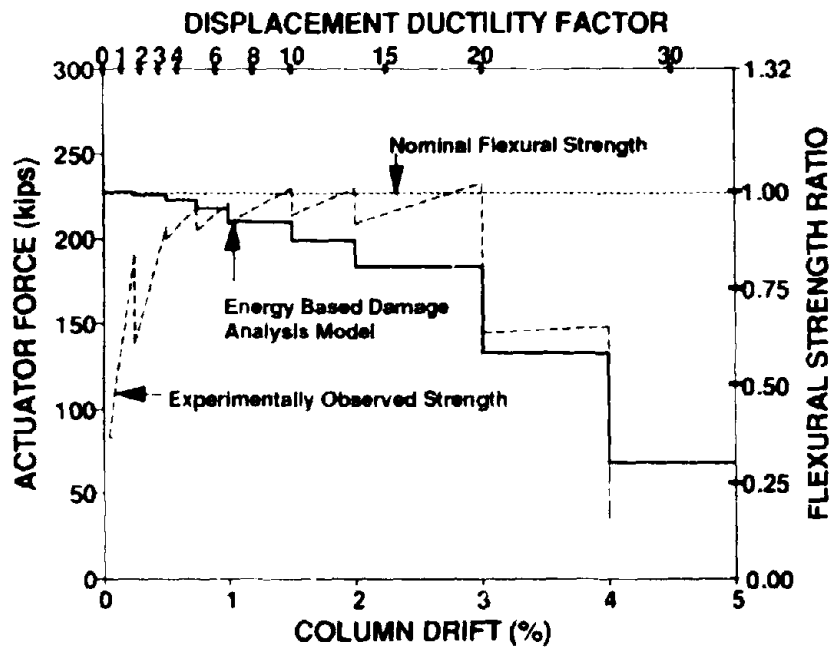
Fig. 6.8   Proposed Strength Degradation Model based on Cumulative Drift (For the Prototype)

ACTUAL PIER
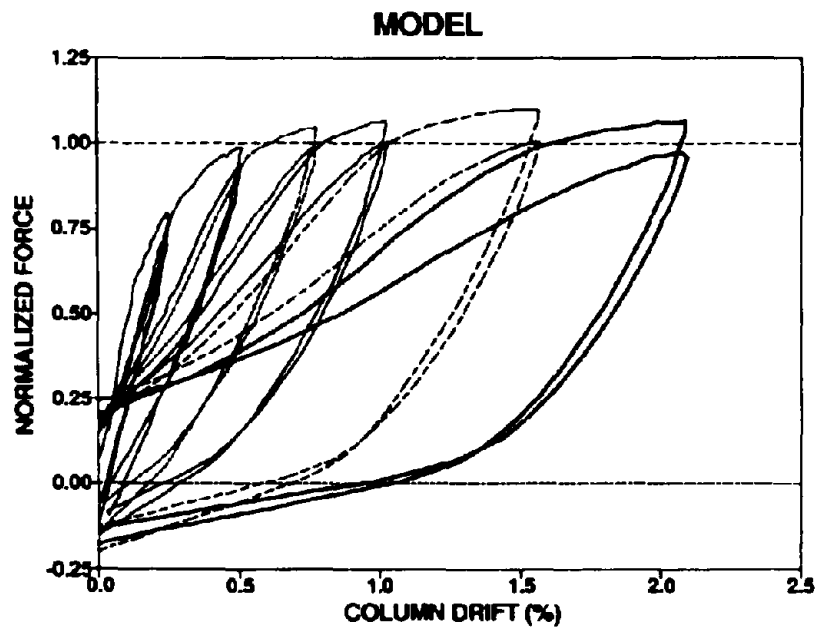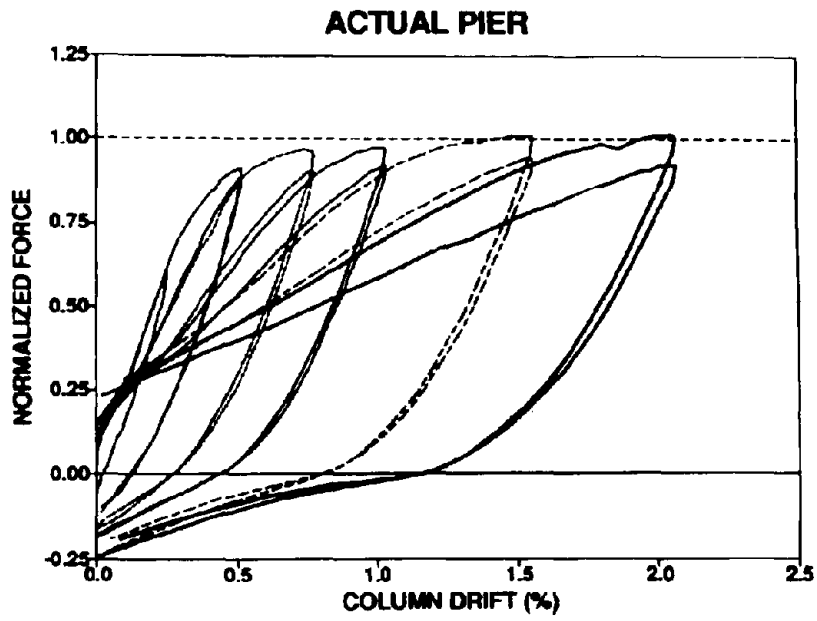
MODEL

Fig. 6.9(a) Force vs Drift Curves of the Model and the Prototype

6-37

ENERGY ABSORPTION
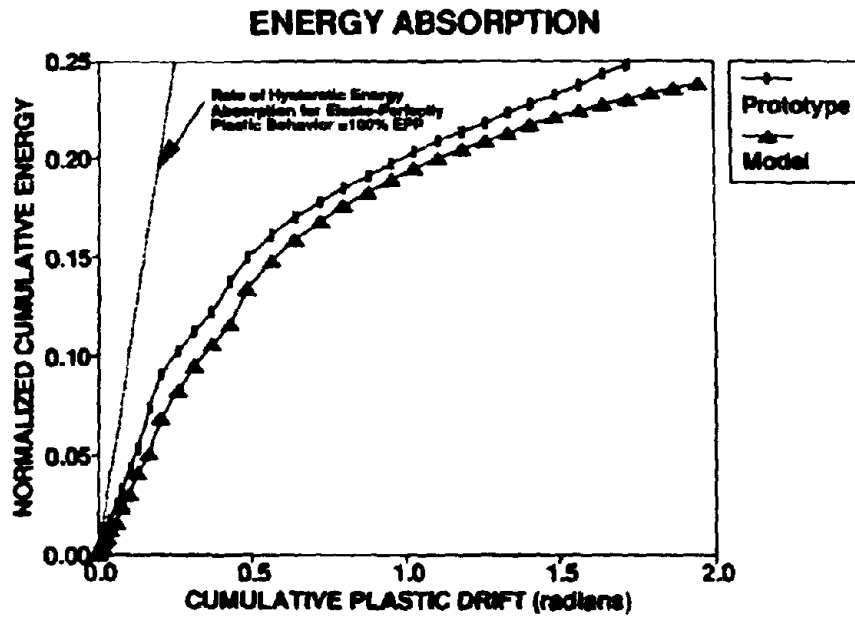
Fig. 6.9(b)   Cumulative Energy vs Cumulative Drift Relationships for the Model and the Prototype
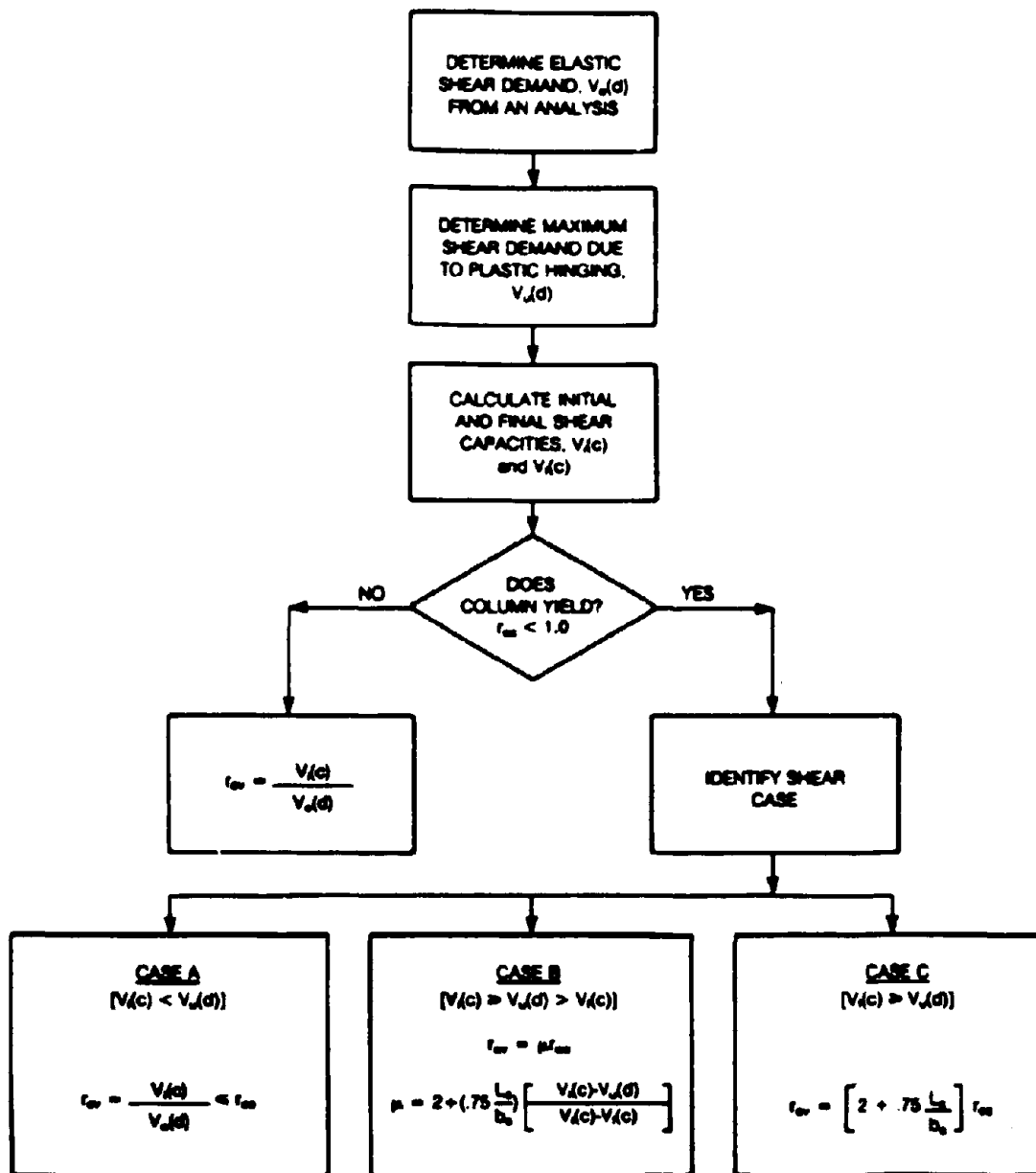
Fig. 6.10 Prodecure for Determining Capacity/Demand Ratios for Column Shear (After ATC 6-2, 1983)

SEISMIC PERFORMANCE CATEGORY
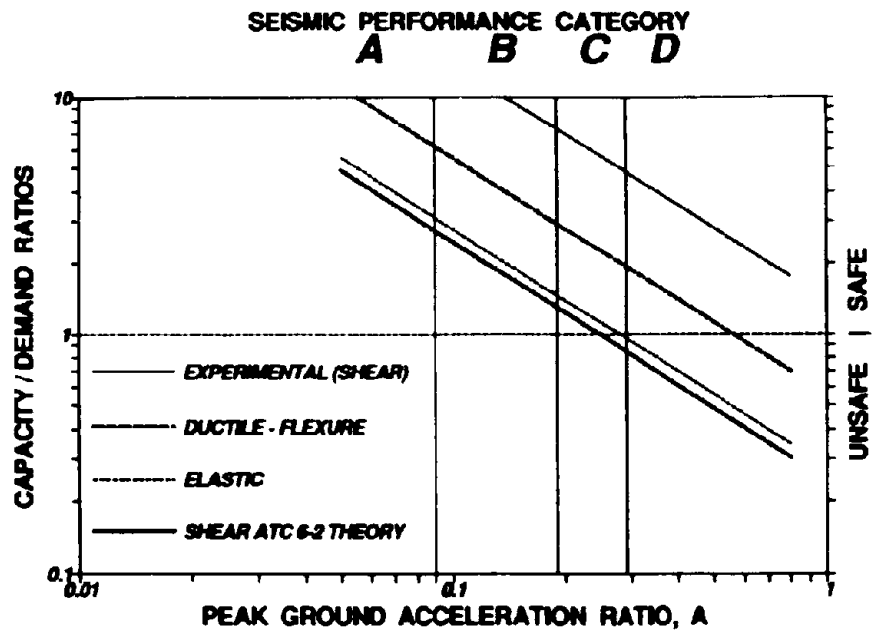
Fig. 6.11 C/D Ratios for the Prototype Bridge Located in Any Seismic Risk Zone

6-40

SECTION 7
SUMMARY AND CONCLUSIONS

This report has presented an investigation of the behavior of a beam to column joint of a 32 year old shear-critical bridge pier and a companion one-quarter scale model of the two column prototype bent under reversed cyclic lateral loading. The prototype specimen was retrieved from the field and prepared for testing by welding a self equilibrating reaction frame onto the reinforcing steel of the cap beam. The model and the prototype were tested under constant vertical (gravity) loads. The cyclic lateral loading was applied through a horizontally connected actuator in case of the model and two parallel actuators inclined at 24° with the horizontal were used for the prototype testing in order to simulate lateral force effects in an entire two-column bent.

Lateral loads were applied with increasing drift angles to ±4 percent. A moderately ductile failure initiated through flexure but was later dominated by shear when drift angles exceeded ±2 percent for both model and prototype specimens. Final failure was attributed to fracture and bond deterioration of the longitudinal bars for the model and the prototype respectively. The results of model and the prototype tests were compared with one another. Overall performance of the model and prototype were remarkably similar.

Shear accounted for between 25 and 60 percent of the plastic deformations in the columns. The experimentally observed shear strengths were compared with code-based strength evaluation techniques. The evaluation methods showed that the pier would possess inadequate shear capacity and thus be classified as shear-brittle with no ductility capability. An energy based damage analysis procedure was proposed. This improved evaluation procedure is a rational method and is capable of predicting the cumulative displacement ductility failure limit state. The seismic vulnerability of this class of shear-critical bridge pier was examined using the ATC 6-2 methodology. It was shown that if code-based evaluation procedures are followed, this class of bridge pier is classified as "unsafe" and shear-brittle, but may be capable of resisting minor earthquakes through

elastic response. However, if a dependable ductile mechanism is assumed, as demonstrated by good experimental behavior, a "safe" seismic response can be assumed for all Seismic Performance Categories in the United States.

Some specific conclusions are as follows:

1. The primary purpose of this study was to examine the seismic performance of a particular class of existing bridge piers, that was not specifically designed for earthquake loads thus possessing detailing deficiencies. The principal deficiency of the bridge pier considered in this study was a general lack of transverse reinforcement for shear. It has been shown herein that present code-based evaluation techniques do not adequately predict the strength and deformation capacity. Use of the existing code techniques that provide overly conservative predictions of shear strength and deformation characteristics can lead to a false picture that indicates many existing bridge piers may be unsafe in earthquakes. However, in reality they may perform satisfactorily, particularly in moderate seismic zones.

2. Even though the transverse reinforcing steel was insufficient with respect to a contemporary design, both the prototype and the model performed well up to column drift angles of 2 percent, at which level the flexural strength was sustained under cyclic loading. Thereafter degradation in strength took place at a rate that was directly proportional to the cumulative plastic drift (about 80 percent for both model and the prototype) until the residual base strength

   $C_e \approx 0.15$ was left with no significant reduction during the successive cycles

   of loading.

3. The shear carrying capacities evaluated by various code-based approaches were generally lower than the nominal flexural strength. The shear strength degradation pattern suggested in Ang et al (1989) was found to provide an improved

7-2

approximation, although that is still conservative.

4. The existing flexural plastic hinge method for predicting maximum displacement needs further refinement to include the shear component of the plastic displacement. For the members tested in this study (where MV/D = 1.1 to 1.5) results showed that the total displacement typically included between 40 to 65 percent of shear displacement, the higher value occurring for higher axial loads.

5. A new energy based strength deterioration model is proposed. Although this still needs some further refinement it shows promise for making a rational prediction of the maximum cumulative ductility (energy absorption) capacity.

6. Similarities in the performances of the model and the prototype show that the model studies can be relied on when investigating the behavior of this class of structure. It should be noted however, that bond and anchorage in model studies may not be reliably represented. The general nature of the hysteretic performance however, is almost identical between model and prototype.

REFERENCES

AASHTO (1983), "Guide Specifications for Seismic Design of Highway Bridges" American Association of State Highway and transportation Officials, Washington D.C., 106 pp.

AASHTO (1989), "Standard Specifications for Highway Bridges", American Association of State Highway and transportation Officials, Washington D.C., 426 pp.

ACI Committee 318 (1989),"Building Code Requirements for Reinforced Concrete (ACI 318-89) and Commentary -ACI 318 R-89", American Concrete Institute, Detroit, 353 pp.

Ang, B.G., Priestley, M.N.J. and Paulay, T. (1989), "Seismic Shear Strength of Circular Reinforced Concrete Columns", *ACI Structural Journal*, Jan-Feb, V.86, No.1, pp. 45-59.

ATC 6-2 (1983), "Seismic Retrofitting Guidelines For Highway Bridges", Applied Technology Council, 220 pp.

Aycardi, L.E., Mander, J.B., and Reinhorn, A.M. (1992), "Seismic Resistance of Reinforced Concrete Frame Structures Designed only for Gravity Loads: Part II Experimental Performance of Subassemblages", Technical Report NCEER-92-0028, National Center For Earthquake Engineering and Research, SUNY at Buffalo.

Bracci, J.M., Reinhorn, A.M., and Mander, J.B. (1992a), "Seismic Resistance of Reinforced Concrete Frame Structures Designed only for Gravity Loads: Part I Design and Properties of a One-Third Scale Model Structure", Technical Report NCEER-92-0027, National Center For Earthquake Engineering and Research, SUNY at Buffalo.

Paulay, T. and Priestley, M.J.N (1992), " Seismic Design of Reinforced Concrete and Masonry Buildings", J. Wiley.

Priestley, M.J.N. and Park, R. (1987), "Strength and Ductility of Concrete Bridge Columns Under Seismic Loading", *ACI Structural Journal*, Jan-Feb, V.84, No.1, pp. 61-76.

NATIONAL CENTER FOR EARTHQUAKE ENGINEERING RESEARCH
LIST OF TECHNICAL REPORTS

The National Center for Earthquake Engineering Research (NCEER) publishes technical reports on a variety of subjects related to earthquake engineering written by authors funded through NCEER. These reports are available from both NCEER's Publications Department and the National Technical Information Service (NTIS). Requests for reports should be directed to the Publications Department, National Center for Earthquake Engineering Research, State University of New York at Buffalo, Red Jacket Quadrangle, Buffalo, New York 14261. Reports can also be requested through NTIS, 5285 Port Royal Road, Springfield, Virginia 22161. NTIS accession numbers are shown in parenthesis, if available.

NCEER-87-0001 "First Year Program in Research, Education and Technology Transfer," 3/5/87, (PB88 134275/AS).

NCEER-87-0002 "Experimental Evaluation of Instantaneous Optimal Algorithms for Structural Control," by R.C. Lin, T.T. Soong and A.M. Reinhorn, 4/20/87, (PB88-134341/AS).

NCEER-87-0003 "Experimentation Using the Earthquake Simulation Facilities at University at Buffalo," by A.M. Reinhorn and R.L. Ketter, to be published.

NCEER-87-0004 "The System Characteristics and Performance of a Shaking Table," by J.S. Hwang, K.C. Chang and G.C. Lee, 6/1/87, (PB88-134259/AS). This report is available only through NTIS (see address given above).

NCEER-87-0005 "A Finite Element Formulation for Nonlinear Viscoplastic Material Using a Q Model," by O. Gyebi and G. Dasgupta, 11/2/87, (PB88-213764/AS).

NCEER-87-0006 "Symbolic Manipulation Program (SMP) - Algebraic Codes for Two and Three Dimensional Finite Element Formulations," by X. Lee and G. Dasgupta, 11/9/87, (PB88-219522/AS).

NCEER-87-0007 "Instantaneous Optimal Control Laws for Tall Buildings Under Seismic Excitations," by J.N. Yang, A. Akbarpour and P. Ghaemmaghami, 6/10/87, (PB88-134333/AS).

NCEER-87-0008 "IDARC: Inelastic Damage Analysis of Reinforced Concrete Frame - Shear-Wall Structures," by Y.J. Park, A.M. Reinhorn and S.K. Kunnath, 7/20/87, (PB88-134325/AS).

NCEER-87-0009 "Liquefaction Potential for New York State: A Preliminary Report on Sites in Manhattan and Buffalo," by M. Budhu, V. Vijayakumar, R.F. Giese and L. Baumgras, 8/31/87, (PB88-163704/AS). This report is available only through NTIS (see address given above).

NCEER-87-0010 "Vertical and Torsional Vibration of Foundations in Inhomogeneous Media," by A.S. Veletsos and K.W. Dotson, 6/1/87, (PB88-134291/AS).

NCEER-87-0011 "Seismic Probabilistic Risk Assessment and Seismic Margins Studies for Nuclear Power Plants," by Howard H.M. Hwang, 6/15/87, (PB88-134267/AS).

NCEER-87-0012 "Parametric Studies of Frequency Response of Secondary Systems Under Ground-Acceleration Excitations," by Y. Yong and Y.K. Lin, 6/10/87, (PB88-134309/AS).

NCEER-87-0013 "Frequency Response of Secondary Systems Under Seismic Excitation," by J.A. HoLung, J. Cai and Y.K. Lin, 7/31/87, (PB88-134317/AS).

NCEER-87-0014 "Modelling Earthquake Ground Motions in Seismically Active Regions Using Parametric Time Series Methods," by G.W. Ellis and A.S. Cakmak, 8/25/87, (PB88-134283/AS).

NCEER-87-0015 "Detection and Assessment of Seismic Structural Damage," by E. DiPasquale and A.S. Cakmak, 8/25/87, (PB88-163712/AS).

A-1

NCEER-88-0006 "Combining Structural Optimization and Structural Control," by F.Y. Cheng and C.P. Pantelides, 1/10/88, (PB88-213814/AS).

NCEER-88-0007 "Seismic Performance Assessment of Code-Designed Structures," by H.H-M. Hwang, J-W. Jaw and H-J. Shau, 3/20/88, (PB88-219423/AS).

NCEER-88-0008 "Reliability Analysis of Code-Designed Structures Under Natural Hazards," by H.H-M. Hwang, H. Ushiba and M. Shinozuka, 2/29/88, (PB88-229471/AS).

NCEER-88-0009 "Seismic Fragility Analysis of Shear Wall Structures," by J-W Jaw and H.H-M. Hwang, 4/30/88, (PB89-102867/AS).

NCEER-88-0010 "Base Isolation of a Multi-Story Building Under a Harmonic Ground Motion - A Comparison of Performances of Various Systems," by F-G Fan, G. Ahmadi and I.G. Tadjbakhsh, 5/18/88, (PB89-122238/AS).

NCEER-88-0011 "Seismic Floor Response Spectra for a Combined System by Green's Functions," by F.M. Lavelle, L.A. Bergman and P.D. Spanos, 5/1/88, (PB89-102875/AS)

NCEER-88-0012 "A New Solution Technique for Randomly Excited Hysteretic Structures," by G.Q. Cai and Y.K. Lin, 5/16/88, (PB89-102883/AS).

NCEER-88-0013 "A Study of Radiation Damping and Soil-Structure Interaction Effects in the Centrifuge," by K. Weissman, supervised by J.H. Prevost, 5/24/88, (PB89-144703/AS).

NCEER-88-0014 "Parameter Identification and Implementation of a Kinematic Plasticity Model for Frictional Soils," by J.H. Prevost and D.V. Griffiths, to be published.

NCEER-88-0015 "Two- and Three- Dimensional Dynamic Finite Element Analyses of the Long Valley Dam," by D.V. Griffiths and J.H. Prevost, 6/17/88, (PB89-144711/AS).

NCEER-88-0016 "Damage Assessment of Reinforced Concrete Structures in Eastern United States," by A.M. Reinhorn, M.J. Seidel, S.K. Kunnath and Y.J. Park, 6/15/88, (PB89-122220/AS).

NCEER-88-0017 "Dynamic Compliance of Vertically Loaded Strip Foundations in Multilayered Viscoelastic Soils," by S. Ahmad and A.S.M. Israil, 6/17/88, (PB89-102891/AS).

NCEER-88-0018 "An Experimental Study of Seismic Structural Response With Added Viscoelastic Dampers," by R.C. Lin, Z. Liang, T.T. Soong and R.H. Zhang, 6/30/88, (PB89-122212/AS). This report is available only through NTIS (see address given above).

NCEER-88-0019 "Experimental Investigation of Primary - Secondary System Interaction," by G.D. Manolis, G. Juhn and A.M. Reinhorn, 5/27/88, (PB89-122204/AS).

NCEER-88-0020 "A Response Spectrum Approach For Analysis of Nonclassically Damped Structures," by J.N. Yang, S. Sarkani and F.X. Long, 4/22/88, (PB89-102909/AS).

NCEER-88-0021 "Seismic Interaction of Structures and Soils: Stochastic Approach," by A.S. Veletsos and A.M. Prasad, 7/21/88, (PB89-122196/AS).

NCEER-88-0022 "Identification of the Serviceability Limit State and Detection of Seismic Structural Damage," by E. DiPasquale and A.S. Cakmak, 6/15/88, (PB89-122188/AS). This report is available only through NTIS (see address given above).

NCEER-88-0023 "Multi-Hazard Risk Analysis: Case of a Simple Offshore Structure," by B.K. Bhartia and E.H. Vanmarcke, 7/21/88, (PB89-145213/AS).

NCEER 88-0024 "Automated Seismic Design of Reinforced Concrete Buildings," by Y.S. Chung, C. Meyer and M. Shinozuka, 7/5/88, (PB89-122170/AS). This report is available only through NTIS (see address given above)

NCEER-88-0025 "Experimental Study of Active Control of MDOF Structures Under Seismic Excitations," by L.L. Chung, R.C. Lin, T.T. Soong and A.M. Reinhorn, 7/10/88, (PB89-122600/AS)

NCEER-88-0026 "Earthquake Simulation Tests of a Low-Rise Metal Structure," by J.S. Hwang, K.C. Chang, G.C. Lee and R.L. Ketter, 8/1/88, (PB89-102917/AS).

NCEER-88-0027 "Systems Study of Urban Response and Reconstruction Due to Catastrophic Earthquakes," by F. Kozin and H.K. Zhou, 9/22/88, (PB90-162348/AS).

NCEER-88-0028 "Seismic Fragility Analysis of Plane Frame Structures," by H.H-M. Hwang and Y.K. Low, 7/31/88, (PB89-131445/AS).

NCEER-88-0029 "Response Analysis of Stochastic Structures," by A. Kardara, C. Bucher and M. Shinozuka, 9/22/88, (PB89-174429/AS).

NCEER-88-0030 "Nonnormal Accelerations Due to Yielding in a Primary Structure," by D.C.K. Chen and L.D. Lutes, 9/19/88, (PB89-131437/AS).

NCEER-88-0031 "Design Approaches for Soil-Structure Interaction," by A.S. Veletsos, A.M. Prasad and Y. Tang, 12/30/88, (PB89-174437/AS). This report is available only through NTIS (see address given above).

NCEER-88-0032 "A Re-evaluation of Design Spectra for Seismic Damage Control," by C.J. Turkstra and A.G. Tallin, 11/7/88, (PB89-145221/AS).

NCEER-88-0033 "The Behavior and Design of Noncontact Lap Splices Subjected to Repeated Inelastic Tensile Loading," by V.E. Sagan, P. Gergely and R.N. White, 12/8/88, (PB89-163737/AS).

NCEER-88-0034 "Seismic Response of Pile Foundations," by S.M. Mamoon, P.K. Banerjee and S. Ahmad, 11/1/88, (PB89-145239/AS).

NCEER-88-0035 "Modeling of R/C Building Structures With Flexible Floor Diaphragms (IDARC2)," by A.M. Reinhorn, S.K. Kunnath and N. Panahshahi, 9/7/88, (PB89-207153/AS).

NCEER-88-0036 "Solution of the Dam-Reservoir Interaction Problem Using a Combination of FEM, BEM with Particular Integrals, Modal Analysis, and Substructuring," by C-S. Tsai, G.C. Lee and R.L. Ketter, 12/31/88, (PB89-207146/AS).

NCEER-88-0037 "Optimal Placement of Actuators for Structural Control," by F.Y. Cheng and C.P. Pantelides, 8/15/88, (PB89-162846/AS).

NCEER-88-0038 "Teflon Bearings in Aseismic Base Isolation: Experimental Studies and Mathematical Modeling," by A. Mokha, M.C. Constantinou and A.M. Reinhorn, 12/5/88, (PB89-218457/AS). This report is available only through NTIS (see address given above).

NCEER-88-0039 "Seismic Behavior of Flat Slab High-Rise Buildings in the New York City Area," by P. Weidlinger and M. Ettouney, 10/15/88, (PB90-145681/AS).

NCEER-88-0040 "Evaluation of the Earthquake Resistance of Existing Buildings in New York City," by P. Weidlinger and M. Ettouney, 10/15/88, to be published.

NCEER-88-0041 "Small-Scale Modeling Techniques for Reinforced Concrete Structures Subjected to Seismic Loads," by W. Kim, A. El-Attar and R.N. White, 11/22/88, (PB89-189625/AS).

A-4

NCEER-88-0042 "Modeling Strong Ground Motion from Multiple Event Earthquakes," by G.W. Ellis and A.S. Cakmak, 10/15/88, (PB89-174445/AS).

NCEER-88-0043 "Nonstationary Models of Seismic Ground Acceleration," by M. Grigoriu, S.E. Ruiz and E. Rosenblueth, 7/15/88, (PB89-189617/AS).

NCEER-88-0044 "SARCF User's Guide: Seismic Analysis of Reinforced Concrete Frames," by Y.S. Chung, C. Meyer and M. Shinozuka, 11/9/88, (PB89-174452/AS).

NCEER-88-0045 "First Expert Panel Meeting on Disaster Research and Planning," edited by J. Pantelic and J. Stoyle, 9/15/88, (PB89-174460/AS).

NCEER-88-0046 "Preliminary Studies of the Effect of Degrading Infill Walls on the Nonlinear Seismic Response of Steel Frames," by C.Z. Chrysostomou, P. Gergely and J.F. Abel, 12/19/88, (PB89-208383/AS).

NCEER-88-0047 "Reinforced Concrete Frame Component Testing Facility - Design, Construction, Instrumentation and Operation," by S.P. Pessiki, C. Conley, T. Bond, P. Gergely and R.N. White, 12/16/88, (PB89-174478/AS).

NCEER-89-0001 "Effects of Protective Cushion and Soil Compliancy on the Response of Equipment Within a Seismically Excited Building," by J.A. HoLung, 2/16/89, (PB89-207179/AS).

NCEER-89-0002 "Statistical Evaluation of Response Modification Factors for Reinforced Concrete Structures," by H.H.M. Hwang and J-W. Jaw, 2/17/89, (PB89-207187/AS).

NCEER-89-0003 "Hysteretic Columns Under Random Excitation," by G-Q. Cai and Y.K. Lin, 1/9/89, (PB89-196513/AS).

NCEER 89 0004 "Experimental Study of 'Elephant Foot Bulge' Instability of Thin-Walled Metal Tanks," by Z-H. Jia and R.L. Ketter, 2/22/89, (PB89-207195/AS).

NCEER-89-0005 "Experiment on Performance of Buried Pipelines Across San Andreas Fault," by J. Isenberg, E. Richardson and T.D. O'Rourke, 3/10/89, (PB89-218440/AS).

NCEER-89-0006 "A Knowledge-Based Approach to Structural Design of Earthquake-Resistant Buildings," by M. Subramani, P. Gergely, C.H. Conley, J.F. Abel and A.H. Zaghw, 1/15/89, (PB89-218465/AS).

NCEER-89-0007 "Liquefaction Hazards and Their Effects on Buried Pipelines," by T.D. O'Rourke and P.A. Lane, 2/1/89, (PB89-218481).

NCEER-89-0008 "Fundamentals of System Identification in Structural Dynamics," by H. Imai, C-B. Yun, O. Maruyama and M. Shinozuka, 1/26/89, (PB89-207211/AS).

NCEER-89-0009 "Effects of the 1985 Michoacan Earthquake on Water Systems and Other Buried Lifelines in Mexico," by A.G. Ayala and M.J. O'Rourke, 3/8/89, (PB89-207229/AS).

NCEER-89-R010 "NCEER Bibliography of Earthquake Education Materials," by K.E.K. Ross, Second Revision, 9/1/89, (PB90-125352/AS).

NCEER-89-0011 "Inelastic Three-Dimensional Response Analysis of Reinforced Concrete Building Structures (IDARC-3D), Part I - Modeling," by S.K. Kunnath and A.M. Reinhorn, 4/17/89, (PB90-114612/AS).

NCEER-89-0012 "Recommended Modifications to ATC-14," by C.D. Poland and J.O. Malley, 4/12/89, (PB90-108648/AS).

NCEER-89-0013 "Repair and Strengthening of Beam-to-Column Connections Subjected to Earthquake Loading," by M. Corazao and A.J. Durrani, 2/28/89, (PB90-109885/AS).

A-5

NCEER-89-0014 "Program EXKAL2 for Identification of Structural Dynamic Systems," by O. Maruyama, C-B. Yun, M. Hoshiya and M. Shinozuka, 5/19/89, (PB90-109877/AS).

NCEER-89-0015 "Response of Frames With Bolted Semi-Rigid Connections, Part I - Experimental Study and Analytical Predictions," by P.J. DiCorso, A.M. Reinhorn, J.R. Dickerson, J.B. Radziminski and W.L. Harper, 6/1/89, to be published.

NCEER-89-0016 "ARMA Monte Carlo Simulation in Probabilistic Structural Analysis," by P.D. Spanos and M.P. Mignolet, 7/10/89, (PB90-109893/AS).

NCEER-89-P017 "Preliminary Proceedings from the Conference on Disaster Preparedness - The Place of Earthquake Education in Our Schools," Edited by K.E.K. Ross, 6/23/89.

NCEER-89-0017 "Proceedings from the Conference on Disaster Preparedness - The Place of Earthquake Education in Our Schools," Edited by K.E.K. Ross, 12/31/89, (PB90-207895). This report is available only through NTIS (see address given above).

NCEER-89-0018 "Multidimensional Models of Hysteretic Material Behavior for Vibration Analysis of Shape Memory Energy Absorbing Devices, by E.J. Graesser and F.A. Cozzarelli, 6/7/89, (PB90-164146/AS).

NCEER-89-0019 "Nonlinear Dynamic Analysis of Three Dimensional Base Isolated Structures (3D-BASIS)," by S. Nagarajaiah, A.M. Reinhorn and M.C. Constantinou, 8/3/89, (PB90-161936/AS). This report is available only through NTIS (see address given above).

NCEER-89-0020 "Structural Control Considering Time-Rate of Control Forces and Control Rate Constraints," by F.Y. Cheng and C.P. Pantelides, 8/3/89, (PB90-120445/AS).

NCEER-89-0021 "Subsurface Conditions of Memphis and Shelby County," by K.W. Ng, T-S. Chang and H-H.M. Hwang, 7/26/89, (PB90-120437/AS).

NCEER-89-0022 "Seismic Wave Propagation Effects on Straight Jointed Buried Pipelines," by K. Elhmadi and M.J. O'Rourke, 8/24/89, (PB90-162322/AS).

NCEER-89-0023 "Workshop on Serviceability Analysis of Water Delivery Systems," edited by M. Grigoriu, 3/6/89, (PB90-127424/AS).

NCEER-89-0024 "Shaking Table Study of a 1/5 Scale Steel Frame Composed of Tapered Members," by K.C. Chang, J.S. Hwang and G.C. Lee, 9/18/89, (PB90-160169/AS).

NCEER-89-0025 "DYNA1D: A Computer Program for Nonlinear Seismic Site Response Analysis - Technical Documentation," by Jean H. Prevost, 9/14/89, (PB90-161944/AS). This report is available only through NTIS (see address given above).

NCEER-89-0026 "1:4 Scale Model Studies of Active Tendon Systems and Active Mass Dampers for Aseismic Protection," by A.M. Reinhorn, T.T. Soong, R.C. Lin, Y.P. Yang, Y. Fukao, H. Abe and M. Nakai, 9/15/89, (PB90-173246/AS).

NCEER-89-0027 "Scattering of Waves by Inclusions in a Nonhomogeneous Elastic Half Space Solved by Boundary Element Methods," by P.K. Hadley, A. Askar and A.S. Cakmak, 6/15/89, (PB90-145699/AS).

NCEER-89-0028 "Statistical Evaluation of Deflection Amplification Factors for Reinforced Concrete Structures," by H.H.M. Hwang, J-W. Jaw and A.L. Ch'ng, 8/31/89, (PB90-164633/AS).

NCEER-89-0029 "Bedrock Accelerations in Memphis Area Due to Large New Madrid Earthquakes," by H.H.M. Hwang, C.H.S. Chen and G. Yu, 11/7/89, (PB90-162330/AS).

A-6

NCEER-89-0030 "Seismic Behavior and Response Sensitivity of Secondary Structural Systems," by Y.Q. Chen and T.T. Soong. 10/23/89, (PB90-164658/AS).

NCEER-89-0031 "Random Vibration and Reliability Analysis of Primary-Secondary Structural Systems," by Y. Ibrahim, M. Grigoriu and T.T. Soong, 11/10/89, (PB90-161951/AS).

NCEER-89-0032 "Proceedings from the Second U.S. - Japan Workshop on Liquefaction, Large Ground Deformation and Their Effects on Lifelines, September 26-29, 1989," Edited by T.D. O'Rourke and M. Hamada, 12/1/89, (PB90-209388/AS).

NCEER-89-0033 "Deterministic Model for Seismic Damage Evaluation of Reinforced Concrete Structures," by J.M. Bracci, A.M. Reinhorn, J.B. Mander and S.K. Kunnath, 9/27/89.

NCEER-89-0034 "On the Relation Between Local and Global Damage Indices," by E. DiPasquale and A.S. Cakmak, 8/15/89, (PB90-173865).

NCEER-89-0035 "Cyclic Undrained Behavior of Nonplastic and Low Plasticity Silts," by A.J. Walker and H.E. Stewart, 7/26/89, (PB90-183518/AS).

NCEER-89-0036 "Liquefaction Potential of Surficial Deposits in the City of Buffalo, New York," by M. Budhu, R. Giese and L. Baumgrass, 1/17/89, (PB90-208455/AS).

NCEER-89-0037 "A Deterministic Assessment of Effects of Ground Motion Incoherence," by A.S. Veletsos and Y. Tang, 7/15/89, (PB90-164294/AS).

NCEER-89-0038 "Workshop on Ground Motion Parameters for Seismic Hazard Mapping," July 17-18, 1989, edited by R.V. Whitman, 12/1/89, (PB90-173923/AS).

NCEER-89-0039 "Seismic Effects on Elevated Transit Lines of the New York City Transit Authority," by C.J. Costantino, C.A. Miller and E. Heymsfield, 12/26/89, (PB90-207887/AS).

NCEER-89-0040 "Centrifugal Modeling of Dynamic Soil-Structure Interaction," by K. Weissman, Supervised by J.H. Prevost, 5/10/89, (PB90-207879/AS).

NCEER-89-0041 "Linearized Identification of Buildings With Cores for Seismic Vulnerability Assessment," by I-K. Ho and A.E. Aktan, 11/1/89, (PB90-251943/AS).

NCEER-90-0001 "Geotechnical and Lifeline Aspects of the October 17, 1989 Loma Prieta Earthquake in San Francisco," by T.D. O'Rourke, H.E. Stewart, F.T. Blackburn and T.S. Dickerman, 1/90, (PB90-208596/AS).

NCEER-90-0002 "Nonnormal Secondary Response Due to Yielding in a Primary Structure," by D.C.K. Chen and L.D. Lutes, 2/28/90, (PB90-251976/AS).

NCEER-90-0003 "Earthquake Education Materials for Grades K-12," by K.E.K. Ross, 4/16/90, (PB91-113415/AS).

NCEER-90-0004 "Catalog of Strong Motion Stations in Eastern North America," by R.W. Busby, 4/3/90, (PB90-251984)/AS.

NCEER-90-0005 "NCEER Strong-Motion Data Base: A User Manual for the GeoBase Release (Version 1.0 for the Sun3)," by P. Friberg and K. Jacob, 3/31/90 (PB90-258062/AS).

NCEER-90-0006 "Seismic Hazard Along a Crude Oil Pipeline in the Event of an 1811-1812 Type New Madrid Earthquake," by H.H.M. Hwang and C-H.S. Chen, 4/16/90(PB90-258054).

NCEER-90-0007 "Site-Specific Response Spectra for Memphis Sheahan Pumping Station," by H.H.M. Hwang and C.S. Lee, 5/15/90, (PB91-108811/AS).

A-7

NCEER-90-0008 "Pilot Study on Seismic Vulnerability of Crude Oil Transmission Systems," by T. Ariman, R. Dobry, M. Grigoriu, F. Kozin, M. O'Rourke, T. O'Rourke and M. Shinozuka, 5/25/90, (PB91-108837/AS).

NCEER-90-0009 "A Program to Generate Site Dependent Time Histories: EQGEN," by G.W. Ellis, M. Srinivasan and A.S. Cakmak, 1/30/90, (PB91-108829/AS).

NCEER-90-0010 "Active Isolation for Seismic Protection of Operating Rooms," by M.E. Talbott, Supervised by M. Shinozuka, 6/8/9, (PB91-110205/AS).

NCEER-90-0011 "Program LINEARID for Identification of Linear Structural Dynamic Systems," by C-B Yun and M. Shinozuka, 6/25/90, (PB91-110312/AS).

NCEER-90-0012 "Two-Dimensional Two-Phase Elasto-Plastic Seismic Response of Earth Dams," by A.N. Yiagos, Supervised by J.H. Prevost, 6/20/90, (PB91-110197/AS).

NCEER-90-0013 "Secondary Systems in Base-Isolated Structures: Experimental Investigation, Stochastic Response and Stochastic Sensitivity," by G.D. Manolis, G. Juhn, M.C. Constantinou and A.M. Reinhorn, 7/1/90, (PB91-110320/AS).

NCEER-90-0014 "Seismic Behavior of Lightly-Reinforced Concrete Column and Beam-Column Joint Details," by S.P. Pessiki, C.H. Conley, P. Gergely and R.N. White, 8/22/90, (PB91-108795/AS).

NCEER-90-0015 "Two Hybrid Control Systems for Building Structures Under Strong Earthquakes," by J.N. Yang and A. Danielians, 6/29/90, (PB91-125393/AS).

NCEER-90-0016 "Instantaneous Optimal Control with Acceleration and Velocity Feedback," by J.N. Yang and Z. Li, 6/29/90, (PB91-125401/AS).

NCEER-90-0017 "Reconnaissance Report on the Northern Iran Earthquake of June 21, 1990," by M. Mehrain, 10/4/90, (PB91-125377/AS).

NCEER-90-0018 "Evaluation of Liquefaction Potential in Memphis and Shelby County," by T.S. Chang, P.S. Tang, C.S. Lee and H. Hwang, 8/10/90, (PB91-125427/AS).

NCEER-90-0019 "Experimental and Analytical Study of a Combined Sliding Disc Bearing and Helical Steel Spring Isolation System," by M.C. Constantinou, A.S. Mokha and A.M. Reinhorn, 10/4/90, (PB91-125385/AS).

NCEER-90-0020 "Experimental Study and Analytical Prediction of Earthquake Response of a Sliding Isolation System with a Spherical Surface," by A.S. Mokha, M.C. Constantinou and A.M. Reinhorn, 10/11/90, (PB91-125419/AS).

NCEER-90-0021 "Dynamic Interaction Factors for Floating Pile Groups," by G. Gazetas, K. Fan, A. Kaynia and E. Kausel, 9/10/90, (PB91-170381/AS).

NCEER-90-0022 "Evaluation of Seismic Damage Indices for Reinforced Concrete Structures," by S. Rodriguez-Gomez and A.S. Cakmak, 9/30/90, PB91-171322/AS).

NCEER-90-0023 "Study of Site Response at a Selected Memphis Site," by H. Desai, S. Ahmad, E.S. Gazetas and M.R. Oh, 10/11/90, (PB91-196857/AS).

NCEER-90-0024 "A User's Guide to Strongmo: Version 1.0 of NCEER's Strong-Motion Data Access Tool for PCs and Terminals," by P.A. Friberg and C.A.T. Susch, 11/15/90, (PB91-171272/AS).

NCEER-90-0025 "A Three-Dimensional Analytical Study of Spatial Variability of Seismic Ground Motions," by L-L. Hong and A.H.-S. Ang, 10/30/90, (PB91-170399/AS).

NCEER-90-0026 "MUMOID User's Guide - A Program for the Identification of Modal Parameters," by S. Rodriguez-Gomez and E. DiPasquale, 9/30/90, (PB91-171298/AS)

NCEER-90-0027 "SARCF-II User's Guide - Seismic Analysis of Reinforced Concrete Frames," by S. Rodriguez-Gomez, Y.S. Chung and C. Meyer, 9/30/90, (PB91-171280/AS).

NCEER-90-0028 "Viscous Dampers: Testing, Modeling and Application in Vibration and Seismic Isolation," by N. Makris and M.C. Constantinou, 12/20/90 (PB91-190561/AS).

NCEER-90-0029 "Soil Effects on Earthquake Ground Motions in the Memphis Area," by H. Hwang, C.S. Lee, K.W. Ng and T.S. Chang, 8/2/90, (PB91-190751/AS).

NCEER-91-0001 "Proceedings from the Third Japan-U.S. Workshop on Earthquake Resistant Design of Lifeline Facilities and Countermeasures for Soil Liquefaction, December 17-19, 1990," edited by T.D. O'Rourke and M. Hamada, 2/1/91, (PB91-179259/AS).

NCEER-91-0002 "Physical Space Solutions of Non-Proportionally Damped Systems," by M. Tong, Z. Liang and G.C. Lee, 1/15/91, (PB91-179242/AS).

NCEER-91-0003 "Seismic Response of Single Piles and Pile Groups," by K. Fan and G. Gazetas, 1/10/91, (PB92-174994/AS).

NCEER-91-0004 "Damping of Structures: Part 1 - Theory of Complex Damping," by Z. Liang and G. Lee, 10/10/91, (PB92-197235/AS).

NCEER-91-0005 "3D-BASIS - Nonlinear Dynamic Analysis of Three Dimensional Base Isolated Structures: Part II," by S. Nagarajaiah, A.M. Reinhorn and M.C. Constantinou, 2/28/91, (PB91-190553/AS).

NCEER-91-0006 "A Multidimensional Hysteretic Model for Plasticity Deforming Metals in Energy Absorbing Devices," by E.J. Graesser and F.A. Cozzarelli, 4/9/91, (PB92-108364/AS).

NCEER-91-0007 "A Framework for Customizable Knowledge-Based Expert Systems with an Application to a KBES for Evaluating the Seismic Resistance of Existing Buildings," by E.G. Ibarra-Anaya and S.J. Fenves, 4/9/91, (PB91-210930/AS).

NCEER-91-0008 "Nonlinear Analysis of Steel Frames with Semi-Rigid Connections Using the Capacity Spectrum Method," by G.G. Deierlein, S-H. Hsieh, Y-J. Shen and J.F. Abel, 7/2/91, (PB92-113828/AS).

NCEER-91-0009 "Earthquake Education Materials for Grades K-12," by K.E.K. Ross, 4/30/91, (PB91-212142/AS).

NCEER-91-0010 "Phase Wave Velocities and Displacement Phase Differences in a Harmonically Oscillating Pile," by N. Makris and G. Gazetas, 7/8/91, (PB92-108356/AS).

NCEER-91-0011 "Dynamic Characteristics of a Full-Size Five-Story Steel Structure and a 2/5 Scale Model," by K.C. Chang, G.C. Yao, G.C. Lee, D.S. Hao and Y.C. Yeh," 7/2/91.

NCEER-91-0012 "Seismic Response of a 2/5 Scale Steel Structure with Added Viscoelastic Dampers," by K.C. Chang, T.T. Soong, S-T. Oh and M.L. Lai, 5/17/91 (PB92-110816/AS).

NCEER-91-0013 "Earthquake Response of Retaining Walls; Full-Scale Testing and Computational Modeling," by S. Alampalli and A-W.M. Elgamal, 6/20/91, to be published.

NCEER-91-0014 "3D-BASIS-M: Nonlinear Dynamic Analysis of Multiple Building Base Isolated Structures," by P.C. Tsopelas, S. Nagarajaiah, M.C. Constantinou and A.M. Reinhorn, 5/28/91, (PB92-113885/AS).

A-9

NCEER-91-0015 "Evaluation of SEAOC Design Requirements for Sliding Isolated Structures," by D. Theodossiou and M.C. Constantinou, 6/10/91, (PB92-114602/AS).

NCEER-91-0016 "Closed-Loop Modal Testing of a 27-Story Reinforced Concrete Flat Plate-Core Building," by H.R. Somaprasad, T. Toksoy, H. Yoshiyuki and A.E. Aktan, 7/15/91, (PB92-129980/AS).

NCEER-91-0017 "Shake Table Test of a 1/6 Scale Two-Story Lightly Reinforced Concrete Building," by A.G. El-Attar, R.N. White and P. Gergely, 2/28/91, (PB92-222447/AS).

NCEER-91-0018 "Shake Table Test of a 1/8 Scale Three-Story Lightly Reinforced Concrete Building," by A.G. El-Attar, R.N. White and P. Gergely, 2/28/91.

NCEER-91-0019 "Transfer Functions for Rigid Rectangular Foundations," by A.S. Veletsos, A.M. Prasad and W.H. Wu, 7/31/91

NCEER-91-0020 "Hybrid Control of Seismic-Excited Nonlinear and Inelastic Structural Systems," by J.N. Yang, Z. Li and A. Danielians, 8/1/91, (PB92-143171/AS).

NCEER-91-0021 "The NCEER-91 Earthquake Catalog: Improved Intensity-Based Magnitudes and Recurrence Relations for U.S. Earthquakes East of New Madrid," by L. Seeber and J.G. Armbruster, 8/28/91, (PB92-176742/AS).

NCEER-91-0022 "Proceedings from the Implementation of Earthquake Planning and Education in Schools: The Need for Change - The Roles of the Changemakers," by K.E.K. Ross and F. Winslow, 7/23/91, (PB92-129998/AS).

NCEER-91-0023 "A Study of Reliability-Based Criteria for Seismic Design of Reinforced Concrete Frame Buildings," by H.H.M. Hwang and H-M. Hsu, 8/10/91, (PB92-140235/AS).

NCEER-91-0024 "Experimental Verification of a Number of Structural System Identification Algorithms," by R.G. Ghanem, H. Gavin and M. Shinozuka, 9/18/91, (PB92-176577/AS).

NCEER-91-0025 "Probabilistic Evaluation of Liquefaction Potential," by H.H.M. Hwang and C.S. Lee," 11/25/91, (PB92-143429/AS).

NCEER-91-0026 "Instantaneous Optimal Control for Linear, Nonlinear and Hysteretic Structures - Stable Controllers," by J.N. Yang and Z. Li, 11/15/91, (PB92-163807/AS).

NCEER-91-0027 "Experimental and Theoretical Study of a Sliding Isolation System for Bridges," by M.C. Constantinou, A. Kartoum, A.M. Reinhorn and P. Bradford, 11/15/91, (PB92-176973/AS).

NCEER-92-0001 "Case Studies of Liquefaction and Lifeline Performance During Past Earthquakes, Volume 1: Japanese Case Studies," Edited by M. Hamada and T. O'Rourke, 2/17/92, (PB92-197243/AS).

NCEER-92-0002 "Case Studies of Liquefaction and Lifeline Performance During Past Earthquakes, Volume 2: United States Case Studies," Edited by T. O'Rourke and M. Hamada, 2/17/92, (PB92-197250/AS).

NCEER-92-0003 "Issues in Earthquake Education," Edited by K. Ross, 2/3/92, (PB92-222389/AS).

NCEER-92-0004 "Proceedings from the First U.S. - Japan Workshop on Earthquake Protective Systems for Bridges," 2/4/92, to be published.

NCEER-92-0005 "Seismic Ground Motion from a Haskell-Type Source in a Multiple-Layered Half-Space," A.P. Theoharis, G. Deodatis and M. Shinozuka, 1/2/92, to be published.

NCEER-92-0006 "Proceedings from the Site Effects Workshop," Edited by R. Whitman, 2/29/92, (PB92-127201/AS).

A-10

NCEER-92-0007   "Engineering Evaluation of Permanent Ground Deformations Due to Seismically-Induced Liquefaction," by M.H. Baziar, R. Dobry and A-W.M. Elgamal, 3/24/92, (PB92-222421/AS).

NCEER-92-0008   "A Procedure for the Seismic Evaluation of Buildings in the Central and Eastern United States," by C.D. Poland and J.O. Malley, 4/2/92, (PB92-222439/AS).

NCEER-92-0009   "Experimental and Analytical Study of a Hybrid Isolation System Using Friction Controllable Sliding Bearings," by M.Q. Feng, S. Fujii and M. Shinozuka, 5/15/92, (PB93-150282/AS).

NCEER-92-0010   "Seismic Resistance of Slab-Column Connections in Existing Non-Ductile Flat-Plate Buildings," by A.J. Durrani and Y. Du, 5/18/92.

NCEER-92-0011   "The Hysteretic and Dynamic Behavior of Brick Masonry Walls Upgraded by Ferrocement Coatings Under Cyclic Loading and Strong Simulated Ground Motion," by H. Lee and S.P. Prawel, 5/11/92, to be published.

NCEER-92-0012   "Study of Wire Rope Systems for Seismic Protection of Equipment in Buildings," by G.F. Demetriades, M.C. Constantinou and A.M. Reinhorn, 5/20/92.

NCEER-92-0013   "Shape Memory Structural Dampers: Material Properties, Design and Seismic Testing," by P.R. Witting and F.A. Cozzarelli, 5/26/92.

NCEER-92-0014   "Longitudinal Permanent Ground Deformation Effects on Buried Continuous Pipelines," by M.J. O'Rourke, and C. Nordberg, 6/15/92.

NCEER-92-0015   "A Simulation Method for Stationary Gaussian Random Functions Based on the Sampling Theorem," by M. Grigoriu and S. Balopoulou, 6/11/92, (PB93-127496/AS).

NCEER-92-0016   "Gravity-Load-Designed Reinforced Concrete Buildings: Seismic Evaluation of Existing Construction and Detailing Strategies for Improved Seismic Resistance," by G.W. Hoffmann, S.K. Kunnath, J.B. Mander and A.M. Reinhorn, 7/15/92, to be published.

NCEER-92-0017   "Observations on Water System and Pipeline Performance in the Limón Area of Costa Rica Due to the April 22, 1991 Earthquake," by M. O'Rourke and D. Ballantyne, 6/30/92, (PB93-126811/AS).

NCEER-92-0018   "Fourth Edition of Earthquake Education Materials for Grades K-12," Edited by K.E.K. Ross, 8/10/92.

NCEER-92-0019   "Proceedings from the Fourth Japan-U.S. Workshop on Earthquake Resistant Design of Lifeline Facilities and Countermeasures for Soil Liquefaction," Edited by M. Hamada and T.D. O'Rourke, 8/12/92, (PB93-163939/AS).

NCEER-92-0020   "Active Bracing System: A Full Scale Implementation of Active Control," by A.M. Reinhorn, T.T. Soong, R.C. Lin, M.A. Riley, Y.P. Wang, S. Aizawa and M. Higashino, 8/14/92, (PB93-127512/AS).

NCEER-92-0021   "Empirical Analysis of Horizontal Ground Displacement Generated by Liquefaction-Induced Lateral Spreads," by S.F. Bartlett and T.L. Youd, 8/17/92.

NCEER-92-0022   "IDARC Version 3.0: Inelastic Damage Analysis of Reinforced Concrete Structures," by S.K. Kunnath, A.M. Reinhorn and R.F. Lobo, 8/31/92, to be published.

NCEER-92-0023   "A Semi-Empirical Analysis of Strong-Motion Peaks in Terms of Seismic Source, Propagation Path and Local Site Conditions, by M. Kamiyama, M.J. O'Rourke and R. Flores-Berrones, 9/9/92, (PB93-150266/AS).

NCEER-92-0024   "Seismic Behavior of Reinforced Concrete Frame Structures with Nonductile Details, Part I: Summary of Experimental Findings of Full Scale Beam-Column Joint Tests," by A. Beres, R.N. White and P. Gergely, 9/30/92, to be published.

NCEER-92-0025   "Experimental Results of Repaired and Retrofitted Beam-Column Joint Tests in Lightly Reinforced Concrete Frame Buildings," by A. Beres, S. El-Borgi, R.N. White and P. Gergely, 10/29/92, to be published.

A-11

NCEER-92-0026   "A Generalization of Optimal Control Theory: Linear and Nonlinear Structures," by J.N. Yang, Z. Li and S. Vongchavalitkul, 11/2/92.

NCEER-92-0027   "Seismic Resistance of Reinforced Concrete Frame Structures Designed Only for Gravity Loads: Part I - Design and Properties of a One-Third Scale Model Structure," by J.M. Bracci, A.M. Reinhorn and J.B. Mander, 12/1/92.

NCEER-92-0028   "Seismic Resistance of Reinforced Concrete Frame Structures Designed Only for Gravity Loads: Part II - Experimental Performance of Subassemblages," by L.E. Aycardi, J.B. Mander and A.M. Reinhorn, 12/1/92.

NCEER-92-0029   "Seismic Resistance of Reinforced Concrete Frame Structures Designed Only for Gravity Loads: Part III - Experimental Performance and Analytical Study of a Structural Model," by J.M. Bracci, A.M. Reinhorn and J.B. Mander, 12/1/92.

NCEER-92-0030   "Evaluation of Seismic Retrofit of Reinforced Concrete Frame Structures: Part I - Experimental Performance of Retrofitted Subassemblages," by D. Choudhuri, J.B. Mander and A.M. Reinhorn, 12/8/92.

NCEER-92-0031   "Evaluation of Seismic Retrofit of Reinforced Concrete Frame Structures: Part II - Experimental Performance and Analytical Study of a Retrofitted Structural Model," by J.M. Bracci, A.M. Reinhorn and J.B. Mander, 12/8/92

NCEER-92-0032   "Experimental and Analytical Investigation of Seismic Response of Structures with Supplemental Fluid Viscous Dampers," by M.C. Constantinou and M.D. Symans, 12/21/92.

NCEER-92-0033   "Reconnaissance Report on the Cairo, Egypt Earthquake of October 12, 1992," by M. Khater, 12/23/92.

NCEER-92-0034   "Low-Level Dynamic Characteristics of Four Tall Flat-Plate Buildings in New York City," by H. Gavin, S. Yuan, J. Grossman, E. Pekelis and K. Jacob, 12/28/92.

NCEER-93-0001   "An Experimental Study on the Seismic Performance of Brick-Infilled Steel Frames With and Without Retrofit," by J.B. Mander, B. Nair, K. Wojkowski and J. Ma, 1/29/93.

NCEER-93-0002   "Social Accounting for Disaster Preparedness and Recovery Planning," by S. Cole, E. Pantoja and V. Razak, 2/22/93, to be published.

NCEER-93-0003   "Assessment of 1991 NEHRP Provisions for Nonstructural Components and Recommended Revisions," by T.T. Soong, G. Chen, Z. Wu, R-H. Zhang and M. Grigoriu, 3/1/93.

NCEER-93-0004   "Evaluation of Static and Response Spectrum Analysis Procedures of SEAOC/UBC for Seismic Isolated Structures," by C.W. Winters and M.C. Constantinou, 3/23/93.

NCEER-93-0005   "Earthquakes in the Northeast - Are We Ignoring the Hazard? A Workshop on Earthquake Science and Safety for Educators," edited by K.E.K. Ross, 4/2/93, to be published.

NCEER-93-0006   "Inelastic Response of Reinforced Concrete Structures with Viscoelastic Braces," by R.F. Lobo, J.M. Bracci, K.L. Shen, A.M. Reinhorn and T.T. Soong, 4/5/93.

NCEER-93-0007   "Seismic Testing of Installation Methods for Computers and Data Processing Equipment," by K. Kosar, T.T. Soong, K.L. Shen, J.A. HoLung and Y.K. Lin, 4/12/93.

NCEER-93-0008   "Retrofit of Reinforced Concrete Frames Using Added Dampers," by A. Reinhorn, M. Constantinou and C. Li, to be published.

NCEER-93-0009   "Seismic Applications of Viscoelastic Dampers to Steel Frame Structures," by K.C. Chang and T.T. Soong, to be published.

NCEER-93-0010   "Seismic Performance of Shear-Critical Reinforced Concrete Bridge Piers," by J.B. Mander, S.M. Waheed, M.T.A. Chaudhary and S.S. Chen, 5/12/93.

NCEER-89-0030 "Seismic Behavior and Response Sensitivity of Secondary Structural Systems," by Y.Q. Chen and T.T. Soong, 10/23/89, (PB90-164658/AS).

NCEER-89-0031 "Random Vibration and Reliability Analysis of Primary-Secondary Structural Systems," by Y. Ibrahim, M. Grigoriu and T.T. Soong, 11/10/89, (PB90-161951/AS).

NCEER-89-0032 "Proceedings from the Second U.S. - Japan Workshop on Liquefaction, Large Ground Deformation and Their Effects on Lifelines, September 26-29, 1989," Edited by T.D. O'Rourke and M. Hamada, 12/1/89, (PB90-209188/AS).

NCEER-89-0033 "Deterministic Model for Seismic Damage Evaluation of Reinforced Concrete Structures," by J.M. Bracci, A.M. Reinhorn, J.B. Mander and S.K. Kunnath, 9/27/89.

NCEER-89-0034 "On the Relation Between Local and Global Damage Indices," by E. DiPasquale and A.S. Cakmak, 8/15/89, (PB90-173865).

NCEER-89-0035 "Cyclic Undrained Behavior of Nonplastic and Low Plasticity Silts," by A.J. Walker and H.E. Stewart, 7/26/89, (PB90-183518/AS).

NCEER-89-0036 "Liquefaction Potential of Surficial Deposits in the City of Buffalo, New York," by M. Budhu, R. Giese and L. Baumgrass, 1/17/89, (PB90-208455/AS).

NCEER-89-0037 "A Deterministic Assessment of Effects of Ground Motion Incoherence," by A.S. Veletsos and Y. Tang, 7/15/89, (PB90-164294/AS).

NCEER-89-0038 "Workshop on Ground Motion Parameters for Seismic Hazard Mapping," July 17-18, 1989, edited by R.V. Whitman, 12/1/89, (PB90-173923/AS).

NCEER-89-0039 "Seismic Effects on Elevated Transit Lines of the New York City Transit Authority," by C.J. Costantino, C.A. Miller and E. Heymsfield, 12/26/89, (PB90-207887/AS).

NCEER-89-0040 "Centrifugal Modeling of Dynamic Soil-Structure Interaction," by K. Weissman, Supervised by J.H. Prevost, 5/10/89, (PB90-207879/AS).

NCEER-89-0041 "Linearized Identification of Buildings With Cores for Seismic Vulnerability Assessment," by I-K. Ho and A.E. Aktan, 11/1/89, (PB90-251943/AS).

NCEER-90-0001 "Geotechnical and Lifeline Aspects of the October 17, 1989 Loma Prieta Earthquake in San Francisco," by T.D. O'Rourke, H.E. Stewart, F.T. Blackburn and T.S. Dickerman, 1/90, (PB90-208596/AS).

NCEER-90-0002 "Nonnormal Secondary Response Due to Yielding in a Primary Structure," by D.C.K. Chen and L.D. Lutes, 2/28/90, (PB90-251976/AS).

NCEER-90-0003 "Earthquake Education Materials for Grades K-12," by K.E.K. Ross, 4/16/90, (PB91-113415/AS).

NCEER-90-0004 "Catalog of Strong Motion Stations in Eastern North America," by R.W. Busby, 4/3/90, (PB90-251984)/AS.

NCEER-90-0005 "NCEER Strong-Motion Data Base: A User Manual for the GeoBase Release (Version 1.0 for the Sun3)," by P. Friberg and K. Jacob, 3/31/90 (PB90-258062/AS).

NCEER-90-0006 "Seismic Hazard Along a Crude Oil Pipeline in the Event of an 1811-1812 Type New Madrid Earthquake," by H.H.M. Hwang and C-H.S. Chen, 4/16/90(PB90-258054).

NCEER-90-0007 "Site-Specific Response Spectra for Memphis Sheahan Pumping Station," by H.H.M. Hwang and C.S. Lee, 5/15/90, (PB91-108811/AS).

B-7

NCEER-90-0008 "Pilot Study on Seismic Vulnerability of Crude Oil Transmission Systems," by T. Ariman, R. Dobry, M. Grigoriu, F. Kozin, M. O'Rourke, T. O'Rourke and M. Shinozuka, 5/25/90, (PB91-108837/AS).

NCEER-90-0009 "A Program to Generate Site Dependent Time Histories: EQGEN," by G.W. Ellis, M. Srinivasan and A.S. Cakmak, 1/30/90, (PB91-108829/AS).

NCEER-90-0010 "Active Isolation for Seismic Protection of Operating Rooms," by M.E. Talbott, Supervised by M. Shinozuka, 6/8/9, (PB91-110205/AS).

NCEER-90-0011 "Program LINEARID for Identification of Linear Structural Dynamic Systems," by C-B. Yun and M. Shinozuka, 6/25/90, (PB91-110312/AS).

NCEER-90-0012 "Two-Dimensional Two-Phase Elasto-Plastic Seismic Response of Earth Dams," by A.N. Yiagos, Supervised by J.H. Prevost, 6/20/90, (PB91-110197/AS).

NCEER-90-0013 "Secondary Systems in Base-Isolated Structures: Experimental Investigation, Stochastic Response and Stochastic Sensitivity," by G.D. Manolis, G. Juhn, M.C. Constantinou and A.M. Reinhorn, 7/1/90, (PB91-110320/AS).

NCEER-90-0014 "Seismic Behavior of Lightly-Reinforced Concrete Column and Beam-Column Joint Details," by S.P. Pessiki, C.H. Conley, P. Gergely and R.N. White, 8/22/90, (PB91-108795/AS).

NCEER-90-0015 "Two Hybrid Control Systems for Building Structures Under Strong Earthquakes," by J.N. Yang and A. Danielians, 6/29/90, (PB91-125393/AS).

NCEER-90-0016 "Instantaneous Optimal Control with Acceleration and Velocity Feedback," by J.N. Yang and Z. Li, 6/29/90, (PB91-125401/AS).

NCEER-90-0017 "Reconnaissance Report on the Northern Iran Earthquake of June 21, 1990," by M. Mehrain, 10/4/90, (PB91-125377/AS).

NCEER-90-0018 "Evaluation of Liquefaction Potential in Memphis and Shelby County," by T.S. Chang, P.S. Tang, C.S. Lee and H. Hwang, 8/10/90, (PB91-125427/AS).

NCEER-90-0019 "Experimental and Analytical Study of a Combined Sliding Disc Bearing and Helical Steel Spring Isolation System," by M.C. Constantinou, A.S. Mokha and A.M. Reinhorn, 10/4/90, (PB91-125385/AS).

NCEER-90-0020 "Experimental Study and Analytical Prediction of Earthquake Response of a Sliding Isolation System with a Spherical Surface," by A.S. Mokha, M.C. Constantinou and A.M. Reinhorn, 10/11/90, (PB91-125419/AS).

NCEER-90-0021 "Dynamic Interaction Factors for Floating Pile Groups," by G. Gazetas, K. Fan, A. Kaynia and E. Kausel, 9/10/90, (PB91-170381/AS).

NCEER-90-0022 "Evaluation of Seismic Damage Indices for Reinforced Concrete Structures," by S. Rodriguez-Gomez and A.S. Cakmak, 9/30/90, PB91-171322/AS).

NCEER-90-0023 "Study of Site Response at a Selected Memphis Site," by H. Desai, S. Ahmad, E.S. Gazetas and M.R. Oh, 10/11/90, (PB91-196857/AS).

NCEER-90-0024 "A User's Guide to Strongmo: Version 1.0 of NCEER's Strong-Motion Data Access Tool for PCs and Terminals," by P.A. Friberg and C.A.T. Susch, 11/15/90, (PB91-171272/AS).

NCEER-90-0025 "A Three-Dimensional Analytical Study of Spatial Variability of Seismic Ground Motions," by L-L. Hong and A.H.-S. Ang, 10/30/90, (PB91-170399/AS).

NCEER-90-0026 "MUMOID User's Guide - A Program for the Identification of Modal Parameters," by S. Rodriguez-Gomez and E. DiPasquale, 9/30/90, (PB91-171298/AS).

NCEER-90-0027 "SARCF-II User's Guide - Seismic Analysis of Reinforced Concrete Frames," by S. Rodriguez-Gomez, Y.S. Chung and C. Meyer, 9/30/90, (PB91-171280/AS).

NCEER-90-0028 "Viscous Dampers: Testing, Modeling and Application in Vibration and Seismic Isolation," by N. Makris and M.C. Constantinou, 12/20/90 (PB91-190561/AS).

NCEER-90-0029 "Soil Effects on Earthquake Ground Motions in the Memphis Area," by H. Hwang, C.S. Lee, K.W. Ng and T.S. Chang, 8/2/90, (PB91-190751/AS).

NCEER-91-0001 "Proceedings from the Third Japan-U.S. Workshop on Earthquake Resistant Design of Lifeline Facilities and Countermeasures for Soil Liquefaction, December 17-19, 1990," edited by T.D. O'Rourke and M. Hamada, 2/1/91, (PB91-179259/AS).

NCEER-91-0002 "Physical Space Solutions of Non-Proportionally Damped Systems," by M. Tong, Z. Liang and G.C. Lee, 1/15/91, (PB91-179242/AS).

NCEER-91-0003 "Seismic Response of Single Piles and Pile Groups," by K. Fan and G. Gazetas, 1/10/91, (PB92-174994/AS).

NCEER-91-0004 "Damping of Structures: Part 1 - Theory of Complex Damping," by Z. Liang and G. Lee, 10/10/91, (PB92-197235/AS).

NCEER-91-0005 "3D-BASIS - Nonlinear Dynamic Analysis of Three Dimensional Base Isolated Structures: Part II," by S. Nagarajaiah, A.M. Reinhorn and M.C. Constantinou, 2/28/91, (PB91-190553/AS).

NCEER-91-0006 "A Multidimensional Hysteretic Model for Plasticity Deforming Metals in Energy Absorbing Devices," by E.J. Graesser and F.A. Cozzarelli, 4/9/91, (PB92-108364/AS).

NCEER-91-0007 "A Framework for Customizable Knowledge-Based Expert Systems with an Application to a KBES for Evaluating the Seismic Resistance of Existing Buildings," by E.G. Ibarra-Anaya and S.J. Fenves, 4/9/91, (PB91-210930/AS).

NCEER-91-0008 "Nonlinear Analysis of Steel Frames with Semi-Rigid Connections Using the Capacity Spectrum Method," by G.G. Deierlein, S-H. Hsieh, Y-J. Shen and J.F. Abel, 7/2/91, (PB92-113828/AS).

NCEER-91-0009 "Earthquake Education Materials for Grades K-12," by K.E.K. Ross, 4/30/91, (PB91-212142/AS).

NCEER-91-0010 "Phase Wave Velocities and Displacement Phase Differences in a Harmonically Oscillating Pile," by N. Makris and G. Gazetas, 7/8/91, (PB92-108356/AS).

NCEER-91-0011 "Dynamic Characteristics of a Full-Size Five-Story Steel Structure and a 2/5 Scale Model," by K.C. Chang, G.C. Yao, G.C. Lee, D.S. Hao and Y.C. Yeh," 7/2/91.

NCEER-91-0012 "Seismic Response of a 2/5 Scale Steel Structure with Added Viscoelastic Dampers," by K.C. Chang, T.T. Soong, S-T. Oh and M.L. Lai, 5/17/91 (PB92-110816/AS).

NCEER-91-0013 "Earthquake Response of Retaining Walls; Full-Scale Testing and Computational Modeling," by S. Alampalli and A-W.M. Elgamal, 6/20/91, to be published.

NCEER-91-0014 "3D-BASIS-M: Nonlinear Dynamic Analysis of Multiple Building Base Isolated Structures," by P.C. Tsopelas, S. Nagarajaiah, M.C. Constantinou and A.M. Reinhorn, 5/28/91, (PB92-113885/AS).

B-9

NCEER-91-0015   "Evaluation of SEAOC Design Requirements for Sliding Isolated Structures," by D. Theodossiou and M.C. Constantinou, 6/10/91, (PB92-114602/AS).

NCEER-91-0016   "Closed Loop Modal Testing of a 27-Story Reinforced Concrete Flat Plate-Core Building," by H.R. Somaprasad, T. Toksoy, H. Yoshiyuki and A.E. Aktan, 7/15/91, (PB92-129980/AS).

NCEER-91-0017   "Shake Table Test of a 1/6 Scale Two-Story Lightly Reinforced Concrete Building," by A.G. El-Attar, R.N. White and P. Gergely, 2/28/91, (PB92-222447/AS).

NCEER-91-0018   "Shake Table Test of a 1/8 Scale Three-Story Lightly Reinforced Concrete Building," by A.G. El-Attar, R.N. White and P. Gergely, 2/28/91.

NCEER-91-0019   "Transfer Functions for Rigid Rectangular Foundations," by A.S. Veletsos, A.M. Prasad and W.H. Wu, 7/31/91.

NCEER-91-0020   "Hybrid Control of Seismic-Excited Nonlinear and Inelastic Structural Systems," by J.N. Yang, Z. Li and A. Danielians, 8/1/91, (PB92-143171/AS).

NCEER-91-0021   "The NCEER-91 Earthquake Catalog: Improved Intensity-Based Magnitudes and Recurrence Relations for U.S. Earthquakes East of New Madrid," by L. Seeber and J.G. Armbruster, 8/28/91, (PB92-176742/AS).

NCEER-91-0022   "Proceedings from the Implementation of Earthquake Planning and Education in Schools: The Need for Change - The Roles of the Changemakers," by K.E.K. Ross and F. Winslow, 7/23/91, (PB92-129998/AS).

NCEER-91-0023   "A Study of Reliability Based Criteria for Seismic Design of Reinforced Concrete Frame Buildings," by H.H.M. Hwang and H-M. Hsu, 8/10/91, (PB92-140235/AS).

NCEER-91-0024   "Experimental Verification of a Number of Structural System Identification Algorithms," by R.G. Ghanem, H. Gavin and M. Shinozuka, 9/18/91, (PB92-176577/AS).

NCEER-91-0025   "Probabilistic Evaluation of Liquefaction Potential," by H.H.M. Hwang and C.S. Lee," 11/25/91, (PB92-143429/AS).

NCEER-91-0026   "Instantaneous Optimal Control for Linear, Nonlinear and Hysteretic Structures - Stable Controllers," by J.N. Yang and Z. Li, 11/15/91, (PB92-163807/AS).

NCEER-91-0027   "Experimental and Theoretical Study of a Sliding Isolation System for Bridges," by M.C. Constantinou, A. Kartoum, A.M. Reinhorn and P. Bradford, 11/15/91, (PB92-176973/AS).

NCEER-92-0001   "Case Studies of Liquefaction and Lifeline Performance During Past Earthquakes, Volume 1: Japanese Case Studies," Edited by M. Hamada and T. O'Rourke, 2/17/92, (PB92-197243/AS).

NCEER-92-0002   "Case Studies of Liquefaction and Lifeline Performance During Past Earthquakes, Volume 2: United States Case Studies," Edited by T. O'Rourke and M. Hamada, 2/17/92, (PB92-197250/AS).

NCEER-92-0003   "Issues in Earthquake Education," Edited by K. Ross, 2/3/92, (PB92-222389/AS).

NCEER-92-0004   "Proceedings from the First U.S. - Japan Workshop on Earthquake Protective Systems for Bridges," 2/4/92, to be published.

NCEER-92-0005   "Seismic Ground Motion from a Haskell-Type Source in a Multiple-Layered Half-Space," A.P. Theoharis, G. Deodatis and M. Shinozuka, 1/2/92, to be published.

NCEER-92-0006   "Proceedings from the Site Effects Workshop," Edited by R. Whitman, 2/29/92, (PB92-197201/AS).

B-10

NCEER-92-0007 "Engineering Evaluation of Permanent Ground Deformations Due to Seismically-Induced Liquefaction," by M.H. Baziar, R. Dobry and A.W.M. Elgamal, 3/24/92, (PB92-222421/AS).

NCEER-92-0008 "A Procedure for the Seismic Evaluation of Buildings in the Central and Eastern United States," by C.D. Poland and J.O. Malley, 4/2/92, (PB92-222439/AS).

NCEER-92-0009 "Experimental and Analytical Study of a Hybrid Isolation System Using Friction Controllable Sliding Bearings," by M.Q. Feng, S. Fujii and M. Shinozuka, 5/15/92, (PB93-150282/AS).

NCEER-92-0010 "Seismic Resistance of Slab-Column Connections in Existing Non-Ductile Flat-Plate Buildings," by A.J. Durrani and Y. Du, 5/18/92.

NCEER-92-0011 "The Hysteretic and Dynamic Behavior of Brick Masonry Walls Upgraded by Ferrocement Coatings Under Cyclic Loading and Strong Simulated Ground Motion," by H. Lee and S.P. Prawel, 5/11/92, to be published.

NCEER-92-0012 "Study of Wire Rope Systems for Seismic Protection of Equipment in Buildings," by G.F. Demetriades, M.C. Constantinou and A.M. Reinhorn, 5/20/92.

NCEER-92-0013 "Shape Memory Structural Dampers: Material Properties, Design and Seismic Testing," by P.R. Witting and F.A. Cozzarelli, 5/26/92.

NCEER-92-0014 "Longitudinal Permanent Ground Deformation Effects on Buried Continuous Pipelines," by M.J. O'Rourke, and C. Nordberg, 6/15/92.

NCEER-92-0015 "A Simulation Method for Stationary Gaussian Random Functions Based on the Sampling Theorem," by M. Grigoriu and S. Balopoulou, 6/11/92, (PB93-127496/AS).

NCEER-92-0016 "Gravity-Load-Designed Reinforced Concrete Buildings: Seismic Evaluation of Existing Construction and Detailing Strategies for Improved Seismic Resistance," by G.W. Hoffmann, S.K. Kunnath, J.B. Mander and A.M. Reinhorn, 7/15/92, to be published.

NCEER-92-0017 "Observations on Water System and Pipeline Performance in the Limón Area of Costa Rica Due to the April 22, 1991 Earthquake," by M. O'Rourke and D. Ballantyne, 6/30/92, (PB93-126811/AS).

NCEER-92-0018 "Fourth Edition of Earthquake Education Materials for Grades K-12," Edited by K.E.K. Ross, 8/10/92.

NCEER-92-0019 "Proceedings from the Fourth Japan-U.S. Workshop on Earthquake Resistant Design of Lifeline Facilities and Countermeasures for Soil Liquefaction," Edited by M. Hamada and T.D. O'Rourke, 8/12/92, (PB93-163939/AS).

NCEER-92-0020 "Active Bracing System: A Full Scale Implementation of Active Control," by A.M. Reinhorn, T.T. Soong, R.C. Lin, M.A. Riley, Y.P. Wang, S. Aizawa and M. Higashino, 8/14/92, (PB93-127512/AS).

NCEER-92-0021 "Empirical Analysis of Horizontal Ground Displacement Generated by Liquefaction-Induced Lateral Spreads," by S.F. Bartlett and T.L. Youd, 8/17/92.

NCEER-92-0022 "IDARC Version 3.0: Inelastic Damage Analysis of Reinforced Concrete Structures," by S.K. Kunnath, A.M. Reinhorn and R.F. Lobo, 8/31/92, to be published.

NCEER-92-0023 "A Semi-Empirical Analysis of Strong-Motion Peaks in Terms of Seismic Source, Propagation Path and Local Site Conditions, by M. Kamiyama, M.J. O'Rourke and R. Flores-Berrones, 9/9/92, (PB93-150266/AS).

NCEER-92-0024 "Seismic Behavior of Reinforced Concrete Frame Structures with Nonductile Details, Part I: Summary of Experimental Findings of Full Scale Beam-Column Joint Tests," by A. Beres, R.N. White and P. Gergely, 9/30/92, to be published.

NCEER-92-0025 "Experimental Results of Repaired and Retrofitted Beam-Column Joint Tests in Lightly Reinforced Concrete Frame Buildings," by A. Beres, S. El-Borgi, R.N. White and P. Gergely, 10/29/92, to be published.

B-11

NCEER-92-0026 "A Generalization of Optimal Control Theory: Linear and Nonlinear Structures," by J.N. Yang, Z. Li and S. Vongchavalitkul, 11/2/92.

NCEER-92-0027 "Seismic Resistance of Reinforced Concrete Frame Structures Designed Only for Gravity Loads: Part I - Design and Properties of a One Third Scale Model Structure," by J.M. Bracci, A.M. Reinhorn and J.B. Mander, 12/1/92.

NCEER-92-0028 "Seismic Resistance of Reinforced Concrete Frame Structures Designed Only for Gravity Loads: Part II - Experimental Performance of Subassemblages," by L.E. Aycardi, J.B. Mander and A.M. Reinhorn, 12/1/92.

NCEER-92-0029 "Seismic Resistance of Reinforced Concrete Frame Structures Designed Only for Gravity Loads: Part III - Experimental Performance and Analytical Study of a Structural Model," by J.M. Bracci, A.M. Reinhorn and J.B. Mander, 12/1/92, to be published.

NCEER-92-0030 "Evaluation of Seismic Retrofit of Reinforced Concrete Frame Structures: Part I - Experimental Performance of Retrofitted Subassemblages," by D. Choudhuri, J.B. Mander and A.M. Reinhorn, 12/8/92.

NCEER-92-0031 "Evaluation of Seismic Retrofit of Reinforced Concrete Frame Structures: Part II - Experimental Performance and Analytical Study of a Retrofitted Structural Model," by J.M. Bracci, A.M. Reinhorn and J.B. Mander, 12/8/92.

NCEER-92-0032 "Experimental and Analytical Investigation of Seismic Response of Structures with Supplemental Fluid Viscous Dampers," by M.C. Constantinou and M.D. Symans, 12/21/92.

NCEER-92-0033 "Reconnaissance Report on the Cairo, Egypt Earthquake of October 12, 1992," by M. Khater, 12/23/92.

NCEER-92-0034 "Low-Level Dynamic Characteristics of Four Tall Flat-Plate Buildings in New York City," by H. Gavin, S. Yuan, J. Grossman, E. Pekelis and K. Jacob, 12/28/92.

NCEER-93-0001 "An Experimental Study on the Seismic Performance of Brick-Infilled Steel Frames With and Without Retrofit," by J.B. Mander, B. Nair, K. Wojkowski and J. Ma, 1/29/93.

NCEER-93-0002 "Social Accounting for Disaster Preparedness and Recovery Planning," by S. Cole, E. Pantoja and V. Razak, 2/22/93, to be published.

NCEER-93-0003 "Assessment of 1991 NEHRP Provisions for Nonstructural Components and Recommended Revisions," by T.T. Soong, G. Chen, Z. Wu, R-H. Zhang and M. Grigoriu, 3/1/93.

NCEER-93-0004 "Evaluation of Static and Response Spectrum Analysis Procedures of SEAOC/UBC for Seismic Isolated Structures," by C.W. Winters and M.C. Constantinou, 3/23/93.

NCEER-93-0005 "Earthquakes in the Northeast - Are We Ignoring the Hazard? A Workshop on Earthquake Science and Safety for Educators," edited by K.E.K. Ross, 4/2/93, to be published.

NCEER-93-0006 "Inelastic Response of Reinforced Concrete Structures with Viscoelastic Braces," by R.F. Lobo, J.M. Bracci, K.L. Shen, A.M. Reinhorn and T.T. Soong, 4/5/93.